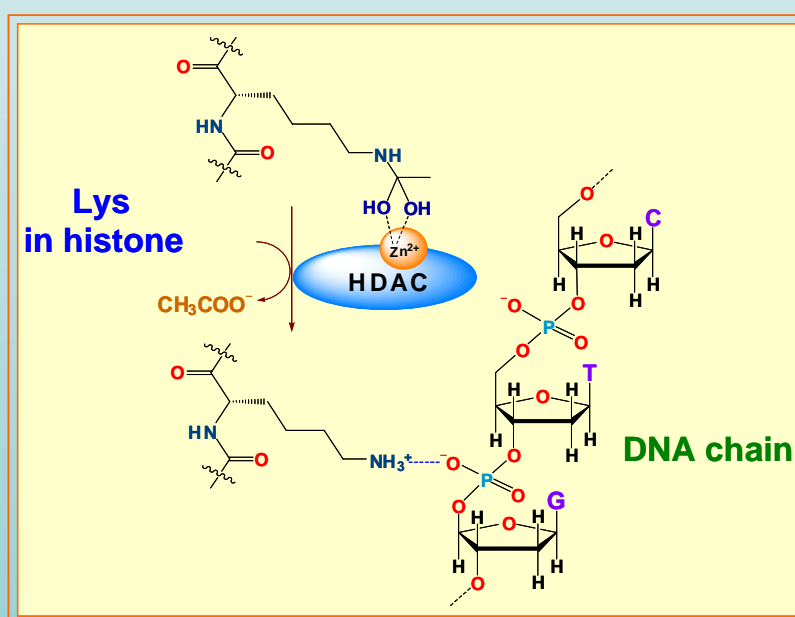


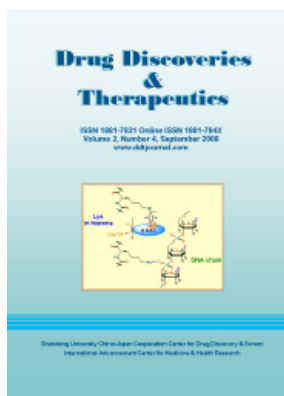
Drug Discoveries & Therapeutics

ISSN 1881-7831 Online ISSN 1881-784X
Volume 2, Number 4, September 2008
www.ddtjournal.com



Shandong University China-Japan Cooperation Center for Drug Discovery & Screen
International Advancement Center for Medicine & Health Research

Drug Discoveries & Therapeutics



Editor-in-Chief:

Kazuhisa SEKIMIZU
(The University of Tokyo, Tokyo, Japan)

Associate Editor:

Norihiro KOKUDO
(The University of Tokyo, Tokyo, Japan)

Drug Discoveries & Therapeutics is a peer-reviewed international journal published bimonthly by *Shandong University China-Japan Cooperation Center for Drug Discovery & Screen (SDU-DDSC)* and *International Advancement Center for Medicine & Health Research Co., Ltd. (IACMHR Co., Ltd.)*.

Drug Discoveries & Therapeutics mainly publishes articles related to basic and clinical pharmaceutical research such as pharmaceutical and therapeutical chemistry, pharmacology, pharmacy, pharmacokinetics, industrial pharmacy, pharmaceutical manufacturing, pharmaceutical technology, drug delivery, toxicology, and traditional herb medicine. Studies on drug-related fields such as biology, biochemistry, physiology, microbiology, and immunology are also within the scope of this journal.

Subject Coverage: Basic and clinical pharmaceutical research including Pharmaceutical and therapeutical chemistry, Pharmacology, Pharmacy, Pharmacokinetics, Industrial pharmacy, Pharmaceutical manufacturing, Pharmaceutical technology, Drug delivery, Toxicology, and Traditional herb medicine.

Language: English

Issues/Year: 6

Published by: IACMHR and SDU-DDSC

ISSN: 1881-7831 (Online ISSN 1881-784X)

Editorial and Head Office

Wei TANG, MD PhD
Secretary-in-General

TSUIN-IKIZAKA 410
2-17-5 Hongo, Bunkyo-ku
Tokyo 113-0033, Japan
Tel: 03-5840-9697

Fax: 03-5840-9698

E-mail: office@ddtjournal.com

URL: www.ddtjournal.com



Drug Discoveries & Therapeutics

Editorial Board

Editor-in-Chief:

Kazuhisa SEKIMIZU (*The University of Tokyo, Tokyo, Japan*)

Associate Editor:

Norihiro KOKUDO (*The University of Tokyo, Tokyo, Japan*)

Secretary-in-General:

Wei TANG (*The University of Tokyo, Tokyo, Japan*)

Office Manager:

Munehiro NAKATA (*Tokai University, Kanagawa, Japan*)

Web Editor:

Yu CHEN (*The University of Tokyo, Tokyo, Japan*)

English Editor:

Curtis BENTLEY (*Roswell, GA, USA*)

China Office:

Wenfang XU (*Shandong University, Shandong, China*)

Editors:

Yoshihiro ARAKAWA (<i>Tokyo, Japan</i>)	Hongxiang LOU (<i>Jinan, China</i>)
Santad CHANPRAPAPH (<i>Bangkok, Thailand</i>)	Ken-ichi MAFUNE (<i>Tokyo, Japan</i>)
Fen Er CHEN (<i>Shanghai, China</i>)	Norio MATSUKI (<i>Tokyo, Japan</i>)
Zilin CHEN (<i>Wuhan, China</i>)	Tohru MIZUSHIMA (<i>Kumamoto, Japan</i>)
Guanhua DU (<i>Beijing, China</i>)	Abdulla M. MOLOKHIA (<i>Alexandria, Egypt</i>)
Chandradhar DWIVEDI (<i>Brookings, SD, USA</i>)	Masahiro MURAKAMI (<i>Osaka, Japan</i>)
Mohamed F. EL-MILIGI (<i>Cairo, Egypt</i>)	Yoshinobu NAKANISHI (<i>Ishikawa, Japan</i>)
Harald HAMACHER (<i>Tuebingen, Germany</i>)	Yutaka ORIHARA (<i>Tokyo, Japan</i>)
Hiroshi HAMAMOTO (<i>Tokyo, Japan</i>)	Xiao-Ming OU (<i>Jackson, MS, USA</i>)
Xiao-Jiang HAO (<i>Kunming, China</i>)	Wei-San PAN (<i>Shenyang, China</i>)
Langchong HE (<i>Xi'an, China</i>)	Shafiqur RAHMAN (<i>Brookings, SD, USA</i>)
David A. HORNE (<i>Duarte, CA, USA</i>)	Adel SAKR (<i>Cincinnati, OH, USA</i>)
Yongzhou HU (<i>Hangzhou, China</i>)	Abdel Aziz M. SALEH (<i>Cairo, Egypt</i>)
Wei HUANG (<i>Shanghai, China</i>)	Tomofumi SANTA (<i>Tokyo, Japan</i>)
Yu HUANG (<i>Hong Kong, China</i>)	Yasufumi SAWADA (<i>Tokyo, Japan</i>)
Hans E. JUNGINGER (<i>Phitsanulok, Thailand</i>)	Brahma N. SINGH (<i>Commack, NY, USA</i>)
Toshiaki KATADA (<i>Tokyo, Japan</i>)	Hongbin SUN (<i>Nanjing, China</i>)
Ibrahim S. KHATTAB (<i>Safat, Kuwait</i>)	Benny K. H. TAN (<i>Singapore, Singapore</i>)
Hiromichi KIMURA (<i>Tokyo, Japan</i>)	Ren-Xiang TAN (<i>Nanjing, China</i>)
Shiroh KISHIOKA (<i>Wakayama, Japan</i>)	Murat TURKOGLU (<i>Istanbul, Turkey</i>)
Kam Ming KO (<i>Hong Kong, China</i>)	Stephen G. WARD (<i>Bath, UK</i>)
Nobuyuki KOBAYASHI (<i>Nagasaki, Japan</i>)	Takako YOKOZAWA (<i>Toyama, Japan</i>)
Toshiro KONISHI (<i>Tokyo, Japan</i>)	Liangren ZHANG (<i>Beijing, China</i>)
Masahiro KUROYANAGI (<i>Hiroshima, Japan</i>)	Jian-Ping ZUO (<i>Shanghai, China</i>)
Chun Guang LI (<i>Victoria, Australia</i>)	
Hongmin LIU (<i>Zhengzhou, China</i>)	
Ji-Kai LIU (<i>Kunming, China</i>)	

(as of September 29, 2008)

Review

200 - 210 Spermicidal agents.

Heeshma C. Shah, Pratima Tatke, Kamalinder K. Singh

Brief Reports

211 - 215 Novel *N*-hydroxybenzamide histone deacetylase inhibitors as potential anti-cancer agents.

Jie Jiao, Hao Fang, Wenfang Xu

216 - 218 Synthesis and antifungal activity of 3-substituted thiochromanones.

Yang Liu, Wei Luo, Li Sun, Chun Guo

Original Articles

219 - 228 Transdermal patch incorporating salbutamol sulphate: *In vitro* and clinical characterization.

Nashwa A. El-Gendy, Nirmeen A. Sabry, Mai El-Attar, Emad Omar, Manal Mahmoud

229 - 233 Establishment of a cell-based assay to screen insulin-like hypoglycemic drugs.

Li Zhang, Juan-juan Hu, Guan-hua Du

234 - 244 Inhibition of *in vivo* angiogenesis by *Anacardium occidentale* L. involves repression of the cytokine VEGF gene expression.

Sheela M. Lingaraju, Kaveri Keshavaiah, Bharathi P. Salimath

CONTENTS

(Continued)

- 245 - 253** **Production of a human antibody fragment against the insulin-like growth factor I receptor as a fusion protein.**

Yu Kusada, Toru Morizono, Keiko Sakai, Atsushi Takayanagi, Nobuyoshi Shimizu, Yoko Fujita-Yamaguchi

- 254 - 261** **The effects of dietary obesity on protein expressions of insulin signaling pathway in rat aorta.**

Sameer H. Fatani, Ebrahim K. Naderali, Sunil Panchiani, Feisal Shah, Chris Wong

Notification

Guide for Authors

Copyright

Review

Spermicidal agents

Heeshma C. Shah, Pratima Tatke, Kamalinder K. Singh*

C.U.Shah College of Pharmacy, S.N.D.T. Women's University, Mumbai, India.

ABSTRACT: In recent years, there is a development of vaginal contraceptives incorporating potent spermicides. Many compounds with different pharmacological activity have been evaluated *in vitro* for their spermicidal activity. Drugs such as surface-active agents (synthetic and natural), ionophores, antiliquefying agents, antimicrobial agents and miscellaneous agents such as gossypol, *Azadirachta indica*, vanadocenes have all been demonstrated to possess good spermicidal activity. Nonoxynol is the only spermicidal agent currently marketed and widely used. But there is still a need to develop alternative compounds for future use as safe spermicide.

Keywords: Spermicidal agents, Nonoxynol, Neem, Plants with spermicidal activity, Antifertility agents

1. Introduction

The world population continues to grow at an alarming rate, with a projected 50% increase in current world population to approximately 9 billion by 2050. Many methods such as condoms, oral contraceptives and intrauterine devices are available since long but there is still a quest for alternative means. A vaginal topical is the primary, if not the only, technique whereby, a woman can prevent both pregnancy and infections. The serious development of chemical spermicides for public use dates back to the 1930's. Research has focused on the development of safe, highly effective and inexpensive spermicidal agents as one of the several alternative methods for family planning.

Spermicides are a biologically obvious way of interrupting fertility and have advantage that they do not depend on high skilled personnel for their prescription

*Correspondence to: Dr. Kamalinder K. Singh, C.U.Shah College of Pharmacy, S.N.D.T. Women's University, Sir Vithaldas Vidya Vihar, Santacruz (W), Mumbai-400049, India;
e-mail: kksingh35@rediffmail.com

and use. Spermicidal agents are defined as drugs that have the ability to immobilize or kill the sperm upon contact. An ideal spermicide should immediately and irreversibly produce immobilization of the sperm, non-irritating to the vaginal and penile mucosa, not have adverse effects on the developing fetus, free from long-term topical and systemic toxicity and should not be systemically absorbed.

Hence, the spermicidal agents should be critically evaluated for these aspects. Understanding the morphology of spermatozoa is essential to appreciate the mechanism of action of spermicide.

2. Morphology of spermatozoa

Each normal spermatozoon is made up of two parts a head and a tail. The head consists of two main parts, the nucleus and acrosome. The nucleus contains the whole of the chromatin content of the sperm and the acrosome is made up of collection of enzymes that will aid penetration of the zona-pellucida by the sperm. The connecting piece is a small area in a very short segment that joins the head to the tail. The sperm tail is the means by which the sperm moves. The tail of the sperm consists of three parts the middle piece, the principle piece and the terminal segment. Overall the tail measures around 50 μm . The whole length of the tail contains a central contractile unit known as axoneme. In the middle piece, a central axoneme is present which is surrounded by closely packed helix of mitochondria. The principle piece makes up more than 90% of the length of the tail followed by the terminal segment. The sperm plasma membrane serves as a continuous limiting cell boundary, maintaining cell integrity and forming a dynamic interface between the cell boundary and its immediate environment (1,2).

One of the most challenging pursuits in the realm of pharmaceutical and medical sciences is the search for newer and more potent spermicides with little or no toxic effects and available at reasonable cost. A review of spermicidal agents which are in various stages of preclinical and/or clinical stage of development are given as follows:

3. Spermicides acting through pH modification

The spermatozoa are motile between pH 6.7 to 8.5. Therefore, one of the oldest approaches for achieving spermicidal action has been to modify vaginal pH. The normal human vaginal pH is 3.8-4.2. This naturally acidic environment is maintained by the production of lactic acid by the vaginal flora. HIV, several STD-causing microbes and spermatozoa are inactivated at this low pH. When semen enters the vagina, the pH rises to above 6.0 because of the buffering activity of the ejaculate (pH 7.2-8.0) (3). It is well documented that sperm are sensitive to low pH and acidic solution can immobilize sperm within minutes (4).

ACIDFORM, an acid buffering vaginal formulation that maintains the acidic vaginal pH below 5.0 when ejaculate is deposited in the vagina or when a vaginal infection is present. In women, the desired acidification of semen can be achieved with a 3-5 mL dose because the average volume of the human ejaculate is about 3 mL, which would require less than 1 g of ACIDFORM to buffer the semen to a pH lower than 5.0. ACIDFORM is slightly off-white in appearance with a pH of about 3.55. The formulation consists of gelling agents, buffer salts, humectants, preservatives and water that are all GRAS except for one, which although not GRAS, is currently used in marketed vaginal formulations. A recently completed Phase I clinical safety study with ACIDFORM confirms its safety. No patient complaints (symptoms) have been recorded when ACIDFORM was applied vaginally for six consecutive days and no vaginal or cervical irritation was noted on visual or coloscopic inspection (5-8).

Lemon juice has been used as traditional intravaginal contraceptive throughout the Mediterranean region for hundreds of years. The spermicidal properties of lemon juice are possibly due to the high concentration of citric acid (9). Investigations have demonstrated that dyein ATPase in the sperm midpiece is required to energize the sperm tail. The acidic pH of lemon juice may immobilize sperm by denaturing dyein ATPase (10). Clarke *et al.* have demonstrated that a minimum concentration of 200 $\mu\text{L}/\text{mL}$ lemon juice would be required to irreversibly immobilize 100% of spermatozoa. Ejaculate volume in normal men rarely exceeds 5 mL, so it would be necessary to deliver at least 1.5 mL of lemon juice into the vagina to obtain the desired concentration (9). Lemon juice would be a cheap and widely available vaginal contraceptive if its safety and efficacy were demonstrated (11).

4. Synthetic surface active agents

4.1. Non-ionic surfactants

In the category of non-ionic surfactants octoxynol and nonoxynol are the two commonly reported surfactants.

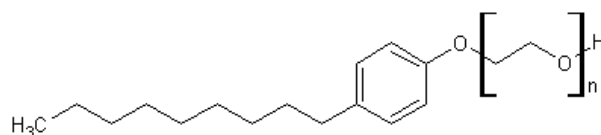


Figure 1. Structure of Nonoxynol-9.

Nonoxynol is more potent spermicide than octoxynol. Among the different nonoxynol derivatives designated as N1-N15, *p*-nonyl phenoxy polyethoxy ethanol (N-9) is reported to be the most potent spermicide (Figure 1) (12). At present N-9 is the only marketed contact spermicide available worldwide.

N-9 destroys the cell membrane of the neck of spermatozoa. The SEM/TEM of spermatozoa have revealed that after contact with N-9 the plasma membrane and the acrosomal membrane complex were removed, the midpiece membrane was absent, the normal cristae of the mitochondria were empty and the fibers were exposed. Damage to all membranes was first evident as vesiculations. Membranes then became loose and detached. The observed irreversible severe membrane alterations cause an immediate devitalization of the spermatozoa (13,14). At the dose of 50 $\mu\text{g}/\text{mL}$ N-9 completely abolishes all sperm movement within one minute of addition. Although, N-9 has been employed as a contact spermicide for the last 30 years and is well tolerated, reports have appeared suggesting that the frequent use of surface active spermicides, can be associated with vaginal irritation and the appearance of lesions in the epithelium. The most common abnormality reported has been superficial de-epithelization of either the cervix or the vaginal walls, though there have been no reports of vaginal inflammation (15,16). In contrast, more recent studies reports that the use of N-9 as a microbicide or N-9 used in limiting the transmission of STD's should be discontinued since N-9 interferes with the lipid bilayer of the vaginal epithelium and facilitates the process of absorption and transmission of the viral particle into the blood stream (17-20).

Nonoxynol-9 is commercially available as gel, cream, foam and pessary formulations in various strengths (Table 1).

Ahmad N *et al.* have designed a new bioadhesive suppository of N-9 called Long Acting, Sustained Release of Spermicide (LASRS). The formulation is reported to adhere well to cellulose membranes *in vitro* and was completely spermicidal in the primate (stumptailed macaque) on post-coital tests even when mating was delayed for 12 h. Vaginal irritation studies in the rabbit and primate showed LASRS to be acceptable even with a nonoxynol-9 dose as high as 22.5% (w/w) (21). No coloscopic or visual vaginal lesions were induced when LASRS with 20% N-9 was used for 7 consecutive days by the volunteers participating in a pilot clinical trial. These studies

Table 1. List of marketed spermicidal formulations of nonoxynol

Sr. No.	Brand name	Nonoxynol-9	Formulations	Companies
1.	Advantage 24	3.5%	Gel	Columbia Laboratories
2.	Conceptrol Gel	4%	Gel	Advanced Care
3.	Koromex Crystal Clear gel	3%	Gel	Quality Health
4.	Ramses Personal Spermicidal Lubricant Gel	3%	Gel	London International U. S. Holdings
5.	VCF Gel	3%	Gel	Apothecus Pharmaceutical
6.	Encare	100 mg	Suppository	Thompson Medical Co.
7.	Semicid	100 mg	Suppository	Whitehall Robbins Healthcare
8.	Koromex	125 mg	Suppository	Quality Health
9.	Gynol II	2%	Jelly	Advanced Care
10.	K-Y Plus	2.2%	Jelly	Johnson & Johnson
11.	Koromex	3%	Jelly	Quality Health
12.	Ortho- Gynol	1%	Jelly	Advanced Care
13.	Shur-Seal	2%	Jelly	Milex Products
14.	Delfen	12.5%	Foam	Advanced Care
15.	Emko	12%	Foam	Schering-Plough Healthcare
16.	Koromex	12.5%	Foam	Quality Health
17.	Ortho-Creme	2%	Cream	Advanced Care
18.	Today	5%	Pessary	Bliss Pharmaceuticals

suggest that LASRS possess advantages over presently marketed formulations by having long-term efficacy and by forming a bioadhesive, protective layer over the genital tract epithelium (22).

4.2. Cationic surfactants

Benzalkonium chloride is a bactericidal cationic surfactant, of the ammonium series that ceases the sperm flagellar motility immediately upon contact with spermatozoa. Four seconds after contact, the midpiece and head are destroyed. In concentrations of 70-300 µg/mL, the spermatozoon motility decreases, acrosomal proteins disappear, the fecundity capacity is lost as determined by hamster-ova penetration test and the enzymes of carbohydrate metabolism are disturbed. Benzalkonium chloride also coagulates ovulatory cervical mucus, its colloid network structure disappears and results in a magma with mesh of less than 5 µm, which is not permeable to spermatozoa. This action might be added mechanism of barrier to sperms in addition to its spermicidal activity. Vaginal suppository containing 18.9 mg of benzalkonium chloride have shown cervico-vaginal erosion/inflammation with the use of this suppository, which disappeared after cessation of use (23). It is interesting to note that concentration of benzalkonium chloride required for its spermicidal action is much less than that permitted for its preservative action (0.01-0.25%). Benzalkonium bromide in the concentration of 0.27 mg/mL also significantly affects the motility of human sperm and can be used as a spermicide (24,25).

Other cationic detergents like cetyl ammonium chloride and cetyl trimethyl ammonium bromide are also potent spermicides and instantly immobilize the spermatozoa at the concentration of 1 mg/mL. However, changes in the permeability of vaginal membrane on continuous use of these agents have been reported, and thus none of these agents are suitable for human use (26).

5. Natural surface-active agents: Saponins

Saponins are natural surfactants widely occurring in many plants and are reported to have spermicidal action. A common lipid bilayer, which contains external, internal and transmembrane proteins, is fundamental feature of the plasma membrane of the sperm. Saponin molecules interact with this lipid bilayer, affect the glycoproteins of the cellular membrane and modify the ionic transport across the membrane, leading to surface changes. These changes, namely vesiculation, vacuolation or dissolution of head region may occur due to stretching, loosening, breakdown of the membrane and ultimate removal of the acrosome (27).

Some of the saponin containing plants includes:

5.1. *Acacia auriculiformis*

Mixtures of two partially isolated triterpenoid saponins from the powdered seeds of *Acacia auriculiformis* (Acaciaside A and B) have shown spermicidal activity at the concentration of 0.35 mg/mL. The aglycone parts of these two saponins were characterized as acacic acid lactone and monosaccharide constituents were identified as D-glucose, D-xylose, L-arabinose and L-rhamnose. The complete chemical structures of these compounds are given in Figure 2. Electron microscopic observation showed that the plasma membrane was disintegrated and total dissolution of the acrosomal cap was observed (28,29).

5.2. *Sapindus mukorosii (reetha)*

Saponins isolated from *Sapindus mukorosii* (reetha) have shown most potent spermicidal activity. The saponins reported are derivatives of hederagenin namely mukurozi-saponins E₁, G, X, Y₁, Y₂, Z₁ and Z₂ (30). After incubation with saponins at 0.5 mg/mL for 1 min, the spermatozoa did not exhibit

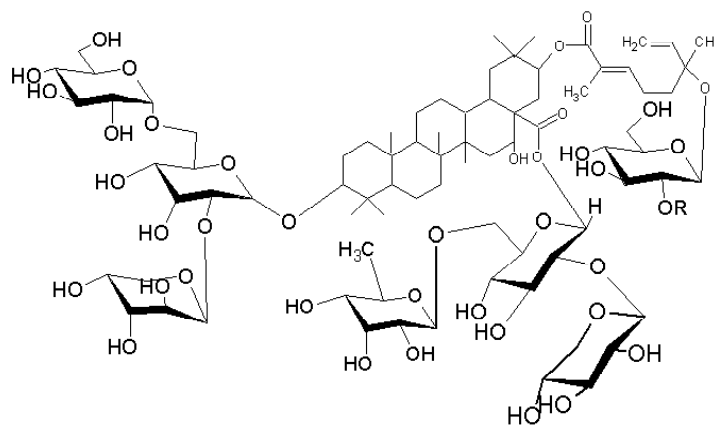


Figure 2. Structure of Acaciaside A and B. Acaciaside A: R= H; Acaciaside B: R= Xylose.

any significant morphological changes, though at the same concentration, immobilization of the sperms was observed. At higher concentrations of saponins (1-50 mg/mL) spermatozoa displayed marked disruption, vacuolation, vesiculation and erosion of the membrane covering the head region. Coiling of the tail was also noticeable with higher concentrations of saponins though no damage was evident under SEM in the flagellar region of the sperm (27,31). These saponins were formulated into a contraceptive cream named 'CONSAP'. This cream has completed Phase III clinical trials successfully in India (32).

5.3. *Molluga pentaphylla*

The ethyl acetate fraction of *Molluga pentaphylla*, a tropical herb contains an antifungal triterpenoid saponin, Mollugogenol-A (Figure 3) which has demonstrated spermicidal activity at 300 µg/mL. Electronic microscopic observation showed that the fragmentation or loss of plasma membrane, vesiculation of periacrosomal membrane and dissolution of the organelle as a whole are suggestive of sperm degeneration (33).

Other plants containing saponins, which have shown spermicidal activity, include *Phytolacca dodecadra*, *Calendula officinalis*, *Acacia caesia*, *Acacia concinna*, *Trigonella foenum-graecum* (34), *Chenopodium album*

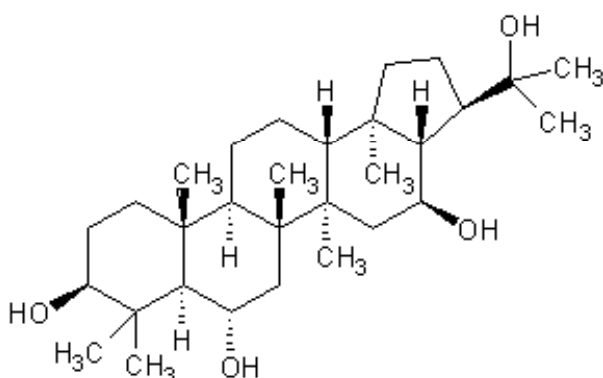


Figure 3. Structure of Mollugogenol-A.

(35) and *Cestrum parqui* (36). Saponins are naturally occurring and there is no report of their systemic toxicity. However, due to their interfacial tension reducing property they may alter the permeability of the vaginal membrane on frequent use. In addition, reduction in interfacial tension may in fact, lead to decreased viscosity of the mucus and hence, result in an increased rate of transfer of spermatozoa through the vaginal mucosa. Therefore, it is necessary to critically evaluate these effects before advocating the use of saponins as spermicidal agents (12).

6. Spermicides with additional antimicrobial activity

6.1. Chlorhexidine

A contraceptive method, which additionally protects against venereal infections, will be of immense value. One such compound being investigated for its spermicidal action is the antiseptic, chlorhexidine. The mechanism of the spermicidal action of chlorhexidine is not fully understood, however its antiseptic action is attributed to its high positive charge density resulting in non-specific binding to the negatively charged elements on the microbial cell wall. Disruption of cellular permeability, cell wall fluidity and altered metabolic activity has been suggested as a possible cause of the antiseptic action. Chlorhexidine shows spermicidal activity at the dose of 4.81 mg/mL within 20 sec, however hypersensitivity to chlorhexidine upon topical use has been reported (37,38).

6.2. Magainins

Magainins are class of peptides initially isolated from the skin of the African clawed frog, *Xenopus laevis*. Magainins A and G are two natural peptides having 23 amino acids and differ by only two substitutions, have been found to have a wide spectrum *in vitro* antimicrobial activity against gram positive and negative bacteria, fungi, and protozoa. They exhibit

spermicidal action, besides antimicrobial activity (39). Magainins are membrane active compounds and the decreased motility and viability of sperm has been observed in the presence of Magainins may be attributed to the loss of permeability of the plasma membrane, which leads to cell-death. Magainin-A was found to be more potent than Magainin-G. Intravaginal administration of magainin-A 200 µg to rats (40) and 1 mg to rabbits and monkeys once before mating resulted in 100% sperm immobilization (41,42). Magainin-A does not have overt cytotoxic properties and is safe for intravaginal application. It is also active against various STI-causing pathogens but not against HIV-1 and HIV-2. It is reported that effectiveness of magainin as a contraceptive *in vivo* is possibly due in part to the removal of cholesterol from sperm membranes (43).

6.3. Nisin

Nisin, a 34 amino acid, naturally occurring antimicrobial cationic peptide is known to be produced by bacteria *Lactococcus lactis*. Nisin has been used as a food preservative throughout the world and the World Health Organization (WHO) and US, Food & Drug Administration have conferred GRAS status to this peptide. At the dose of 300-400 µg, complete immobilization of human spermatozoa was observed within 20 sec. *In vivo* contraceptive efficacy studies in rats showed complete arrest of sperm motility and no pregnancy in any of the animals. At the contraceptive dose of 200 µg, Nisin did not alter the morphology of the vaginal epithelial cells, nor did it cause any histopathological lesions in the vaginal epithelium when administered intravaginally for 14 consecutive days. The mechanism by which Nisin exerts its rapid spermicidal action is not known. However, the existing evidence suggests that Nisin possesses an overall positive charge and interacts preferentially with anionic phospholipids. The sperm plasma membrane contains high concentration of phosphatidylglycerol, a strong anionic phospholipid moiety and thus, Nisin may have high affinity towards spermatozoa (44).

6.4. Zidovudine derivatives

Zidovudine *i.e.* 3'-azido-3'-deoxythymidine though lacks spermicidal activity by itself, its two novel phenyl phosphate derivatives WHI-05 [5-bromo-6-methoxy-5,6-dihydro-3'-azidothymidine-5'-(*p*-methoxyphenyl) methoxyalaninyl phosphate] (Figure 4) and WHI-07 [5-bromo-6-methoxy-5,6-dihydro-3'-azidothymidine-5'-(*p*-bromophenyl) methoxyalaninyl phosphate] (Figure 5) have been identified to exhibit potent anti-HIV and spermicidal activity (45,46). They are dual-functional microbicides lacking detergent-type membrane toxicity, which would have advantages over

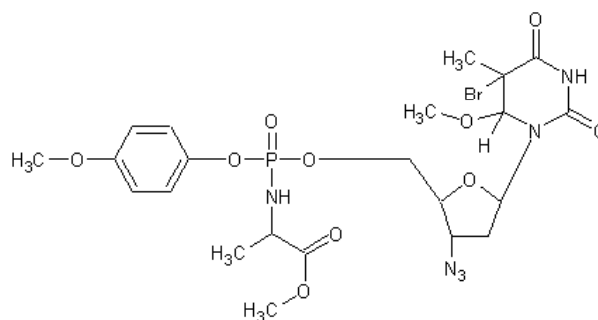


Figure 4. Structure of WHI-05.

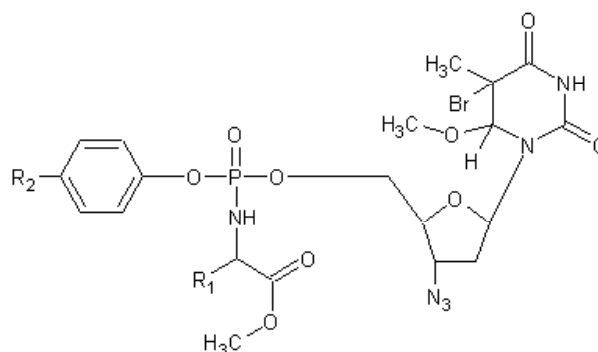


Figure 5. Structure of WHI-07. R₁ = CH₃; R₂ = Br.

the currently available vaginal microbicides. Unlike, N-9, the spermicidal activity of WHI-05 and WHI-07 was not associated with cytotoxicity to reproductive tract epithelial cells (47,48). A repeated intravaginal exposure of gel microemulsion formulations of WHI-05 and WHI-07 in mice and rabbits indicated these are non-cytotoxic and lacks inflammation-inducing properties (49,50). D'Cruz *et al.* also demonstrated that an intravaginal application of 2% WHI-07 *via* a gel microemulsion in rabbit model resulted in marked contraceptive activity (51).

6.5. C31G

C31G, a spermicide composed of an equimolar mixture of *n*-dodecyl-dimethylamine-*N*-oxide (C₁₂-N-O) and *N*-(*n*-dodecyl), *N*-dimethyl-glycine (C₁₂-betaine) offers a potential alternative to nonoxynol-9, both as a spermicide and as a microbicide/virucide. C31G has shown *in vitro* activity against a large number of gram-negative, gram-positive bacterial strains and anti-fungal properties. It is a potent virucidal agent with activity against HIV and herpes simplex virus (52). A phase I double-blind randomized study of 1.2% C31G with hydroxyethyl cellulose (HEC) suggested that physical epithelial changes after 7 consecutive days of product use were similar to changes seen with a marketed 2% nonoxynol-9 product (Gynol-II). The subjective symptoms of genital burning or heat, however, were much greater with the C31G HEC product, which limits its usefulness (53).

7. Antiliquefying agents

The active antiliquefying agents immediately coagulate ejaculated semen, possibly through a denaturing effect on the glycoproteins present in coagulated material. Highly effective antiliquefying property has been exhibited by mercury (2.7 mg/mL), nitrophenols (6.9 mg/mL), sodium naphthyl phosphate and tannic acid. A combination of antiliquefying and a potent spermicidal agent may offer highly promising approach towards vaginal contraception. However, the safety index of the currently evaluated antiliquefying compounds is too low to permit their use in pharmaceutical formulation for *in vivo* use (54).

8. Calcium ion and sperm motility

Calcium ions have an apparently paradoxical effect on sperm motility. Hong CY *et al.* states that in epididymis, calcium ions stimulate immature sperms but in ejaculated semen, calcium ions inhibit sperm motility. Thus calcium chelators such as ethylene glycol-bis β -aminoethyl ether *N,N,N',N'*-tetraacetic acid (EGTA) and ethylenediamine tetraacetic acid (EDTA), as well as calcium antagonists such as diltiazem, flunarizine and verapamil stimulate sperm motility in ejaculated human semen (55).

However, Lee C *et al.* stated that a decrease in calcium ion concentration in semen will inhibit sperm motility. After exposure to EDTA, the calcium ion concentration in semen was found decreased with increasing EDTA concentration. Thus EDTA appears to exert the spermicidal activity by modulating calcium ion concentration in semen. EGTA 5.5 mg/mL, EDTA 5 mg/L showed activity within 2 min (56).

The sperm membrane is reported to possess a Na^+ - Ca^{2+} exchanger and a Ca^{2+} -ATPase pump. Both these systems play a vital role in extrusion of Ca^{2+} from the sperm cell. 2',4'-dichlorobenzamil hydrochloride (Benzamil), has been reported to inhibit both the above systems and thus benzamil exhibits spermicidal activity due to the elevation of intracellular Ca^{2+} . Benzamil at 2.0 mM concentration showed 100% immotility at 60 min. But when used in combination with propranolol (2.0 mM), the spermicidal activity was seen within 8 min. Propranolol is also reported to produce sperm death due to an increase in intracellular Ca^{2+} . This action may be due to its membrane stabilizing property and not related to its β -blocking property (57,58). When 2',4'-dichlorobenzamil hydrochloride (DBZ) was combined with any one of the three H_2 -receptor antagonists, cimetidine, ranitidine and famotidine, the time required to produce complete loss of sperm viability was found to be reduced by minimum of 2.7, 1.9 and 3.4 fold, respectively. The elevation of intrasperm Ca^{2+} by H_2 -receptor antagonists can be attributed to their ability to inhibit Na^+ - K^+ ATPase

enzyme system that is reported to be present on the sperm membrane. Thus the rate of increase of intrasperm Ca^{2+} was found to be faster when DBZ was used in combination with any H_2 -receptor antagonists (59).

9. Ionophores

Ionophores are compounds that form lipid soluble complexes with specific cations and act as vehicles for transporting these cations across biological membrane. The calcium ionophore, A23187, increases the intracellular calcium concentration and inhibits human sperm motility at the concentration of 20 μM within 120 sec. However, local effects of ionophores on vaginal tissue and their systemic effects after absorption are yet to be evaluated (60).

10. Miscellaneous agents

10.1. Gossypol

Gossypol, a disesquiterpene aldehyde (Figure 6) isolated from the seeds of cotton (*Gossypium* species) plant, is reported to be a spermicidal agent (61). The concentration required to immobilize 100% spermatozoa within 20 sec is 40 mg/mL (62). Gossypol inhibits sperm motility by blocking ATP production and utilization. It acts on mitochondria, suppressing oxygen consumption, inhibiting the pyruvate dehydrogenase and ATPase activities and probably on the motility apparatus by blocking dynein ATPase activity and preventing protein phosphorylation (63).

10.2. Lyophilized *Aloe barbadensis*

Aloe barbadensis, one of the worldwide botanicals, has been used for health purposes for thousands of years and comes in a variety of forms including gel and lyophilized powder. Fresh gels are not used intravaginally as they are unstable and also contain

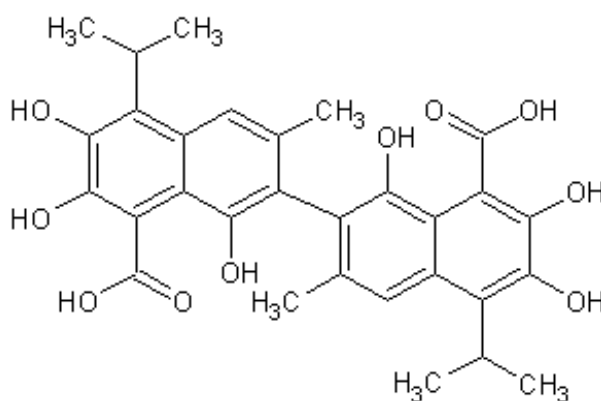


Figure 6. Structure of Gossypol.

sugars, which may accelerate vaginal infections. Lyophilized *Aloe barbadensis* does not contain sugars but eleven different mineral elements in different concentrations, which have shown a toxic effect on the tail of spermatozoa leading to rapid immobilization of spermatozoa. It was seen that the spermatozoa were intact, but their tails were curled after being exposed to lyophilized *Aloe barbadensis* at 100 mg/mL concentration within 30 sec. Rabbit vaginal irritation study showed no irritation of vaginal epithelium after application of 100 mg/mL lyophilized *Aloe barbadensis* for 10 days (64).

10.3. *Azadirachta indica*

The neem tree, *Azadirachta indica* is indigenous to the Indian subcontinent. Neem oil, an oil extracted from the seeds of the neem tree, has been found to possess strong spermicidal activity. By the process of hydrodistillation, the volatile fraction of neem oil has been isolated and coded as NIM-76. A concentration of 25 mg/mL of the compound was found to achieve total spermicidal effect in 20 sec. Vaginal irritation study conducted in rabbits, by intravaginal application of 15 mg of NIM-76 in 2 mL of gelatin jelly for 10 days showed no irritation to the vaginal mucosa (65). Khillare B has revealed that the aqueous extract of old and tender neem leaves is a potent spermicide. The minimum effective concentration required to kill 1 million sperm in 20 sec was 2.91 mg and 2.75 mg for tender and old leaf extract, respectively (66).

10.4. *Allium sativum*

Garlic and its active principle, allitridium (Figure 7) possess bacteriostatic and antimycotic action. Allitridium showed complete immobilization of sperms from human and animals within 20 sec at 7.5 mg/mL and within 3 min at 1.5 mg/mL. Allitridium (7.5 mg/mL) showed no vaginal irritation reaction or other side effects. It had no bacteriostatic action on the lactic acid bacilli, so it would not interfere with the growth of the bacilli in the vagina (67).

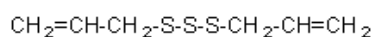


Figure 7. Structure of Allitridium.

10.5. *Curcuma longa* (Turmeric)

Curcumin (diferuloyl methane) (Figure 8), a yellow pigment present in the rhizomes of turmeric and related species and used as a spice, has a wide array of pharmacological and biological activities. Studies have demonstrated that curcumin has anti-tumor, anti-inflammatory and anti-infective activities. Curcumin

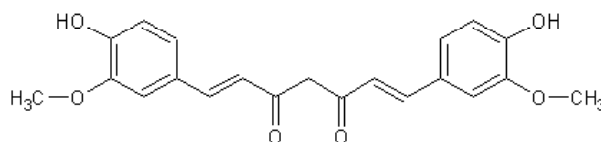


Figure 8. Structure of Curcumin.

has also shown to inhibit the integrase activity of the HIV. When curcumin is used in the concentrations of 30 µg/mL and 100 µg/mL, the human sperm motility was reduced to 53.4% and 4.1% after 120 min. A total 100% immobilization was achieved with a dose of 300 µg/mL at the end of 60 min. Curcumin-induced changes in sperm mitochondrial transmembrane potential indicate that this flavanoid may interfere with sperm energy metabolism. Curcumin in micromolar concentrations inhibits the protein kinase C, which is present in human sperm and is believed to play a role in modulating human sperm flagellar movement (68).

10.6. *Stephania hernandifolia* and *Achyranthes aspera*

A composite extract of the leaves of *Stephania hernandifolia* and the roots of *Achyranthes aspera* were prepared in a ratio of 1:3 and evaluated for spermicidal activity at different concentrations ranging from 0.04 to 0.32 g/mL. Concentration of 0.08 g/mL of the extract affected the motility and at a concentration of 0.16 g/mL, the sperm motility was reduced to 20% immediately within 20 sec. At the concentration of 0.32 g/mL complete sperm immobilization was observed within 2 min after application of the extract. The hypo-osmotic swelling of these sperms was reduced significantly at this highest concentration, indicating that the crude extract may probably cause injury to the sperm plasma membrane. A low concentration of 0.04 g/mL was found to be ineffective (69).

10.7. *Carica papaya* seed extracts

The chloroform extract, the benzene chromatographic fraction of the chloroform extract and its methanol and ethyl acetate subfractions and the isolated compounds ECP 1 and 2 and MCP 1 and 2 have shown a sperm immobilizing effect on human spermatozoa *in vitro*. Total inhibition of motility was observed within 20-25 min at all concentrations of all products. The SEM and TEM of spermatozoa showed membrane damage in the head as well as midpiece suggesting the mode of action appears similar to that of N-9 (70).

10.8. *Praneem polyherbal formulations*

A combination formulation developed as "Praneem polyherbal cream" which includes a purified extract from the dried seeds of *Azadirachta indica* (Neem) (250 mg/mL), extract from the pericarp of fruits of *Sapindus*

mukorosii (0.5 mg/mL) and quinine hydrochloride (3.46 mg/mL) has shown spermicidal activity in 20 sec. The formulation has shown high contraceptive efficacy in rabbits and in monkeys after intravaginal application. Also the formulation was found to be safe with no vaginal irritation when applied intravaginally for 30 days at a daily dose of 1 mL (71).

The Praneem polyherbal pessary and tablet formulated, includes purified ingredients from neem leaves, *Sapindus mukorosii* and *Mentha citrata* oil. The vaginal pessary has shown potent spermicidal action of human spermatozoa *in vitro* and high contraceptive efficacy was demonstrated in rabbits of proven fertility (72,73). Praneem polyherbal formulations have shown *in vitro* activity against HIV and sexually transmitted disease pathogens (73). Praneem vaginal pessaries and tablets were found to be safe for once daily intravaginal use consecutively for 7 and 14 days in healthy women volunteers (74,75).

10.9. Parabens

Parabens are commonly added in food, beverages, pharmaceuticals and cosmetics as antifungal preservatives. Methyl paraben, ethyl paraben, propyl paraben and butyl paraben have shown potent spermicidal activity at the concentrations of 6, 8, 3, and 1 mg/mL, respectively (76).

10.10. Zinc acetate

Zinc acetate at 10 mg/mL concentration has shown spermicidal activity within 30 sec, while the other zinc salts such as zinc gluconate, zinc sulfate and zinc chloride are not spermicidal at the same concentration. It is probably that zinc ion and acetate decrease the availability of oxygen to sperm, which leads to immobilization. Transmission electron microscopy of zinc acetate treated human spermatozoa showed the most visible changes in the mitochondria of the middle portion of the tail. There was a reduction in the electrodensity of mitochondria of the spermatozoa but the sheath was present. Vaginal irritation studies in rabbits with continuous administration of 4 mg zinc acetate/kg or 8 mg zinc acetate/kg for 10 days caused no irritation of highly sensitive rabbit vaginal epithelium. In addition zinc has also been reported to be beneficial to wound healing (64).

10.11. Gel microemulsions

Microemulsions are thermodynamically stable, isotropically clear dispersions of water, oil, and surfactants with potential as drug-delivery vehicles. D'Cruz O *et al.* has formulated novel submicron (30-80 nm) particle gel microemulsion (GM) formulations GM-144 and GM-4. GM-144 prepared from seven non-

toxic pharmaceutical excipients (propylene glycol, Captex 300, Cremophor EL, Phospholipon 90G, Rhodigel, Pluronic F-68 and sodium benzoate) was found to show rapid sperm-immobilizing activity in human semen in less than 30 sec (77). GM-4 formulation containing eight pharmaceutical excipients (Captex 300, Cremophor EL, Phospholipon 90G, Propylene glycol, PEG-200, Seaspan carrageenan, Viscarin carrageenan and sodium benzoate) exhibited potent spermicidal activity in less than 2 min (78). In standard rabbit model, GM-144 and GM-4, when tested as a vaginal contraceptive, GM-144 was as effective as the commercially available N-9 formulation (Gynol II) and GM-4 was far more effective than Gynol-II. No toxic effect was observed on the vaginal mucosa of rabbits after daily exposure for 10 days (77-80).

10.12. Vanadocenes

Spermicidal organometallic complexes of vanadium (IV) with bis(cyclopentadienyl) rings or vanadocenes are a new class of experimental contraceptive agents. Vanadocenes are reported to have rapid, potent and selective sperm immobilizing activity (SIA). Vanadocenes elicited potent SIA at nanomolar to micromolar concentrations. The SIA of representative vanadocenes was 400-fold more potent than that of N-9. Vanadocenes dihalides immobilized human sperm in semen within 15 sec without affecting the sperm membrane integrity or viability of normal human vaginal or cervical epithelial cells. These features of vanadocenes fundamentally differ from those of currently used membrane-active detergent-type spermicides that are cytotoxic to genital tract epithelial cells at spermicidal concentration. The lack of detergent-type membrane toxicity of spermicidal vanadocenes may have particular clinical utility as a new class of contraceptive agents. Spermicidal activity of vanadocenes were shown to be mediated by a unique mechanism involving membrane intercalation that was independent of dynein adenosine triphosphatase activity, protein tyrosine phosphatase activity, and the phosphocreatine/creatine kinase system. Among the 45 vanadocenes that were synthesized and evaluated for human spermicidal activity vanadocene acetylacetonato monotriflate (VDACAC) (Figure 9) and vanadocene dithiocarbamate (VDDTC) (Figure 10)

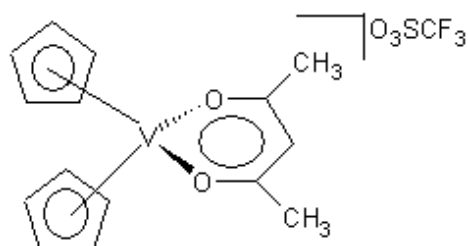


Figure 9. Structure of vanadocene acetylacetonato monotriflate (VDACAC).

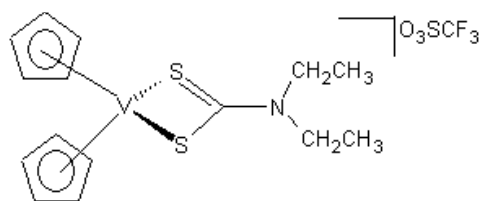


Figure 10. Structure of vanadocene dithiocarbamate (VDDTC).

were the most stable and potent spermicidal vanadocenes (81-88). Repeated intravaginal application of gel formulations of VDACC and VDDTC did not induce local inflammation, toxicity or retention of vanadium in the mice and rabbit vaginal irritation model. D'Cruz OJ *et al.* demonstrated that the intravaginal application of a 0.1% VDDTC in rabbits and pigs results in remarkable contraceptive activity (89-92).

11. Conclusion

This summary of the spermicides pipeline and complementary research clearly shows that much progress has been made in the last decade. Laboratory and clinical research has been complemented by a growing body of research and literature on spermicides acceptability, harm reduction and protection strategies, and potential markets. In recent years, attitudes toward spermicides have generally become more positive in response to public and nonprofit initiatives to address these barriers. However, many challenges remain, including the need for a significant increase in investment to accelerate product development and complementary research, and to plan for availability and access once effective spermicides are available.

References

1. Grudzinskas JG, Yovich JL. Gametes- The spermatozoon. Cambridge University Press, Great Britain, 1995; pp. 45-69.
2. Jequier A, Crich J. Semen analysis-A Practical Guide. Blackwell Scientific Publications, London, 1986; pp. 15-18.
3. Alexander NJ, Baker E, Kaptein M, Karck U, Miller L, Zampaglione E. Why consider vaginal drug administration? *Fertil Steril* 2004; 82:1-12.
4. Olmsted SS, Dubin NH, Cone RA, Moench TR. The rate at which human sperm are immobilized and killed by mild acidity. *Fertil Steril* 2000; 73:687-693.
5. Garg S, Anderson RA, Chany CJ, Waller DP, Diao XH, Vermani K, Zaneveld LJD. Properties of a new acid-buffering bioadhesive vaginal formulation (ACIDFORM). *Contraception* 2001; 64:67-75.
6. Amaral E, Faúndes A, Zaneveld L, Waller D, Garg S. Study of the vaginal tolerance to acidform, an acid-buffering, bioadhesive gel. *Contraception* 1999; 60:361-366.
7. Amaral E, Perdigão A, Souza MH, Mauck C, Waller D, Zaneveld L, Faúndes A. Postcoital testing after the use of a bio-adhesive acid buffering gel (ACIDFORM) and a 2% nonoxynol-9 product. *Contraception* 2004; 70:492-497.
8. Amaral E, Perdigão A, Souza MH, Mauck C, Waller D, Zaneveld L, Faúndes A. Vaginal safety after use of a bioadhesive, acid-buffering, microbicidal contraceptive gel (ACIDFORM) and a 2% nonoxynol-9 product. *Contraception* 2006; 73:542-547.
9. Clarke GN, McCoombe SG, Short RV. Sperm immobilizing properties of lemon juice. *Fertil Steril* 2006; 85:1529-1530.
10. Burgess SA, Walker ML, Sakakibara H, Knight PJ, Oiwa K. Dyein structure and power stroke. *Nature* 2003; 421:715-718.
11. Short RV. New ways of preventing HIV infection: thinking simply, simply thinking. *Philos Trans Roy Soc B* 2006; 361:811-820.
12. Reddy PR, Sharma A, Gupta S, Tiwary AK. Contact spermicides as contraceptives: Efficacy and current status. *Indian J Pharm Sci* 2002; 64:1-9.
13. Schill W, Wolff H. Ultrastructure of human spermatozoa in the presence of the spermicide nonoxynol-9 and a vaginal contraceptive containing nonoxynol-9. *Andrologia* 1981; 13:42-49.
14. Wilborn W, Hahn D, McGuire J. Scanning electron microscopy of human spermatozoa after incubation with spermicide nonoxynol-9. *Fertil Steril* 1983; 39:717-719.
15. Mauck CK, Baker JM, Barr SP, Johanson WM, Archer DF. A phase I comparative study of three contraceptive vaginal films containing nonoxynol-9. Post coital testing and colposcopy. *Contraception* 1997; 56:97-102.
16. Mauck CK, Baker JM, Barr SP, Abercrombie TJ, Archer DF. A phase I comparative study of contraceptive vaginal films containing benzalkonium chloride and nonoxynol-9. Post coital testing and colposcopy. *Contraception* 1997; 56:89-96.
17. Chantler E, Fisher H, Solanki S, Elstein M. Quantification of the *in vitro* activity of some compounds with spermicidal activity. *Contraception* 1992; 46:527-536.
18. Raymond EG, Chen PL, Luoto J. Contraceptive effectiveness and safety of five nonoxynol-9 spermicides: A randomized trial. *Obstet Gynecol* 2004; 103:430-439.
19. Wilkinson D, Tholandi M, Ramjee G, Rutherford GW. Nonoxynol-9 spermicide for prevention of vaginally acquired HIV and other sexually transmitted infections: systematic review and metaanalysis of randomized controlled trials including more than 5000 women. *Lancet Infect Dis* 2002; 2:613-617.
20. Oduka OA, Touitou E. The rationale behind the need to abolish the use of nonoxynol-9, a macrogol ether surfactant, in unprotected sex. *Acta Technologiae et Legis Medicamenti* 2002; 13:85-92.
21. Ahmad N, Ziets GA, Das S. Long lasting contraceptive suppository composition and methods of use. United States Patent No. 4999342, March 12, 1991.
22. Ladipo OA, De Castro MP, Filho LCCT, Coutinho E, Waller DP, Cone F, Zaneveld LJD. A new vaginal antimicrobial contraceptive formulation: Phase I clinical pilot studies. *Contraception* 2000; 62:91-97.
23. Méniez F, Castro A, Ortega A. Use effectiveness of a spermicidal suppository containing benzalkonium chloride. *Contraception* 1986; 34:353-362.
24. Zhang Y, Wu X, Wang Y, Ding X. Effect of benzalkonium bromide on the motility of human sperm. *Weisheng Dulixue Zazhi* 2002; 16:72-75.

25. Zhang Y, Xia VF, Wu X, Wang Y, Ding X. Spermicidal effect of benzalkonium bromide *in vitro* and its irritation effect on rat's vagina. *Shengzhi Yu Biyun* 2002; 22:114-116.
26. Chow PY, Holland MK, Suter DA, White IG. Evaluation of ten potential organic spermicides. *Int J Fertil* 1980; 25:281-286.
27. Dhar JD, Bajpai VK, Setty BS, Kamboj VP. Morphological changes in human spermatozoa as examined under scanning electron microscope after *in vitro* exposure to saponins isolated from *Sapindus mukorossi*. *Contraception* 1989; 39:563-568.
28. Pakrashi A, Ray H, Pal BC, Mahato SB. Sperm immobilizing effect of triterpene saponins from *Acacia auriculiformis*. *Contraception* 1991; 43:475-483.
29. Mahato SB, Pal BC, Nandy AK. Structure elucidation of two acylated triterpenoid bisglycosides from *Acacia auriculiformis* Cunn. *Tetrahedron* 1992; 48:6717-6728.
30. Kimata H, Nakashima T, Kokubun S, Nakayama K, Mitoma Y, Kitahara T, Yata N, Tanaka O. Saponins of pericarps of *Sapindus mukorossi* Gaertn and solubilization of monodesmosides by bisdesmosides. *Chem Pharm Bull* 1983; 31:1998-2005.
31. Setty BS, Kamboj VP, Garg HS, Khanna MN. Spermicidal potential of saponins isolated from Indian medicinal plants. *Contraception* 1976; 14:571-578.
32. Dwivedi AK, Chaudhry M, Sarin JPS. Standardization of a new spermicidal agent *Sapindus* saponin and its estimation in its formulation. *Indian J Pharm Sci* 1990; 52:165-167.
33. Rajasekaran M, Nair AGR, Hellstrom WJG, Sikka SC. Spermicidal activity of an antifungal saponin obtained from the tropical herb *Mollugo pentaphylla*. *Contraception* 1993; 47:401-412.
34. Setty BS, Kamboj VP, Garg HS, Khanna NM. Screening of Indian plants for biological activity. Part VII. Spermicidal activity of Indian plants. *Ind J Exp Biol* 1977; 15:231-232.
35. Kumar S, Biswas S, Mandal D, Roy HN, Chakraborty S, Kabir SN, Banerjee S, Mondal NB. *Chenopodium album* seed extract: a potent sperm-immobilizing agent both *in vitro* and *in vivo*. *Contraception* 2007; 75:71-78.
36. Souad K, Ali S, Mounir A, Mounir TM. Spermicidal activity of extract from *Cestrum parqui*. *Contraception* 2007; 75:152-156.
37. Louis SM, Pearson RM. A Comparison of the effects of nonoxynol-9 and chlorhexidine on sperm motility. *Contraception* 1985; 32:199-205.
38. Chijioke PC, Zaman S, Pearson RM. Comparison of the potency of D-propranolol, chlorhexidine and nonoxynol-9 in the Sander-Cramer test. *Contraception* 1986; 34:207-211.
39. Edelstein MC, Fulgham DL, Gretz JE, Alexander NJ, Bauer TJ, Archer DF. Studies on the *in vitro* spermicidal activity of synthetic magainins. *Fertil Steril* 1991; 55:647-649.
40. Reddy KVR, Shahani S, Meherji P. Spermicidal activity of magainins: *in vitro* and *in vivo* studies. *Contraception* 1996; 53:205-210.
41. Reddy KVR, Manjramkar DD. Evaluation of the antifertility effect of magainin-A in rabbits: *in vitro* and *in vivo* studies. *Fertil Steril* 2000; 73:353-358.
42. Aranha C, Manjramkar DD, Reddy KVR. Preclinical evaluation of magainin-A as a contraceptive antimicrobial agent. *Fertil Steril* 2004; 81:1357-1365.
43. Wojcik C, Sawicki W, Marianowski P, Benchaib M, Czyba JC, Guerin JF. Cyclodextrin enhances spermicidal effects of magainin-2-amide. *Contraception* 2000; 61:99-103.
44. Aranha C, Gupta S, Reddy KVR. Contraceptive efficacy of antimicrobial peptide Nisin: *in vitro* and *in vivo* studies. *Contraception* 2004; 69:333-338.
45. D'Cruz OJ, Uckun FM, Venkatachalam T. AZT derivatives exhibiting spermicidal and anti-viral activity. United States Patent No. 20020022600, February 21, 2002.
46. D'Cruz OJ, Uckun FM, Venkatachalam T. AZT derivatives exhibiting spermicidal and anti-viral activity. United States Patent No. 20020025922, February 28, 2002.
47. D'Cruz OJ, Zhu Z, Yiv SH, Chen CL, Waurzyniak B, Uckun FM. WHI-05, a Novel bromo-methoxy substituted phenyl phosphate derivative of zidovudine, is a dual-action spermicide with potent anti-HIV activity. *Contraception* 1999; 59:319-331.
48. D'Cruz OJ, Venkatachalam TK, Uckun FM. Structural requirements for potent human spermicidal activity of dual-function aryl phosphate derivative of bromo-methoxy zidovudine (compound WHI-07). *Biol Reprod* 2000; 62:37-44.
49. D'Cruz OJ, Waurzyniak B, Yiv SH, Uckun FM. Evaluation of subchronic (13 weeks) and reproductive toxicity potential of intravaginal gel-microemulsion formulation of a dual-function phenyl phosphate derivative of bromo-methoxy zidovudine (compound WHI-05) in B6C3F1 mice. *Contraception* 2000; 61:69-76.
50. D'Cruz OJ, Uckun FM. Preclinical studies on aryl phosphate derivatives of bromo-methoxy zidovudine (compounds WHI-05 and WHI-07): Novel contraceptives with anti-HIV activity. *Fertil Steril* 2000; 74:Supp 1, S72.
51. D'Cruz OJ, Uckun FM. Contraceptive activity of a spermicidal aryl phosphate derivative of bromo-methoxyzidovudine (compound WHI-07) in rabbits. *Fertil Steril* 2003; 79:864-872.
52. Thompson KA, Malamud D, Storey BT. Assessment of the anti-microbial agent C31G as a spermicide: Comparison with nonoxynol-9. *Contraception* 1996; 53:313-318.
53. Ballagh SA, Baker JM, Henry DM, Archer DF. Safety of single daily use for one week of C31G HEC gel in women. *Contraception* 2002; 66:369-375.
54. Mandal A, Bhattacharyya AK. Human seminal antiliquefying agents—A potential approach towards vaginal contraception. *Contraception* 1986; 33:31-38.
55. Hong CY, Chiang BN. Calicium ion is the key regulator of human sperm function. *Lancet* 1984; 2 (8417-8418):1449-1451.
56. Lee C, Anderson M, Chein Y. Characterization of *in vitro* spermicidal activity of chelating agent against human sperm. *J Pharm Sci* 1996; 85:649-654.
57. Patni A, Gupta S, Sharma A, Tiwary A, Garg S. Role of intracellular calcium in the spermicidal action of 2',4'-dichlorobenzamil, a novel contact spermicide. *J Pharm Pharmacol* 2001; 53:1387-1392.
58. White RD, Jane SC, Ratnasooriya WD, Aitken J. Complementary effects of propranolol and nonoxynol-9 upon human sperm motility. *Contraception* 1995; 52:241-247.

59. Gupta A, Gupta S, Tiwary AK. Spermicidal efficacy of H₂-receptor antagonists and potentiation with 2',4'-dichlorobenzamil hydrochloride: role of intrasperm Ca²⁺. *Contraception* 2003; 68:61-64.
60. Hong CY, Huang JJ, Chiang BN, Wei YH. The inhibitory effect of some ionophores on human sperm motility. *Contraception* 1986; 33:301-306.
61. Waller DP, Zanevald LJD, Fond HHS. *In vitro* spermicidal activity of gossypol. *Contraception* 1980; 22:183-187.
62. Kim IC, Waller DP, Marcelle GB, Cordell GA, Fong HH, Pirkle WH, Pilla L, Matlin SA. Comparative *in vitro* spermicidal effects of (+)-gossypol, (+)-gossypol, (-)-gossypol and gossypolone. *Contraception* 1984; 30:253-259.
63. Ueno H, Sahni MK, Segal SJ, Koide SS. Interaction of gossypol with sperm macromolecules and enzymes. *Contraception* 1988; 37:333-341.
64. Fahim MS, Wang M. Zinc acetate and lyophilized *Aloe barbadensis* as vaginal contraceptive. *Contraception* 1996; 53:231-236.
65. Riar SS, Devakumar C, Ilavazhagan G, *et al.* Volatile fraction of neem oil as a spermicide. *Contraception* 1990; 42:479-487.
66. Khillare B, Shrivastav TG. Spermicidal activity of *Azadirachta indica* (neem) leaf extract. *Contraception* 2003; 68:225-229.
67. Qian YX, Shen PJ, Xu RY, Liu GM, Yang HQ, Lu YS, Sun P, Zhang RW, Qi LM, Lu QH. Spermicidal effect *in vitro* by the active principle of garlic. *Contraception* 1986; 34:295-302.
68. Rithaporn T, Monga M, Rajasekaran M. Curcumin: a potential vaginal contraceptive. *Contraception* 2003; 68:219-223.
69. Paul D, Bera S, Jana D, Maiti R, Ghosh D. *In vitro* determination of the contraceptive spermicidal activity of a composite extract of *Achyranthes aspera* and *Stephania hernandifolia* on human semen. *Contraception* 2006; 73:284-288.
70. Lohiya NK, Kothari LK, Manivannan B, Mishra PK, Pathak N. Human sperm immobilization effect of Carica papaya seed extracts: an *in vitro* study. *Asian J Androl* 2000; 2:103-109.
71. Garg S, Taluja V, Upadhyay SN, Talwar GP. Studies on the contraceptive efficacy of Praneem polyherbal cream. *Contraception* 1993; 48:591-596.
72. Raghuvanshi P, Bagga R, Malhotra D, Gopalan S, Talwar GP. Spermicidal & contraceptive properties of Praneem polyherbal pessary. *Indian J Med Res* 2001; 113:135-141.
73. Talwar GP, Raghuvanshi P. Process for the preparation of an improved antimicrobial and spermicidal composition. Application 999/DEL/2003. Published 2005-05-27.
74. Bagga R, Raghuvanshi P, Gopalan S, Das SK, Baweja R, Suri S, Malhotra D, Khare S, Talwar GP. A polyherbal vaginal pessary with spermicidal and antimicrobial action: evaluation of its safety. *Trans R Soc Trop Med Hyg* 2006; 100:1164-1167.
75. Joshi SN, Katti U, Godbole S, Bharucha K, Kumar K, Kulkarni S, Risbud A, Mehendale S. Phase I safety study of Praneem polyherbal vaginal tablet use among HIV-uninfected women in Pune, India. *Trans R Soc Trop Med Hyg* 2005; 99:769-774.
76. Song BL, Li HY, Peng DR. *In vitro* spermicidal activity of parabens against human spermatozoa. *Contraception* 1989; 39:331-335.
77. D'Cruz O, Yiv S, Uckun F. GM-144, a novel lipophilic vaginal contraceptive gel-microemulsion. *AAPS Pharm Sci Tech* 2001; 2:1-10.
78. D'Cruz O, Yiv S, Waurzyniak B, Uckun F. Contraceptive efficacy and safety studies of a novel microemulsion-based lipophilic vaginal spermicide. *Fertil Steril* 2001; 75:115-124.
79. D'Cruz OJ, Uckun FM. Gel-microemulsions as vaginal spermicides and intravaginal drug delivery vehicles. *Contraception* 2001; 64:113-123.
80. Yiv S, Li M, D'Cruz OJ, Uckun FM. Gel-microemulsion formulations. United States Patent No. 20030083314, May 1, 2003.
81. D'Cruz OJ, Ghosh P, Uckun FM. Spermicidal activity of metallocene complexes containing vanadium (IV) in humans. *Biol Reprod* 1998; 58:1515-1526.
82. Ghosh P, Ghosh S, D'Cruz OJ, Uckun FM. Structural and biological characterization of a novel spermicidal vanadium (IV) complex: bis(pi-cyclopentadienyl)-N,N-diethyl dithiocarbamate vanadium (IV) tetrafluoroborate, [VCp₂(DeDtc)](BF₄). *J Inorg Biochem* 1998; 72:89-98.
83. D'Cruz OJ, Ghosh P, Uckun FM. Spermicidal activity of chelated complexes of bis(cyclopentadienyl)vanadium(IV). *Mol Hum Reprod* 1998; 4:683-693.
84. D'Cruz OJ, Vassilev A, Uckun FM. Studies in humans on the mechanism of potent spermicidal and apoptosis-inducing activities of vanadocene complexes. *Biol Reprod* 2000; 62:939-949.
85. D'Cruz OJ, Uckun FM. Vaginal contraceptive activity of a chelated vanadocene. *Contraception* 2005; 72:146-156.
86. D'Cruz O, Ghosh P, Uckun F. Vanadium (IV) metallocene complexes having spermicidal activity. United States Patent No. 20020099087, July 25, 2002.
87. D'Cruz O, Ghosh P, Uckun F. Vanadium (IV) metallocene complexes having spermicidal activity. United States Patent No. 20030018068, January 23, 2003.
88. D'Cruz O, Ghosh P, Uckun F. Vanadium (IV) metallocene complexes having spermicidal activity. United States Patent No. 20050192266, September 1, 2005.
89. D'Cruz OJ, Uckun FM. Intravaginal toxicity studies of a gel-microemulsion formulation of spermicidal vanadocenes in rabbits. *Toxicol Appl Pharmacol* 2001; 170:104-112.
90. D'Cruz OJ, Waurzyniak B, Uckun FM. Subchronic (13-week) toxicity studies of intravaginal administration of spermicidal vanadocene dithiocarbamate in mice. *Contraception* 2001; 64:177-185.
91. D'Cruz OJ, Uckun FM. Lack of subchronic and reproductive toxicity of intravaginal gel formulations of spermicidal vanadocenes in a 13-week study in B6C3F1 and CD-1 mice. *Fertil Steril* 2001; 76:Suppl 1, S17.
92. D'Cruz OJ, Waurzyniak B, Uckun FM. Subchronic (13-week) toxicity studies of intravaginal administration of spermicidal vanadocene acetylacetonato monotriflate in mice. *Toxicology* 2002; 170:31-43.

(Received April 8, 2008; Revised July 8, 2008; Accepted July 14, 2008)

Brief Report

Novel *N*-hydroxybenzamide histone deacetylase inhibitors as potential anti-cancer agents

Jie Jiao, Hao Fang, Wenfang Xu*

Department of Medicinal Chemistry, School of Pharmaceutical Sciences, Shandong University, Ji'nan, China.

ABSTRACT: Histone deacetylases (HDACs) are a class of Zn^{2+} dependent metalloproteases that play an important role in tumorigenesis. Inhibition of HDACs may be a potential strategy for cancer therapy. This study designed and synthesized a series of novel *N*-hydroxybenzamide histone deacetylase inhibitors based on the structural features of suberoylanilide hydroxamic acid (SAHA), the first HDAC inhibitor that came to market. Preliminary biological evaluation *in vitro* found that most of the inhibitors had satisfactory inhibitory activity (IC_{50} = 1-17 μ M) against HDACs and HCT116 tumor cells.

Keywords: HDACs, Inhibitors, *N*-hydroxybenzamide, Antitumor

1. Introduction

Cancer is the most dreaded killer of humans and takes a number of lives every year. In recent years, a class of metalloproteases known as histone deacetylases (HDACs) has been considered as an epigenetic target for cancer therapy. These enzymes play an important role in gene transcription, the cell cycle, differentiation, and tumorigenesis. Inhibitors of these key enzymes are inducers of growth arrest and apoptosis of many tumor cells, so HDAC inhibitors are considered to be a new generation of anti-cancer agents (1).

HDACs are involved in modification and remodeling of chromosomal histones by removing acetyl groups from ϵ - NH_2 of lysine residues in histones through Zn^{2+} -dependent hydrolysis (Figure 1). Deacetylation results in the positive charge density on the *N*-termini of nucleosomal histones increasing, which strengthens the interaction with the negatively charged DNA

chain and blocks the access of transcription factors. In tumor cells, HDACs are over-expressed, resulting in deacetylated histones being tightly packed with DNA to form an abnormal "compact structure" of chromatin. In this process, expression of the onco-suppressors p21^{WAF1} and p27^{KIP1} is inhibited and activity of the onco-suppressor p53 is down-regulated, but tumor activators HIF-1 and VEGF are up-regulated. Therefore, the inhibition of HDAC activity is considered a potential strategy for cancer therapy (2-4).

Suberoylanilide hydroxamic acid (SAHA), a linear chain hydroxamic acid and the first HDAC inhibitor, was approved by the US FDA in 2006 (5). As reported in the literature, there are two rules to the structure-activity relationship (SAR) of SAHA derivatives: 1) introduction of hydrophobic groups to the para-position of the benzene ring results in a higher level of activity, and 2) the optimal chain length between the benzene ring and zinc-binding group (ZBG) is 7-8 atoms (Figure 2) (6-8). *N*-hydroxy-4-(3-phenylpropanamido)benzamide (HPPB) (9) and its cinnamamide analogue provide the molecular formwork for the design of novel *N*-hydroxybenzamide HDAC inhibitors. This design strategy has been shown in Figure 2; ferulic acid, a natural cinnamic acid, was used as the starting material to prepare the HPPB derivatives and their cinnamamide analogues.

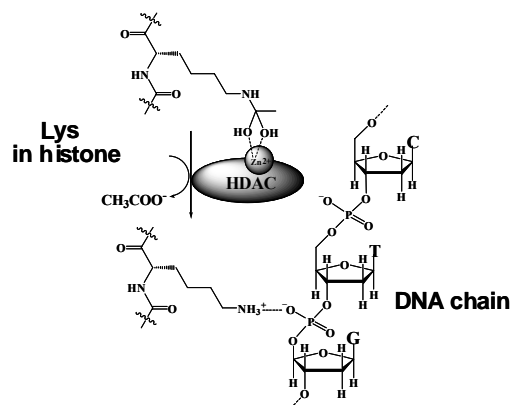


Figure 1. HDACs function of modification of histones.

*Correspondence to: Dr. Wenfang Xu, The Department of Medicinal Chemistry, School of Pharmacy, Shandong University, 44 West Wenhua Road, Ji'nan 250012, Shandong, R.P. China; e-mail: xuwenf@sdu.edu.cn

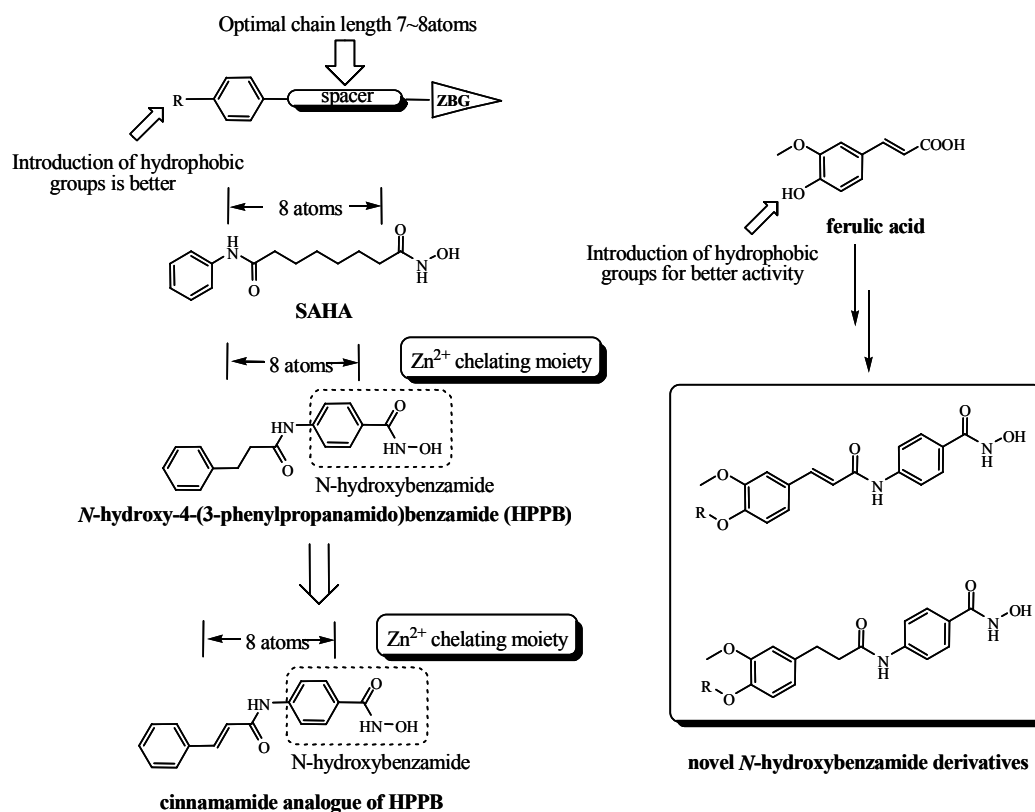


Figure 2. Design of novel *N*-hydroxybenzamide derivatives.

2. Materials and Methods

All material and reagents used in this work are analytical reagents. All reactions were monitored by thin-layer chromatography on 0.25 mm silica gel plates (60GF-254) and visualized with UV light. 1H NMR spectra were determined on a Bruker Avance 300 spectrometer using TMS as an internal standard. ESI-MS were determined on an API 4000 spectrometer. Melting points were determined on an electrothermal melting point apparatus and are uncorrected. The route of synthesis has been shown in Scheme 1.

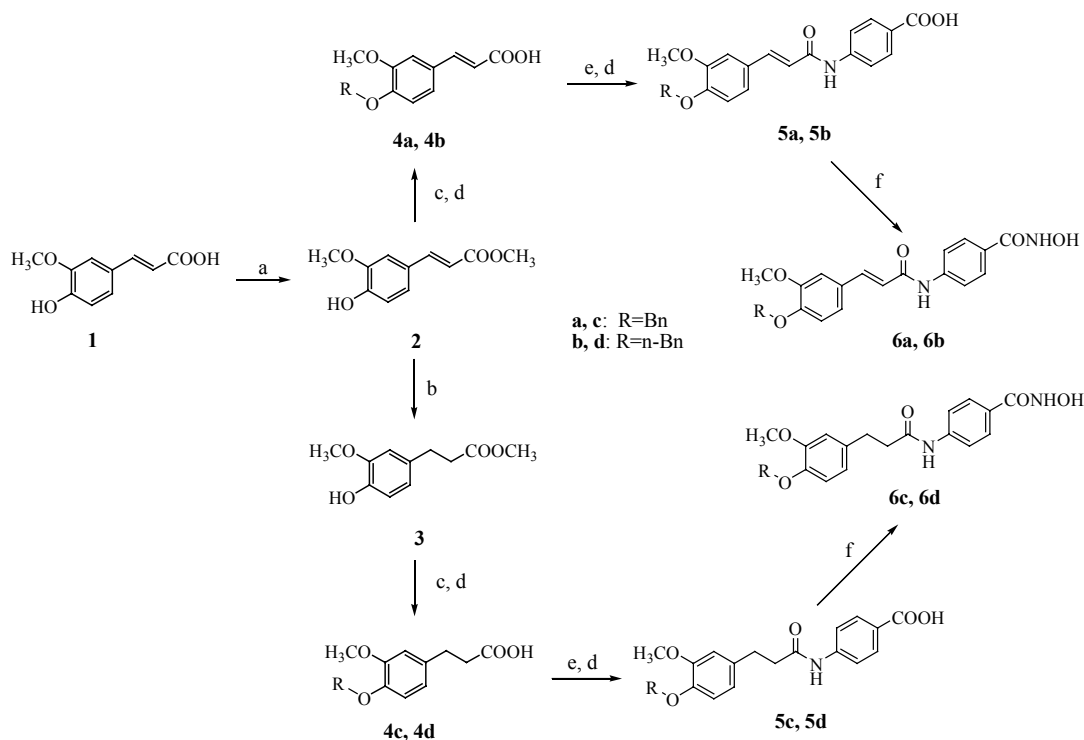
Esterification of ferulic acid **1** with *p*-methyl phenylsulfonic acid (PTS) in methanol yielded methyl ferulic acid **2**, which was reacted with BnBr in DMF by Williamson etherification and then hydrolyzed to provide compound **4a**. Compound **4a** was reacted with $SOCl_2$ to produce acylation of methyl 4-aminobenzoate, and then hydrolysis was performed to yield compound **5a**. Compound **5a** was reacted with $ClCOOBu-i$ to provide a mixed anhydride and then reacted with NH_2OH to yield compound **6a**. Compound **6b** was prepared from compound **2** in the same way as compound **6a** using the *n*-bu substituted 4'-OH of compound **2**. In addition, hydrogenation of compound **2** yielded **3**, which provided compound **6c** and **6d** in the same way as compounds **6a** and **6b**.

3. Results and Discussion

In vitro bioactivity evaluation of compounds **6a-6d** was performed by HDAC activity assays using a HDAC colorimetric activity assay kit (AK501, Biomol Research Laboratories) and MTT assays of human colonic cancer cells (HCT116) because HDACs are highly expressed in this cell type.

3.1. Procedures for HDAC activity assay

The source of HDACs was HeLa nuclear extracts including HDAC1 and HDAC2 (the major contributors to HDAC activity in HeLa nuclear extracts), and the substrate was a type of [3H]acetylated histone peptide. HDAC1 and HDAC2 are known to both be nucleus proteins in charge of the deacetylation of histones (10). Assays we performed according to kit instructions. The compound samples and the control drug were diluted to various concentrations: 20 $\mu g/mL$, 4 $\mu g/mL$, 0.8 $\mu g/mL$, and 0.16 $\mu g/mL$. On the 96-well plate, HDACs (5 $\mu L/well$) were incubated at 37°C with 10 μL of various concentrations of samples and 25 μL of substrate. After reacting for 30 min, Color de Lys Developer (50 $\mu L/well$) was added. Then, after 15 min the ultraviolet absorption of the wells was measured on a microtiter-plate reader at 405 nm. The % inhibition was calculated from the ultraviolet



Scheme 1. Synthetic scheme, reagents and conditions: (a) PTS, CH₃OH, 80°C; (b) H₂, 10% Pd-C, CH₃OH; (c) RBr, KOH, DMF, r.t.; (d) 2 mol/L NaOH, EtOH, 75°C; (e) SOCl₂, THF, methyl 4-aminobenzoate; (f) ClCOOBu-*t*, Et₃N, NH₂OH·HCl, THF, 0°C.

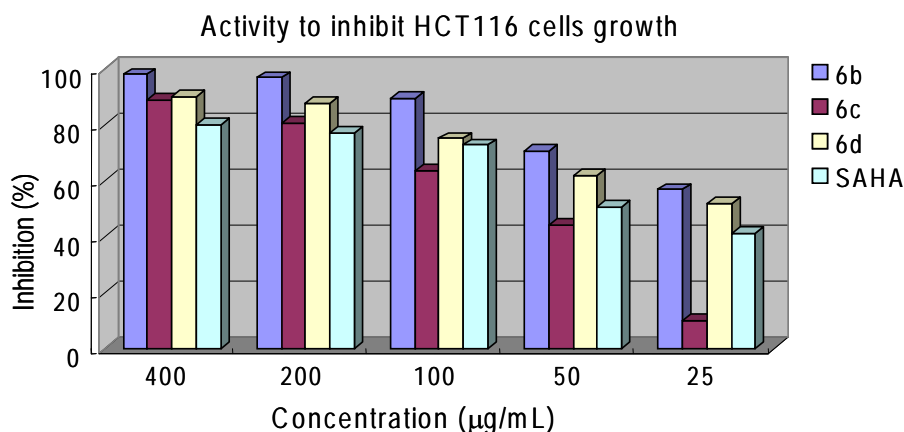


Figure 3. Activity to inhibit HCT116 cells growth of compounds **6b-6d** compared to SAHA.

absorption readings of inhibited wells relative to those of control wells. Finally, the IC₅₀ values were determined using a regression analysis of the concentration/inhibition data.

3.2. Procedures for the MTT assay

The cells, being maintained in McCoy's 5a medium with 10% fetal bovine serum, were plated in 96-well plates (50 µL/well) at the density of 2.0×10^5 /mL. After 4 h, compounds of various concentrations (400 µg/mL, 200 µg/mL, 100 µg/mL, 50 µg/mL, and 25 µg/mL) were dosed, and the cells were cultured for 2 days. Then 0.5% MTT (10 µL/well) were added to each well. After an additional 4 h of incubation, OD₅₇₀ and OD₆₃₀ were measured as a reference, and the

IC₅₀ values were calculated according to a regression analysis of the concentration/inhibition data.

3.3. Inhibitory activity of compounds **6a-6d**

Results indicating the activity of compounds **6a-6d** are shown in Table 1. These compounds all had satisfactory

Table 1. Inhibitory activities of compounds **6a-6d** against HDACs and tumor cells

Compounds	HDACs IC ₅₀ (µM)	HCT 116 IC ₅₀ (µM)
6a	12.7	>1000
6b	16.4	175.6
6c	1.8	208.8
6d	4.0	193.6
SAHA	1.3	245.6

activity ($IC_{50} = 1-17 \mu\text{M}$) at inhibiting HDACs. In general, **HPPB** derivatives **6c** and **6d** were more potent than their cinnamamide analogues **6a** and **6b**. With the exception of **6a**, compounds exhibited a higher level of activity at inhibiting HCT116 cell growth than SAHA (Figure 3). Compound **6b** ($IC_{50} = 16.4 \mu\text{M}$) showed less potency than other compounds, but among these compounds it exhibited the highest level of activity at inhibiting HCT116 cell growth. The **HPPB** derivatives **6c** and **6d** both showed exciting bioactivity *in vitro* and could be used as leading compounds to guide further study on **HPPB** derivatives in the future.

4. Conclusion

A series of novel *N*-hydroxybenzamide HDAC inhibitors was designed and synthesized based on the structural features of SAHA. Preliminary biological evaluation *in vitro* found that most of these inhibitors showed satisfactory activity at inhibiting HDACs and HCT116 cell growth. These compounds could be used as leading compounds in the future.

Acknowledgments

The authors wish to thank Xuejian Wang for his work on the MTT assays of these compounds. This work was supported by the National "863" Foundation of China (Grant No. 2007AA02Z314).

References

1. Saverio M, Pier GP. Histone deacetylase inhibitors and the promise of epigenetic (and more) treatments for cancer. *Nature* 2006; 6:38-51.
2. Dong HK, Minjung K, Ho JK. Histone deacetylase in carcinogenesis and its inhibitors as anti-cancer agents. *J Biochem Mol Biol* 2003; 36:110-119.
3. Marks PA, Rifkind RA, Richon VM, Breslow R, Miller T, Kelly WK. Histone deacetylases and cancer: causes and therapies. *Nat Rev Cancer* 2001; 1:194-202.
4. Meinke PT, Liberator P. Histone deacetylase: a target for antiproliferative and antiprotozoal agents. *Curr Med Chem* 2001; 8:211-235.
5. Marielle P, Marina P, Monica B, Daniela F. Histone deacetylase inhibitors: from bench to clinic. *J Med Chem* 2008; 51:1505-1529.
6. Manfred J, Gerald B, Doris K, Hans S, Clarissa G, Peter L. Amide analogues of Trichostatin A as inhibitors of histone deacetylase and inducers of terminal cell differentiation. *J Med Chem* 1999; 42:4669-4679.
7. Stacy WR, Lidia CS, Peter A, Kenneth WB, Wendy DC, Michael AG, Koborn LH, Manfred J, Paul K, Nancy T, Heather W. Inhibitors of human histone deacetylase: synthesis and enzyme and cellular activity of straight chain hydroxamates. *J Med Chem* 2002; 45:753-757.
8. Soon HW, Sylvie F, Elie AK, Giliane B, Arkadii V, Naomy B, Oscar M, Silvana L, Martin AI, Marielle F, Zuomei L, Jeffrey M, Besterman, Daniel D. Structurally simple Trichostatin A-like straight chain hydroxamates

as potent histone deacetylase inhibitors. *J Med Chem* 2002; 45:2877-2885.

9. Qiang L, Da SW, Chang SC, Yuan DH, Ching SC. Structure-based optimization of phenylbutyrate-derived histone deacetylase inhibitors. *J Med Chem* 2005; 48:5530-5535.
10. Annemieke J M, Albert H, Huib NC, Stephan K. Histone deacetylases (HDACs): characterization of the classical HDAC family. *Biochem Soc* 2003; 370:737-749.

(Received July 23, 2008; Revised August 1, 2008; Accepted August 11, 2008)

Supplementary data

Synthesis of compound **6c**, general procedures, analytical data of the compounds **6a-6d**.

(*E*)-Methyl 3-(4-hydroxy-3-methoxyphenyl)acrylate (**2**)

Ferulic acid (30.0 g, 0.15 mol) was dissolved in dry MeOH (300 mL), then PTS (5.0 g, 0.03 mol) was added. The solution was heated to 80°C to be in reflux for 6 h, and then it was concentrated under vacuum. The residue was added by water (100 mL) and then extracted by EtOAc (100 mL) for 3 times. The organic layer was merged and washed by water and then dried with MgSO_4 . The solution was evaporated to give a yellow crystal product (31.0 g, yield: 96.3%). mp 53-55°C, ESI-MS *m/z*: 209.4 ($\text{M}+\text{H}$)⁺.

Methyl 3-(4-hydroxy-3-methoxyphenyl)propanoate (**3**)

Compound **2** (25.0 g, 0.12 mol) was dissolved in MeOH (240 mL), then 10% Pd-C (0.5 g) was added. The solution was stirred at room temperature and filled with H_2 in one atm and for 12 h. The reaction mixture was filtered off Pd-C, and the filtrate was evaporated to get a diaphanous oil product (25.0 g, yield: 99.0%). ESI-MS *m/z*: 211.3 ($\text{M}+\text{H}$)⁺, 228.4 ($\text{M}+\text{NH}_4$)⁺, 233.3 ($\text{M}+\text{Na}$)⁺.

3-(4-Butoxy-3-methoxyphenyl)propanoic acid (**4c**)

Compound **3** (2.1 g, 0.01 mol) was dissolved in dry DMF (20 mL), then KOH powder (0.62 g, 0.012 mol) was added. The solution was stirred for 1h at room temperature, then *n*-BuBr (1.7 g, 0.01 mol) was dropped into reaction mixture. After stirred for another 5 h, the reaction mixture was diluted by 100 mL water. Then the solution was extracted by ether (50 mL) for 3 times. The organic layer was merged and washed by water and then dried with MgSO_4 . The solution was evaporated to give a yellow solid product which was dissolved in EtOH (50 mL), then 2 mol/L NaOH (10 mL) was added. The solution was stirred at 75°C for 3 h, and then concentrated under vacuum. The residue was added by 1 mol/L HCl (50 mL), then the solution was

filtered to get the sediment which was washed by water for several times. Recrystallisation of the sediment with acetone to get white crystal product 1.3 g. Yield: 45.5%, mp 90-91°C, ESI m/z (M+H)⁺ 287.4, (M+NH₄)⁺ 304.5, (M+Na)⁺ 309.6, (M+K)⁺ 325.5. ¹H NMR (DMSO-*d*₆, δ ppm, *J* Hz): 12.10 (s, 1H), 7.44-7.29 (m, 5H), 6.92-6.68 (m, 3H), 5.02 (s, 2H), 3.75 (s, 3H), 2.75 (t, 2H, 7.5 Hz), 2.50 (t, 2H, 7.5 Hz).

4-(3-(4-(Benzyloxy)-3-methoxyphenyl)propanamido)benzoic acid (5c)

Compound **4c** (1.0 g, 3.5 mmol) was dissolved in dry THF (50 mL), the solution was stirred under 0°C and then SOCl₂ (1.2 g, 10 mmol) was dropped into the solution. After 5 h, the reaction mixture was evaporated to get an oil product of acyl chloride which was dissolved in new dry THF (20 mL). The methyl 4-aminobenzoate (0.53 g, 3.5 mmol) was dissolved in dry THF (20 mL), the Et₃N (0.7 g, 7 mmol) was added into the solution, then the acyl chloride solution was dropped into solution. The reaction mixture was stirred at room temperature for 1 h evaporated under vacuum. The residue was added by water (100 mL) and extracted by EtOAc (50 mL) for 3 times. The organic layer was merged and washed by water and then dried with MgSO₄. The solution was evaporated to give a yellow crude product which was dissolved in EtOH (25 mL), and then 2 mol/L NaOH (5 mL) was added. The reaction mixture was stirred at 75°C for 5 h and then evaporated under vacuum. The residue was added by 1 mol/L HCl (30 mL) and then filtered. The sediment was washed by water for several times and recrystallized with acetone to get white crystal product (1.1 g, yield: 78.6%). Mp: 165-168°C, ESI-MS m/z: 406.4 (M+H)⁺.

4-(3-(4-(Benzyloxy)-3-methoxyphenyl)propanamido)-N-hydroxybenzamide (6c)

Compound **5c** (1.0 g, 2.5 mmol) was dissolved in dry THF (30 mL), then Et₃N (0.50 g, 5 mmol) was added. The solution was cooled to 0°C and then ClCOOBu-*i* (0.34 g, 2.5 mmol) was dropped into the solution. The reaction mixture was stirred under 0°C for 5 min and then NH₂OH/MeOH (2.5 mL, 2 mmol/mL) was dropped into the reaction mixture. After stirred for 5 h, the reaction mixture was filtered and the filtrate

was evaporated under vacuum. The residue was added by 1 mol/L HCl (30 mL) and extracted by EtOAc (20 mL) for 3 times. The organic layer was merged and washed by water and then dried with MgSO₄. The solution was evaporated to give a crude product which was recrystallized with acetone to get a white crystal product 0.3 g, (yield: 28.6%). Mp: 193-195°C, ESI-MS m/z: 421.4 (M+H)⁺, IR (KBr, σ cm⁻¹): 3266, 1674, 1513, and 1256, ¹H NMR (DMSO-*d*₆, δ ppm, *J* Hz): 10.09 (s, 1H), 10.12 (s, 1H), 8.94 (s, 1H), 7.71-7.62 (m, 4H), 7.44-7.29 (m, 5H), 6.92 (d, 1H, *J* = 8.1 Hz), 6.88 (s, 1H, *J* = 8.1 Hz), 6.73 (d, 1H, *J* = 8.1 Hz), 5.02 (s, 2H), 3.73 (s, 3H), 2.85 (t, 2H, *J* = 7.5 Hz), 2.62 (t, 2H, *J* = 7.5 Hz).

4-(3-(4-Butoxy-3-methoxyphenyl)propanamido)-N-hydroxybenzamide (6d)

Mp: 163-165°C, ESI-MS m/z: 387.4 (M+H)⁺, IR (KBr, σ cm⁻¹): 3302, 1668, 1514, and 1255, ¹H NMR (DMSO-*d*₆, δ ppm, *J* Hz): 11.10 (s, 1H), 10.13 (s, 1H), 8.95 (s, 1H), 7.71-7.62 (m, 4H), 6.85-6.82 (m, 2H), 6.72 (d, 1H, *J* = 8.1 Hz), 3.88 (t, 2H, *J* = 6.6 Hz), 3.71 (s, 3H), 2.84 (t, 2H, *J* = 7.5 Hz), 2.62 (t, 2H, *J* = 7.5 Hz), 1.70-1.61 (m, 2H), 1.47-1.35 (m, 2H), 0.91 (t, 3H, *J* = 7.5 Hz).

(E)-4-(3-(4-(Benzyloxy)-3-methoxyphenyl)acrylamido)-N-hydroxybenzamide (6a)

Mp: 214-215°C, ESI-MS m/z: 419.4 (M+H)⁺, IR (KBr, σ cm⁻¹): 3247, 1597, 1512, and 1258, ¹H NMR (DMSO-*d*₆, δ ppm, *J* Hz): 11.10 (s, 1H), 10.34 (s, 1H), 8.94 (s, 1H), 7.74 (s, 4H), 7.56 (d, 1H, *J* = 15.6 Hz), 7.47-7.34 (m, 5H), 7.26-7.09 (m, 3H), 6.72 (d, 1H, *J* = 15.6 Hz), 5.15 (s, 2H), 3.84 (s, 3H).

(E)-4-(3-(4-Butoxy-3-methoxyphenyl)acrylamido)-N-hydroxybenzamide (6b)

Mp: 230-233°C, ESI-MS m/z: 385.5 (M+H)⁺, IR (KBr, σ cm⁻¹): 3181, 1648, 1596, 1511, and 1263, ¹H NMR (DMSO-*d*₆, δ ppm, *J* Hz): 11.10 (s, 1H), 10.33 (s, 1H), 8.94 (s, 1H), 7.74 (s, 1H), 7.55 (d, 2H, *J* = 15.6 Hz), 7.22-7.00 (m, 3H), 6.71 (d, 1H, *J* = 15.6 Hz), 4.01 (t, 2H, *J* = 6.6 Hz), 3.83 (s, 3H), 1.76-1.68 (m, 2H), 1.44 (q, 2H, *J* = 7.2 Hz), 0.94 (t, 3H, *J* = 7.2 Hz).

Brief Report

Synthesis and antifungal activity of 3-substituted thiochromanones

Yang Liu, Wei Luo, Li Sun, Chun Guo*

School of Pharmaceutical Engineering, Shenyang Pharmaceutical University, Shenyang, China.

ABSTRACT: A series of 3-substituted thiochromanones has been prepared. Their structures were confirmed by $^1\text{H-NMR}$ and HRMS. All of the synthesized compounds were screened for antifungal activity against ten fungi species *in vitro*. The compounds 2f and 2g were more efficient than the control drug, ketoconazole.

Keywords: Thiochromanone, Synthesis, Antifungal activity

1. Introduction

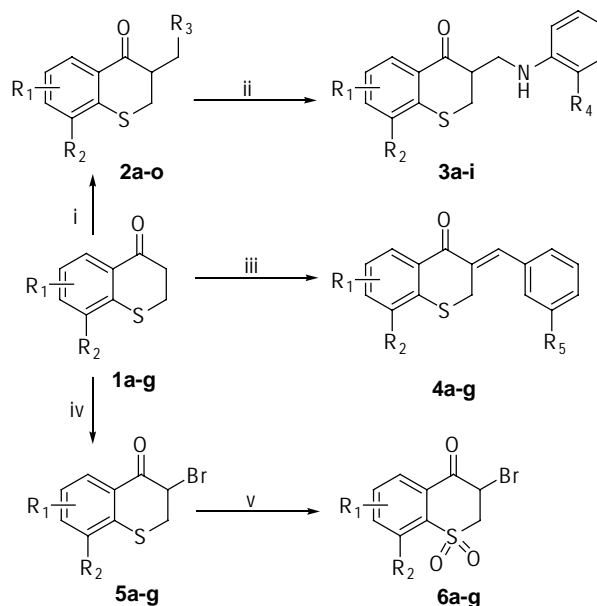
In recent years, the incidence of fungal infections has reached alarming proportions. This is largely due to a number of factors such as intensive uses of chemotherapy for bacterial infections and cancers. At the same time, the number of systemic fungal infections has markedly increased; this has been true for large populations of immunocompromised patients as well as those suffering from various hematological malignancies, those with acquired immune deficiency syndrome (AIDS), and those undergoing organ transplantations (1,2). An initial study on agricultural antibiotics by the current authors revealed an active ingredient with antifungal activity *in vitro*; this was identified as a compound including a scaffold of thiochromanone. Similarly, Nakazumi H *et al.* also reported that thiochromanone derivatives have broad biological activities (3,4). Encouraged by these results, the current authors designed and synthesized a series of 3-substituted thiochromanone derivatives. The preliminary structure-activity relationship has been established based on the results of an *in vitro* antifungal assay. Optimization of the lead scaffold allowed the preparation of several compounds with good antifungal activity *in vitro*.

2. Materials and Methods

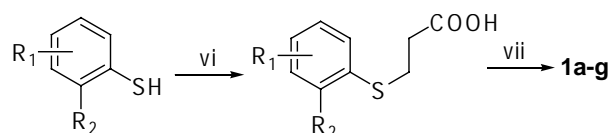
2.1. Synthesis of 3-substituted thiochromanones

The 3-substituted thiochromanones (2, 3, 4, 5 and 6, Table 1) in this paper were prepared from compound 1 as shown in Scheme 1. The starting material compounds 1a-g were obtained by a direct method as outlined in Scheme 2 (5,6). Commercially available substituted thiophenols were condensed with β -chloro-propionic acid under basic conditions in ethanol, followed by cyclization in H_2SO_4 to give compounds 1a-g.

The Mannich base derivatives of secondary saturated amines, compounds 2a-o, were prepared by refluxing the mixtures of 1a-g, paraformaldehyde, and



Scheme 1. (i) Amines/HCHO/HCl, reflux; (ii) Aromatic amines/EtOH, rt; (iii) Arylaldehydes/ H_2SO_4 /EtOH, reflux, 3 h; (iv) Br_2 /HOAc, rt, 3 h; (v) H_2O_2 /HOAc, rt, 48 h.



Scheme 2. (vi) K_2CO_3 /EtOH, reflux, 4 h; (vii) H_2SO_4 , rt, 36 h.

*Correspondence to: Dr. Chun Guo, Shenyang Pharmaceutical University, Shenyang 110016, China; e-mail: chunguo63@yahoo.com.cn

Table 1. Structures and antifungal activities of 3-substituted thiochromanones

Compounds	R ₁	R ₂	R ₃	R ₄	R ₅	Yield (%)	MIC (μM) ^a							
							<i>C.a</i>	<i>C.n</i>	<i>S.s</i>	<i>E.f</i>	<i>T.r</i>	<i>M.g</i>		
1a	5-F	H				50								
1b	5-Cl	H				43								
1c	5-Br	H				47								
1d	6-CF ₃	H				59								
1e	5-CH ₃	H				61								
1f	5-F	6-Cl				64								
1g	6-Cl	8-Cl				56								
2a	5-F	H	N(CH ₃) ₂			57	10	5	2.5	1.25	1.25	1.25	1.25	1.25
2b	5-Cl	H	N(CH ₃) ₂			56	10	10	1.25	0.61	0.61	0.61	0.61	1.25
2c	5-Br	H	N(CH ₃) ₂			78	1.25	5	2.5	0.62	0.08	0.61	0.61	0.61
2d	6-CF ₃	H	N(CH ₃) ₂			67	5	0.61	0.61	0.08	1.25	1.25	1.25	1.25
2e	5-CH ₃	H	N(CH ₃) ₂			49	10	5	1.25	1.25	5	0.61	0.61	0.61
2f	5-F	6-Cl	N(CH ₃) ₂			67	1.25	0.31	1.25	0.08	0.08	0.61	0.61	0.61
2g	6-Cl	8-Cl	N(CH ₃) ₂			80	1.25	0.61	1.25	0.08	0.31	0.08	0.08	0.08
2h	5-F	6-Cl	N(C ₂ H ₅) ₂			69	5	10	10	1.25	0.61	1.25	1.25	1.25
2i	6-Cl	8-Cl	N(C ₂ H ₅) ₂			67	10	5	2.5	1.25	0.08	1.25	1.25	1.25
2j	5-F	H	Piperidine			65	2.5	2.5	2.5	1.25	0.61	0.61	0.61	0.61
2k	5-F	6-Cl	Piperidine			67	5	2.5	5	1.25	0.08	0.31	0.31	0.31
2l	6-Cl	8-Cl	Piperidine			71	1.25	1.25	2.5	0.61	0.61	0.31	0.31	0.31
2m	5-F	H	Morpholine			62	5	2.5	10	1.25	0.31	1.25	1.25	1.25
2n	5-F	6-Cl	Morpholine			78	2.5	1.25	1.25	0.61	1.25	1.25	1.25	1.25
2o	6-Cl	8-Cl	Morpholine			56	2.5	10	10	1.25	1.25	0.31	0.31	0.31
3a	5-F	H		H		69	10	10	2.5	5	1.25	1.25	1.25	1.25
3b	5-F	H		4-SO ₂ NH ₂		75	5	10	10	5	2.5	0.61	0.61	0.61
3c	5-F	H		4-F		75	10	10	10	1.25	1.25	1.25	1.25	1.25
3d	5-F	H		4-Cl		71	2.5	5	1.25	10	1.25	0.31	0.31	0.31
3e	5-F	H		4-Br		79	2.5	5	1.25	2.5	0.61	2.5	2.5	2.5
3f	5-F	H		4-NO ₂		78	5	1.25	5	2.5	1.25	5	5	5
3g	5-F	H		2-NO ₂		75	10	10	5	1.25	0.61	0.61	0.61	0.61
3h	5-F	H		4-CH ₃		80	10	10	5	5	1.25	1.25	1.25	1.25
3i	5-F	H		4-C ₂ H ₅		69	10	10	10	1.25	2.5	0.61	0.61	0.61
4a	5-F	H			H	83	5	10	10	1.25	5	5	5	5
4b	5-F	H			2-Cl	81	10	10	10	5	0.61	1.25	1.25	1.25
4c	6-CF ₃	H			2-Cl	78	10	10	10	2.5	2.5	1.25	1.25	1.25
4d	6-Cl	8-Cl			H	76	5	5	1.25	10	2.5	0.61	0.61	0.61
4e	6-Cl	8-Cl			2-Cl	65	2.5	10	10	5	1.25	10	10	10
4f	6-Cl	8-Cl			2-NO ₂	76	2.5	10	10	1.25	5	5	5	5
4g	6-Cl	8-Cl			4-OCH ₃	87	5	10	5	0.61	5	1.25	1.25	1.25
5a	5-F	H				86	1.25	10	5	5	1.25	0.08	0.08	0.08
5b	5-Cl	H				81	5	2.5	10	1.25	1.25	5	5	5
5c	5-Br	H				85	5	2.5	1.25	5	1.25	1.25	0.61	0.61
5d	6-CF ₃	H				78	10	5	5	1.25	1.25	5	5	5
5e	5-CH ₃	H				67	5	10	2.5	10	1.25	0.61	0.61	0.61
5f	5-F	6-Cl				69	2.5	10	10	10	10	5	5	5
5g	6-Cl	8-Cl				68	2.5	10	10	1.25	2.5	1.25	1.25	1.25
6a	5-F	H				80	2.5	10	10	5	5	0.08	0.08	0.08
6b	5-Cl	H				68	5	5	5	1.25	2.5	5	5	5
6c	5-Br	H				79	10	2.5	1.25	2.5	1.25	1.25	1.25	1.25
6d	6-CF ₃	H				75	5	2.5	5	0.61	0.61	0.61	0.61	0.61
6e	5-CH ₃	H				85	2.5	10	5	5	1.25	2.5	2.5	2.5
6f	5-F	6-Cl				87	5	10	10	2.5	2.5	2.5	2.5	2.5
6g	6-Cl	8-Cl				79	2.5	1.25	10	1.25	1.25	1.25	1.25	1.25
Ketoconazole							2.5	1.25	1.25	0.08	0.61	0.61	0.61	0.61

^a *C.a*, *C. albicans*; *C.n*, *C. newformans*; *S.s*, *S. schenckii*; *E.f*, *E. floccosum*; *T.r*, *T. rubrum*; *M.g*, *M. gypsum*.

appropriate amines in dry benzene. Primary aromatic amines do not usually give corresponding Mannich bases with the above procedure. However, stirring **2a** with primary aromatic amines in ethanol at room temperature was found to give the corresponding Mannich bases in good yield. The 3-benzylmethylene thiochromanones **4a-g** were obtained from an Aldol-condensation reaction of **1a-g** and appropriate arylaldehydes under catalysis of H₂SO₄. Compounds **1a-g** were treated with an equivalent Br₂ in acetic acid to give 3-bromo thiochromanones, compounds **5a-g**, followed by oxidation with H₂O₂ in acetic acid at room temperature to yield **6a-g**. The structures of

all synthesized compounds have been confirmed by elemental analysis, IR, H¹-NMR, and HRMS (*See Supplemental data*).

2.2. Evaluation of antifungal activity

The prepared 3-substituted thiochromanones were evaluated for their *in vitro* antifungal activity against six isolates of fungi in Sabouraud medium according to consecutive double dilution to give their minimum inhibitory concentrations (MIC). Ketoconazole was used as a control drug. In brief, the assay was conducted as follows: the synthesized compounds and

ketoconazole were accurately weighted and dissolved in 0.5 mL of DMSO and diluted with sterile distilled water to 25 mL. The solution was then added to the cells to bring the concentration of tested compound within a range of 0.08 to 10 μ M. The cells were incubated at 28°C for 24 h for *C. albicans*, for 48 h for *C. neoformans*, and for 7 days for other fungi. After incubation, MIC values were determined.

3. Results and Discussion

Table 1 summarizes the structures and antifungal activity of 3-substituted thiochromanones synthesized in the present study. All compounds tested had a certain level of antifungal activity against the fungi tested. On the whole, all compounds demonstrated potent activity against *T. rubrum* and *M. gypsum*. The series of Mannich base derivatives displayed better activity against all fungi tested. Antifungal activity of the most potent compounds, **2f** and **2g**, was more effective than that of the control drug, ketoconazole, against *C. albicans*, *C. neoformans*, and *T. rubrum*. This activity was comparable to that of ketoconazole against *S. schenckii*, *E. floccosum*, and *M. gypsum*. The aromatic Mannich base derivatives, compounds **3a-i**, displayed potent activity against *E. floccosum* and *T. rubrum* but weaker activity against *C. albicans*, *C. neoformans*, and *S. schenckii*. The 3-benzylmethylene derivatives, compounds **4a-g**, demonstrated similar activity; however, compound **4b** was as effective as ketoconazole against *T. rubrum*, **4d** was similarly as effective against *S. schenckii* and *M. gypsum*, and **4e** and **4f** were similarly as effective against *C. albicans*. Among the 3-bromo thiochromanones, **5a** displayed excellent activity against *C. albicans* and *M. gypsum* and was twice as active as ketoconazole. Compound **5d** was as effective as ketoconazole against *M. gypsum*, and other compounds had lower activity. The oxidation derivative compounds **6a-g** did not have clearly increased activity, and did not demonstrate the activity that was expected. The current efforts, though not as successful as hoped, should nonetheless help in the discovery of new antifungal agents.

References

1. Ting PC, Walker SS. New agents to treat life-threatening fungal infections. *Curr Top Med Chem* 2008; 8:592-402.
2. Nosanchuk JD. Current status and future of antifungal therapy for systemic mycoses. *Recent Patents Anti-Infect*

Drug Disc 2006; 1:75-84.

3. Nakazumi H, Ueyama T, Kitao T. Synthesis and antibacterial activity of 2-phenyl 4H-1-benzo[b]thiopyran-4-one. *J Heterocyclic Chem* 1985; 22:1593-1596.
4. Nakib TA, Bezijiak V, Meegan M.J. Synthesis and antifungal activity of some 3-benzylidenechroman-4-one. *Eur J Med Chem* 1990; 25:455-462.
5. Qi P, Jin Y, Guo C, Fang L. Synthesis and antifungal activities of the Mannich bases of thiochromanones. *Chinese Journal of Medicinal Chemistry* 2003; 13:134-137.
6. Yu X, Liu J, Li X, Zhang G, Fang L. Application of uniform design for the synthesis of 3-benzyl-6-chloro-thiochromanone. *West China Journal of Pharmaceutical Science* 1998; 13:250-252.

(Received July 07, 2008; Accepted August 02, 2008)

Supplementary data

All final compounds were characterized by elementary analysis, IR, $^1\text{H-NMR}$ and HRMS. Data for compound:

1g: m.p. 81-82°C; IR (KBr) 1685, 1557, 1475, 880 cm^{-1} ; $^1\text{H-NMR}$ (300 MHz, DMSO- d_6) δ 2.9-3.3 (4H, m), 7.6 (1H, d), 8.1 (1H, d); HRMS (M^+) calcd for $\text{C}_9\text{H}_6\text{Cl}_2\text{OS}$ 231.9516, found 231.9524.

2f: m.p. 165-166°C; IR (KBr) 2670, 1750, 1580, 1320, 1220, 850 cm^{-1} ; $^1\text{H-NMR}$ (300 MHz, DMSO- d_6) δ 3.3-3.9 (6H, m), 4.3-4.7 (5H, m), 7.4 (1H, d), 7.9 (1H, d); HRMS (M^+) calcd for $\text{C}_{12}\text{H}_{13}\text{ClFNOS}$ 273.0390, found 273.0411.

2g: m.p. 176-177°C; IR (KBr) 2700, 1575, 1330, 1225, 845 cm^{-1} ; $^1\text{H-NMR}$ (300 MHz, DMSO- d_6) δ 3.0-3.7 (6H, m), 4.8 (5H, m), 7.3 (1H, d), 7.8 (1H, d); HRMS (M^+) calcd for $\text{C}_{12}\text{H}_{13}\text{Cl}_2\text{NOS}$ 289.0095, found 289.0109.

3e: m.p. 110-112°C; IR (KBr) 3400, 1665, 1600, 1470, 1270, 895, 820 cm^{-1} ; $^1\text{H-NMR}$ (300 MHz, DMSO- d_6) δ 3.1 (3H, m), 3.5-3.7 (2H, q), 4.1-4.8 (1H, s), 6.5 (1H, d), 7.1-7.4 (4H, m), 7.8 (1H, d); HRMS (M^+) calcd for $\text{C}_{16}\text{H}_{13}\text{BrFNOS}$ 364.9885, found 364.9876.

4g: m.p. 148-149°C; IR (KBr) 2830, 1650, 1560, 1545, 1480, 840, 800 cm^{-1} ; $^1\text{H-NMR}$ (300 MHz, DMSO- d_6) δ 3.6 (3H, s), 4.0 (2H, s), 6.6-7.0 (4H, m), 7.1 (1H, s), 7.8 (1H, d), 8.0 (1H, d); HRMS (M^+) calcd for $\text{C}_{17}\text{H}_{12}\text{Cl}_2\text{O}_2\text{S}$ 349.9935, found 349.9950.

5g: m.p. 108-109°C; IR (KBr) 1700, 1575, 1470, 880 cm^{-1} ; $^1\text{H-NMR}$ (300 MHz, DMSO- d_6) δ 3.5-3.8 (2H, m), 4.8-5.0 (1H, m), 7.6 (1H, d), 8.1 (1H, d); HRMS (M^+) calcd for $\text{C}_9\text{H}_5\text{BrCl}_2\text{OS}$ 309.8622, found 309.8637.

Original Article**Transdermal patch incorporating salbutamol sulphate: *In vitro* and clinical characterization**Nashwa A. El-Gendy^{1,*}, Nirmeen A. Sabry², Mai El-Attar³, Emad Omar⁴, Manal Mahmoud⁵¹ *Pharmaceutics Department, Faculty of Pharmacy, Beni-suef University, Beni-suef, Egypt;*² *Department of Clinical Pharmacy, Faculty of Pharmacy, Cairo University, Cairo, Egypt;*³ *Chest Department, Faculty of Medicine, Ain Shams University, Cairo, Egypt;*⁴ *Intensive Care Unit, Faculty of Medicine, Cairo University, Cairo, Egypt;*⁵ *Internal Medicine Department, Faculty of Medicine, Ain Shams University, Cairo, Egypt.*

ABSTRACT: Eudragit patches containing salbutamol sulphate were prepared and evaluated as a rate-controlling membrane for transdermal use. The effect of different Eudragit polymers and various plasticizers on the permeability and mechanical properties of the prepared patches were studied. Drug patches of Eudragit polymers were prepared by a casting method employing methanol as a solvent and dibutylphthalate, polyethylene glycol 400, Propylene glycol, and triacetin as plasticizers. These patches were evaluated for weight and thickness uniformity, swelling index, tensile strength, percentage of elongation, and moisture absorption capacity. *In-vitro* release characteristics of these patches were studied and analyzed. The patches were found to have a uniform thickness. Patches prepared using Eudragit RS 100 (T₈) as well as RS100 + L100 in a ratio of 3:1 (T₁₅) plasticized with triacetin were found to have a tensile strength lower than that of other patches. Permeability characteristics of selected patches were studied. Patch formulations T₈ and T₁₅ containing 10% oleic acid and 5% dimethyl formamide as penetration enhancers, respectively, displayed the highest permeability to salbutamol sulphate. These two formulations were selected for further clinical investigation and although both resulted in improvement in respiratory function tests, only the first formulation resulted in significant improvement.

Keywords: Salbutamol Sulphate, Transdermal patches, Asthma, Respiratory function

*Correspondence to: Dr. Nashwa A. El-Gendy, Pharmaceutics Department, Faculty of Pharmacy, Beni-suef University, Beni-suef, Egypt;
e-mail: papers.sabry@gmail.com

1. Introduction

Salbutamol sulphate (SS) is widely used for the therapeutic management and prophylaxis of asthma and nocturnal asthma in particular (1). Although SS is considered to be the drug of choice for the treatment of asthma, it has several drawbacks such as its short biological half-life of about 4-6 hours (2) and its susceptibility to extensive first-pass metabolism, thus requiring frequent administrations by both oral and inhalation routes. It has a short duration of action, low peak plasma level of 1.2 µg/mL, and poor bioavailability of only 14.8% (3). These factors necessitated formulation of a controlled-release drug delivery system for SS.

A transdermal patch is a medicated adhesive patch that is placed on the skin to deliver a time-released dose of medication through the skin in order to treat systemic illnesses. Such a system offers a variety of significant clinical benefits over other methods of administration. For example, it provides controlled release of the drug to the patient and enables a steady blood-level profile, leading to reduced systemic side effects, and sometimes provides improved efficacy over other dosage forms (4-6). In addition, the dosage form of transdermal patches is user-friendly, convenient, and painless. The generally accepted view is that they offer improved patient compliance (7).

The present work is an attempt to incorporate SS into the transdermal drug delivery system (TDDS) employing various types of Eudragits. The aim is to monitor the release of SS to maintain its therapeutic levels and evaluate it clinically as well. Hence, SS was selected as it undergoes first-pass metabolism and has a short half-life, thus presenting a challenge in terms of achieving controlled transdermal delivery of SS.

2. Materials and Methods

2.1. Materials

SS was donated by Amoun Co., Cairo, Egypt. Eudragit L100-55, RS100, RL100, S100, and L100 were purchased from Rhom Pharm GmbH Weiterstadt, Germany. Triacetin, polyethylene glycol 400 (PEG 400), dibutylphthalate (DBP), *n*-octanol (NO), and dimethyl formamide (DMF) were purchased from Sigma-Aldrich, USA. Propylene glycol (PG), methanol, oleic acid (OA), sodium chloride, potassium dihydrogen phosphate, disodium hydrogen phosphate, magnesium chloride, sodium nitrite, and potassium sulphate were purchased from Adwic, El-Nasr Chemical Co., Cairo, Egypt. Double-distilled water was used throughout the study.

2.2. Preparation of salbutamol sulphate transdermal patches

The transdermal patches of SS were prepared by a solvent casting technique using different types of Eudragit polymers (RS100, RL100, L100-55, L100 and S100) (8). An alcoholic solution of SS was prepared in which the weighed amount (5 mg) of the drug was dispersed in 10 mL methanol. Different Eudragit polymers (5%, w/v) were added to the alcoholic drug solution while stirring to ensure uniform distribution. Lastly, the plasticizer was added to protect the polymeric patches from brittleness upon storage. The plasticizers used were DBP, PEG 400, PG, and triacetin in different concentrations. The dispersion processes were prepared using a magnetic stirrer (Thermolyne Corporation, USA) providing constant stirring (500 rpm) at room temperature until clear solutions were

obtained. The compositions of the tested transdermal patches are shown in Table 1.

Measured volumes (10 mL) of the polymeric solutions were poured onto a plastic substrate (circular dish of 57 mm² diameter and 8 mm depth) and dried on a level bench at room temperature for 24 h with an inverted funnel overhead to provide a uniform rate of evaporation. The formulated patches were allowed to equilibrate in a desiccator over anhydrous calcium chloride for another 24 h before the evaluation process to ensure total hydration and to exclude entrapped air (9). The patches were evaluated within one week of the casting date.

2.3. In-vitro characterization of the prepared salbutamol sulphate transdermal patches

2.3.1. Uniformity of initial drug content

For drug content determination, the total content of transdermal systems ($n = 3$) was placed in a 100 mL volumetric flask and dissolved in methanol. The solution was filtered through a Whatman filter membrane (0.45 μm) prior to spectrophotometric drug analysis at 276 nm (Shimadzu, model UV-1601 PC, Kyoto, Japan).

2.3.2. Uniformity of patch weight and thickness

Three randomly selected patches of each formulation were weighed and their average weight was calculated. Patch thickness was determined using calipers (Vernier Caliper, Shanghai, China) and recorded. Results were reported as the mean (\pm S.D.) of five measurements (the four corners and the center of each patch).

2.3.3. Percent dissolution and swelling index (SI) of the transdermal patches

The patches were dried in a desiccator over anhydrous calcium chloride at ambient temperature until a constant weight was obtained (W_1); then, they were immersed for 3 days in 100 mL distilled water at 37°C. Excess water present on the swollen patches was removed by careful patch blotting with filter paper. The patches were reweighed (W_2), returned to the desiccator, and dried to a constant weight; then, they were reweighed again (W_3) (10).

$$\% \text{ dissolution} = \frac{W_1 - W_3}{W_1} \times 100$$

The swelling index (SI) was determined from the amount of water absorbed per unit weight of undissolved patches retrieved from the distilled water after immersion (10).

$$SI = \frac{W_2 - W_3}{W_3} \times 100$$

Table 1. Composition of SS loaded Eudragit patches in each formula (%)

Formula	Eudragit type	Plasticizer	Plasticizer concentration (%)
T ₁	RL100	PEG 400	40
T ₂		PG	50
T ₃		DBP	30
T ₄		Triacetin	30
T ₅	RS100	PEG 400	50
T ₆		PG	50
T ₇		DBP	30
T ₈		Triacetin	20
T ₉	L100-55	PEG 400	40
T ₁₀		PG	50
T ₁₁		Triacetin	30
T ₁₂	RS100 + L100 (3:1)	PEG 400	40
T ₁₃		PG	50
T ₁₄		DBP	30
T ₁₅		Triacetin	30
T ₁₆	RS100 + S100 (3:1)	PEG 400	40
T ₁₇		PG	50
T ₁₈		DBP	30
T ₁₉		Triacetin	30
T ₂₀	RS 100 + RL100 (3:1)	DBP	30

Results were reported as the mean (\pm S.D.) of three replicates.

2.3.4. Moisture absorption capacity of the patches

The water absorption capacities of various films were determined at 33, 65, and 97% relative humidity (RH). Films were cut into 1 \times 1 cm strips. The strips were conditioned by weighing; they were placed in a desiccator at 40°C for 24 h, removed, and exposed to conditions of 33% RH (containing saturated solution of magnesium chloride), 65% RH (containing saturated solution of sodium nitrate), and 97% RH (containing saturated solution of potassium sulphate) in different desiccators at room temperature. Weight was measured periodically every 48 h for 14 days until a constant weight was obtained. The moisture absorption capacity of the films (weight %) was calculated in terms of percentage increase in the weight of film over the initial weight of the specimen (11,12).

2.3.5. Mechanical properties of salbutamol sulphate patches

The tensile strength, the film's percentage elongation at break, and the modulus of elasticity (Young's Modulus) were determined using a tensile strength tester (TN-30 code N 9112-ID, India). Patch strips 1 cm in width were grasped using an upper and lower flat-faced metal grip laminated with a smooth rubber grip. The distance between the grips was set at 2 cm and this distance, therefore, represented the length of the film under stress. A speed of 5 mm/s was used for all measurements (13).

The load applied to the patch was automatically increased at a specific rate until the patch broke. Only results from films that were observed to break in the middle area of the test strip during testing were used. Results were reported as the mean (\pm S.D.) of five replicates. The tensile strength and elongation at break were calculated as below:

The percentage elongation at break, E_b , of tested films was determined, where E is the film's extension to break and L_0 is its original length (14).

$$E_b = [E/L_0] \times 100$$

The break strength, B , of tested films was determined, where F is the break force of the film and A_R is its cross sectional area (14).

$$B = F/A_R$$

The modulus of elasticity (M_E) of the patch was calculated from Hook's law (15).

$$B = M_E / (E/L_0)$$

2.3.6. In-vitro release studies

The *in-vitro* release of transdermal patches was performed with a paddle over disk method, in

accordance with the US Pharmacopoeia (USP 27 apparatus 5) (16). Briefly, a volume of 250 mL freshly prepared Sorenson's phosphate buffer pH 5.5 (dissolution medium) was placed in the vessel and the temperature of the medium was equilibrated to $32 \pm 0.5^\circ\text{C}$. A patch sample on its plastic substrate was covered with a stainless steel screen disc (mesh size 100 μm) of the same size, with the release surface facing up. The assembly was prevented from floating and hitting the rotating paddle by attaching a glass disc to the bottom of the plastic substrate using cyanoacrylate adhesive. The paddle was then rotated at 50 rpm.

At predetermined time intervals over a total period of 8 h, aliquots (5 mL) were withdrawn and replaced with fresh medium. The samples were filtered through 0.45 μm Whatman filter membranes and spectrophotometrically analyzed for drug content at 276 nm. The results were the mean values of three runs. Cumulative amounts of drug released were plotted against time for different formulations. The obtained data were subsequently analyzed to determine the order of release.

2.4. In-vitro permeation studies of salbutamol patches

Abdominal skin (approximately 1 mm in thickness) from male newborn mice (age 6 days or younger) was carefully excised (Cairo University Labs, Cairo, Egypt). All animals were treated in accordance with the principles of laboratory animal care (Guide for the Care and Use of Laboratory Animals, 1985) (17).

After removing the hypodermal adipose tissue, the skin was used as a barrier membrane for *in-vitro* transdermal permeation. When not used immediately, the skin was kept refrigerated ($2-5^\circ\text{C}$) and used within 3 days (18). *In-vitro* mice skin permeation studies were performed in vertical Franz-type glass single diffusion cells (Keshary-Chien type) (19-21). The volume of the receptor cell was 17 mL and the effective surface area available for permeation was 3.14 cm^2 . Briefly, the freshly excised mice skin was mounted between the donor and receptor cells such that the epidermal surface faced the donor compartment. Each prepared patch was placed on the stratum corneum side of the skin, after which the receptor cells were filled with PBS and thermostated at 37°C by placement in a water bath. The hydrodynamics of the receptor fluid were maintained by stirring the fluid at 600 rpm in order to prevent any boundary layer effects. At predetermined time intervals over a period of 24 h, the receptor solution was sampled (200 μL), filtered through a 0.25- μm filter membrane, and analyzed by HPLC in order to determine the extent of the permeated drug. Briefly, SS concentration was analyzed using a reverse-phase HPLC method in order to determine the extent of the permeated drug. A Shimadzu HPLC system including a solvent delivery

pump (Shimadzu LC-10AT), a controller (Shimadzu SCL-10A), and a UV detector (Shimadzu SPD-10A) was used in this study. A 3.9×150 mm long NOVA-Pack C₁₈ 60A, 4U, cartridge column (Agilent C) with a particle diameter of 3.5 μ m was used. During the assay, SS was eluted isocratically at a flow rate of 1.2 mL/min and monitored with a UV detector operating at 276 nm. The mobile phase for the assay consisted of a mixture of water, methanol, and acetonitrile (70:20:10, v/v) pH-adjusted to 2.5 by 10% phosphoric acid. The run time for the assay was 10 min, and the retention time for SS was 3.0 min (22).

The same volume of fresh PBS was supplied to the receptor after each sampling. Each permeation experiment was replicated at least 3 times.

Three permeation enhancers, namely 10% OA, 5% DMF, and 5% NO (%w/w of the dry polymer weigh), were incorporated separately into selected patch formulations (T₈ and T₁₅) that produced optimum results in all previous tests. Data on the permeation of SS through hairless mice skin was graphically plotted as the cumulative amount of the permeated drug per unit area as a function of time, from which the permeation parameters were calculated including the cumulative amount of the permeated drug per unit area after 24 h (Q₂₄), steady state flux (J_{ss}), apparent permeability coefficient (P_{app}), lag time (t_{lag}), diffusion constant (D), and the enhancement ratio for the permeability coefficient (ER) (23-25).

2.5. Determination of clinical efficacy of the selected formulations

Two optimum formulations (according to the *in-vitro* parameters) were selected for further clinical investigation in asthmatic patients after they satisfied optimum physical, mechanical, and release parameters.

Subjects: Subjects were selected from 30 adult patients who were newly admitted to the Chest Department of Ain Shams University Hospitals and the ICU of El-Kasr El-Aini Teaching Hospital complaining of asthmatic attacks. Patients were recruited to investigate the clinical efficacy of selected patches and all had to be diagnosed with acute asthma to serve as subjects. All selected asthmatics (mild and moderate) were non-smokers and met the criteria mentioned in the new Egyptian guidelines for the diagnosis and management of asthma (26). The study was approved by the Ethics Committee of both Ain Shams University Hospital and El-Kasr El-Aini Teaching Hospital and the research followed the tenets of the Declaration of Helsinki promulgated in 1964.

Protocol: The study adopted an open randomized, parallel design. All patients were subjected to the following after providing written consent:

An initial screening that included a medical history, physical examination, vital signs, ECG, plain chest X-ray, liver function tests, kidney function tests, and

fasting and postprandial blood glucose levels.

Pulmonary function tests with a spirometer (Cosmed Pony Graphics version 3.2 E-MB) at the Pulmonary Function Laboratory of the Chest Department and Critical Care Unit at Ain-Shams University Hospital and Kasr El-Aini Hospital, respectively; tests included FVC, FEV₁, and FEV₁/FVC. All pulmonary function tests were performed for each subject before and after the study.

To objectively assess the impact of intervention, these parameters were scored and a composite score was then calculated. Heart rate and respiratory rate were counted and scored.

NB: The exclusion criteria included evidence of acute or chronic infection, pregnancy, breast-feeding or any chronic medical illness other than asthma, oral steroid therapy, and FEV₁ < 60% of the predicted value (Severe asthmatic patients).

The recruited patients were randomly classified into two groups:

Group I: 15 patients receiving formulation T₈/OA (equivalent to 5 mg Salbutamol).

Group II: 15 patients receiving formulation T₁₅/DMF (equivalent to 5 mg Salbutamol).

The transdermal patch was applied onto the anterior surface of the forearm near the elbow. The patients were instructed not to remove the patch and also to look for any sign of irritation at the site of application. The patch was removed after 24 h. At the conclusion of the study, a physical examination including vital signs and ECG were re-performed. The patients were discharged after suitable medication to ensure a reasonably safe FEV₁ and were asked to continue with their regular medication.

2.6. Statistical analysis

Unless indicated, results are presented as mean \pm standard deviation (S.D.). One-way analysis of variance (ANOVA) was used to determine significance among groups, after which post hoc tests with the Bonferroni correction were used for comparison between individual groups. Other statistical comparisons were done by the Mann-Whitney test for nominal continuous data, Wilcoxon signed rank test to compare mean differences in the data, and the Chi-squared (X²) test for categorical data; a *p* value of < 0.05 was considered significant. Statistical Package for Social Science (SPSS) was used for data analysis.

3. Results and Discussion

3.1. *In-vitro* characterization of the prepared salbutamol sulphate transdermal patches

3.1.1. Uniformity of initial drug content, weight, and thickness

SS patches were evaluated for their physical parameters

Table 2. Physical characterization, drug content, % dissolution and SI of SS transdermal patches

Formula	Drug content (% ± S.D.)	Uniformity of weigh (gm) (average ± S.D.)	Uniformity of thickness (mm) (average ± S.D.)	% Dissolution (average ± S.D.)	SI (average ± S.D.)
T1	91.62 ± 0.877	0.547 ± 0.076	0.131 ± 0.003	14.82 ± 0.255	1.362 ± 0.172
T2	9.31 ± 0.990 ^a	0.525 ± 0.033	0.154 ± 0.030	14.38 ± 0.566	1.858 ± 0.215
T3	94.47 ± 2.046	0.507 ± 0.068	0.144 ± 0.023	11.18 ± 2.574	0.403 ± 0.088
T4	88.24 ± 1.782	0.523 ± 0.016	0.135 ± 0.038	14.32 ± 0.976	0.175 ± 0.011
T5	N/A	N/A	N/A	N/A	N/A
T6	89.52 ± 1.810	0.678 ± 0.017	0.162 ± 0.055	5.57 ± 0.325	0.0814 ± 0.008
T7	92.61 ± 3.521	0.491 ± 0.014	0.156 ± 0.023	1.876 ± 0.461 ^b	0.398 ± 0.020
T8	94.23 ± 1.541	0.603 ± 0.008	0.158 ± 0.011	3.955 ± 0.516	0.255 ± 0.059
T9	N/A ^c	N/A	N/A	N/A	N/A
T10	88.35 ± 0.495	0.563 ± 0.059	0.163 ± 0.003	24.02 ± 0.679 ^b	0.503 ± 0.041
T11	89.24 ± 2.503	0.573 ± 0.008	0.146 ± 0.006	15.92 ± 0.551	0.529 ± 0.037
T12	90.24 ± 2.630	0.549 ± 0.038	0.138 ± 0.006	11.51 ± 0.707	0.438 ± 0.088
T13	93.61 ± 5.020	0.622 ± 0.013	0.129 ± 0.003	12.75 ± 0.650	0.282 ± 0.030
T14	92.57 ± 0.792	0.603 ± 0.012	0.157 ± 0.004	4.38 ± 1.032 ^b	0.149 ± 0.038
T15	88.73 ± 1.457	0.628 ± 0.023	0.159 ± 0.001	4.74 ± 0.720	0.087 ± 0.018
T16	N/A	N/A	N/A	N/A	N/A
T17	N/A	N/A	N/A	N/A	N/A
T18	N/A	N/A	N/A	N/A	N/A
T19	96.23 ± 2.701	0.628 ± 0.054	0.162 ± 0.006	5.97 ± 0.481	0.25 ± 0.071
T20	94.36 ± 1.754	0.622 ± 0.027	0.148 ± 0.004	13.95 ± 0.525	1.355 ± 0.205

^a Statistically significant, ANOVA, $p < 0.05$; ^b Statistically significant, ANOVA, $p < 0.001$; ^c Not applicable.

(thickness and weight uniformity, as well as drug content). The drug content analysis of the prepared formulations showed that the process employed to prepare patches in this study was capable of providing films with a uniform drug content and minimum batch variability. All the prepared patches complied with the pharmacopoeial limits for content uniformity (27). The prepared patches had a thickness ranging from 0.129 to 0.163 mm, and their weight was uniform, varying from 0.491 to 0.678 gm/patch (Table 2). These ranges are suitable for application to the skin as reported by Clearly (28).

3.1.2. Percent dissolution and swelling index (SI) of the transdermal patches

The incorporation of plasticizers in Eudragit patches has weakened its resistance to solubility in distilled water. This can be attributed to the fact that plasticizer molecules increase the flexibility of Eudragit molecules and render the patches more permeable to the water molecules (29). Of the plasticizers used, PG was found to be the most effective in reducing the water resistance of Eudragit patches while DBP was the least effective (Table 2).

As is apparent from Table 2, the percent dissolution increased with the incorporation of Eudragit RL100 (T₁-T₄) and L100-55 (T₁₀ and T₁₁) compared to the patches prepared with RS100 (T₆-T₈). Moreover, addition of Eudragits L100, S100, and RL100 to RS100 in the prepared patches (T₁₂-T₂₀) in a ratio of 1:3 led to increased percent dissolution. This may be attributed to the increase in the freely permeable resin in water as a result of using these polymers (30).

The water uptake capacity of the patch was measured by the swelling index (SI). The data in Table 2 revealed that transdermal patches containing Eudragit L100-55 and RL100 exhibited the highest

SI in comparison to other formulations. These results suggest that these patches would be more permeable to the drug. This may be due to the porosity generated in the remnants of the patches after dissolution (31).

3.1.3. Moisture absorption capacity of the patches

Moisture absorption of polymeric patches affects both the mechanical properties and the drug release pattern. Moisture absorption capacities under different humidity conditions (Figure 1) revealed that the moisture uptake of the patches depended on the type of both Eudragit and plasticizer used.

Moisture absorption in 97% RH is relatively high and the weight of most patches significantly increased in comparison to other levels of RH. The highest absorption capacities within 2 weeks were 4.221%, 7.325%, and 10.73% for those prepared using Eudragit L100-55 and PG while the lowest (1.811, 3.993 and 6.304) were recorded for Eudragit RS100 patches containing DBP at 33%, 65%, and 97% RH, respectively.

As is apparent, Eudragit L100-55 and RL100 formulated patches plasticized with any of the aforementioned plasticizers absorbed water to a greater extent than did patches containing Eudragit RS100. Also obvious is the fact that inclusion of Eudragits L100, S100, or RL100 in RS100 led to increased water absorbing ability of the prepared patches. This could be due to the hydrophilic nature of these Eudragits compared to Eudragit RS100 alone. This hydrophilic nature may be attributed to the fact that Eudragit RL polymers contain double the quaternary ammonium groups of Eudragit RS. Moreover, Eudragit L100-55 is a free-flowing powder that is redispersible in water and dissolves above pH 5.5. The higher methacrylic acid content of Eudragits L100 and S100 increases their hydrophilic characteristics (32).

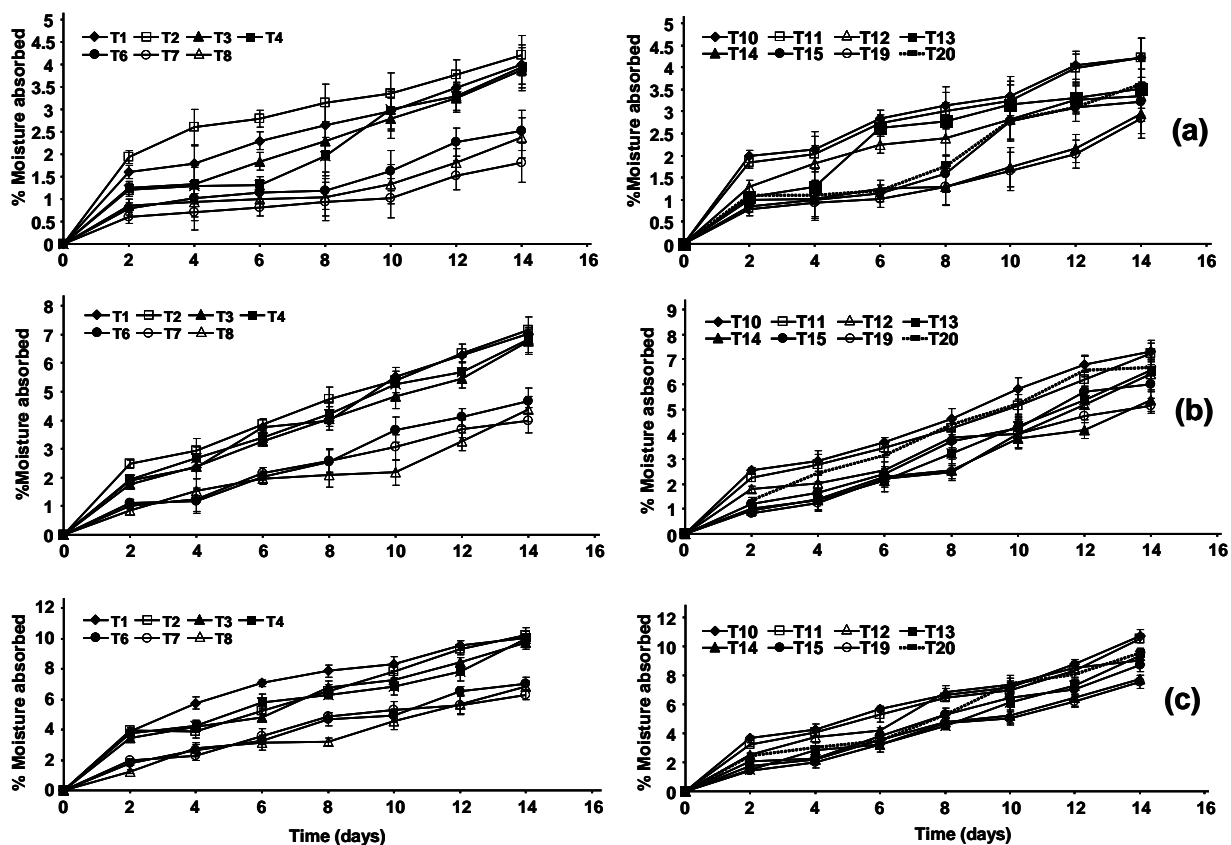


Figure 1. Moisture absorption capacity of salbutamol sulphate transdermal patches at a: 33 % RH, b: 65% RH and c: 97% RH.

Table 3. Mechanical properties of salbutamol sulphate transdermal patches

Formula	Elongation % (average \pm S.D.)	Tensile strength (Kg/cm ²) (average \pm S.D.)	Modulus of elasticity (average \pm S.D.)
T ₁	4.19 \pm 0.438	1.205 \pm 0.177 ^b	28.75 \pm 2.475 ^b
T ₂	9.27 \pm 0.325	0.62 \pm 0.042	6.62 \pm 0.552 ^b
T ₃	24.95 \pm 1.500	0.071 \pm 0.016	0.284 \pm 0.040
T ₄	16.98 \pm 0.480	0.105 \pm 0.057	0.618 \pm 0.1457
T ₅	N/A ^c	N/A	N/A
T ₆	76.03 \pm 1.541 ^b	0.0652 \pm 0.008	0.0857 \pm 0.008
T ₇	91.85 \pm 1.154	0.055 \pm 0.014	0.0598 \pm 0.003
T ₈	208.22 \pm 2.531 ^b	0.015 \pm 0.007	0.0072 \pm 0.003
T ₉	N/A	N/A	N/A
T ₁₀	38.4 \pm 0.990 ^b	0.0659 \pm 0.023	0.1716 \pm 0.042
T ₁₁	14.37 \pm 1.1880	0.11 \pm 0.109	0.765 \pm 0.066
T ₁₂	11.85 \pm 0.976	0.3125 \pm 0.141	2.637 \pm 0.528
T ₁₃	22.71 \pm 1.640	0.72 \pm 0.242	3.17 \pm 0.467
T ₁₄	87.11 \pm 1.432	0.06 \pm 0.038	0.0689 \pm 0.017
T ₁₅	197.99 \pm 2.84 ^b	0.04 \pm 0.008	0.0202 \pm 0.002
T ₁₆	N/A	N/A	N/A
T ₁₇	N/A	N/A	N/A
T ₁₈	N/A	N/A	N/A
T ₁₉	20.19 \pm 1.782	0.075 \pm 0.021	0.371 \pm 0.058
T ₂₀	12.303 \pm 1.427	0.13 \pm 0.143	1.0566 \pm 0.514

^a Statistically significant, ANOVA, $p < 0.05$; ^b Statistically significant, ANOVA, $p < 0.01$; ^c Not applicable.

Also of note is the fact that lower water absorption capacity was achieved in the presence of DBP than with the other plasticizers used. This is possibly attributed to the limited water affinity of DBP (33).

3.1.4. Mechanical properties of salbutamol sulphate transdermal patches

The physicochemical properties of patches are among

the factors that determine the suitability and acceptability of prepared patches. The tensile strength, % elongation, and modulus of elasticity were determined for the prepared patches. All results of mechanical properties are shown in Table 3. The tensile strength ranged from 0.015 kg/cm² for T₈ to 1.205 kg/cm² for T₁. Percent elongation ranged from 4.19% for T₁ to 208.22% for T₈. Optimum mechanical properties were clearly obtained from transdermal SS patches (T₈) containing RS100 and

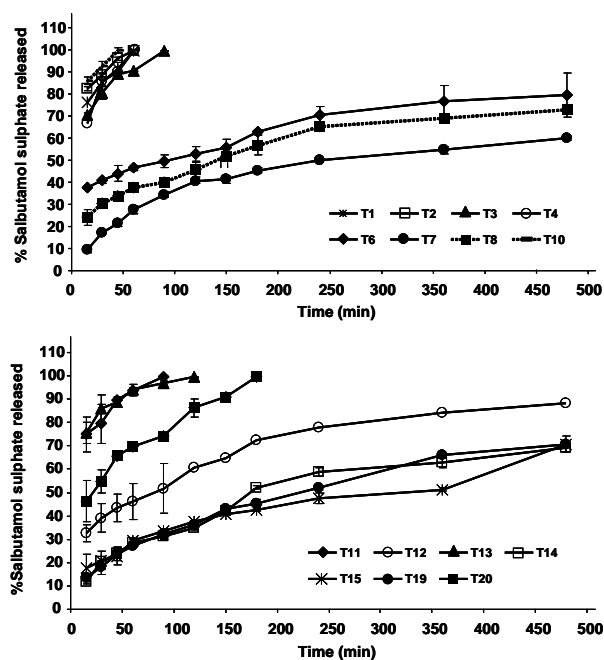


Figure 2. *In-vitro* release profiles of salbutamol sulphate in Sorensen's phosphate buffer (pH 5.5) from patch formulation (T_1 - T_{20}).

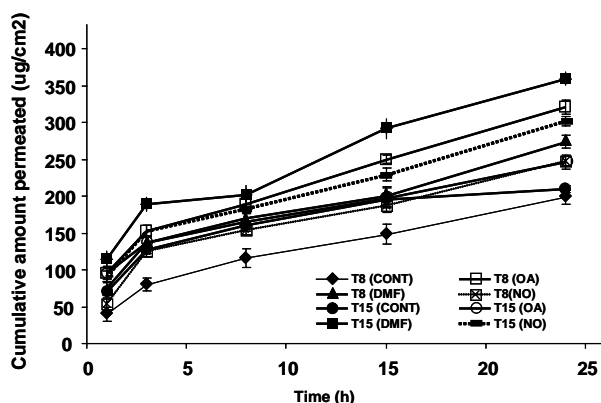


Figure 3. Permeation profiles of salbutamol sulphate from patches a) T_8 and b) T_{15} containing different enhancers through hairless mice skin compared to control.

triacetin, followed by patches (T_{15}) containing RS100 + L100 and triacetin. This could be due to the high affinity of triacetin for water, which contributes to its elongation ability.

3.1.5. *In-vitro* release of salbutamol sulphate from the prepared patches

Drug release testing is a crucial part of the development of transdermal patches as it helps to ensure the batch-to-batch uniformity of each drug delivery system and to evaluate the release rate of the drug from the prepared formulations (34). Even though body temperature is maintained at 37°C, the temperature of the skin surface is 32°C (35). This is why the temperature of the dissolution medium was kept at 32 ± 0.5°C. Sorensen's phosphate buffer of pH 5.5, used as a dissolution medium, simulated the pH of the skin surface (36).

As is apparent in Figures 2 and 3, the amount of

SS released from patches T_{10} was significantly higher ($p < 0.001$) than that released from other patches as it reached ~100% within 45 min. This might be due to the high solubility of Eudragit L100-55 in solutions of pH 5.5 and the high water affinity of PG plasticizer. A point of note is that Eudragit RL100 patches had a higher release of drug than those prepared with Eudragit RS100. This could be attributed to the lower content of quaternary ammonium groups in Eudragit RS100 than in RL100, resulting in less swelling in aqueous media. Thus, it is extensively employed in the pharmaceutical industry because of its potential for the development of controlled-release drug delivery systems (32).

In addition, inclusion of Eudragit RL100 to RS100 (1:3) (T_{20}) led to a slight reduction in the release profile of the drug (~100% within 180 min) compared to the use of RL100 alone. In contrast, incorporation of Eudragit L100 and S100 in RS100 (1:3) (T_{20}) led to a great reduction in the release profile of the drug compared to the use of RL100 alone but still provided a higher release profile than patches containing RS100 alone. Moreover, PG plasticizer resulted in a higher release rate of the drug, followed by PEG and then triacetin and finally DPB. Patches T_7 and T_{14} plasticized with DBP clearly exhibited significantly lower release rates of the drug (59.975 and 69.425%, respectively). That said, a better release profile was provided by Eudragit RS100 plasticized with triacetin (T_8) and Eudragit RS100 + L100 in (3:1) ratio plasticized with triacetin (T_{15}), as they achieved 72.97 and 70.82% within 8 h, respectively.

Linear regression analysis of release data was done to determine the proper order of release. Zero-, first-, and Higuchi diffusion-controlled model equations were applied to all *in-vitro* release results, indicating that the drug is released from all transdermal patches *via* a diffusion-controlled mechanism.

3.2. *In-vitro* drug permeation studies

The *in-vitro* release studies conducted revealed that polymeric patches prepared using RS100 with 20% triacetin (T_8) and a combination of RS100 and L100 in a ratio of 3:1 (T_{15}) with 30% triacetin as a plasticizer were found to be the most suitable with respect to drug content and all of the physical parameters evaluated (Table 2). Thus, the patches T_8 and T_{15} were considered for further *in-vitro* permeation studies.

The major rate-limiting step for the transport of hydrophilic drugs is their permeation through the stratum corneum. Once they have permeated through the stratum corneum, they are rapidly absorbed into the systemic circulation. As a result, hydrophilic drugs elicit poor local pharmacological response due to low retentivity in the skin layers (37). Chemical enhancers are known to enhance the influx of hydrophilic drugs across the stratum corneum. Table 4 summarizes the

Table 4. Percutaneous penetration parameters of salbutamol sulphate across abdominal mouse skin from different transdermal patches

Formula	Q ₂₄ (µg/cm ²)	J _{ss} (µg/cm ² ·h)	Lag time t _{lag} (min)	P _{app} (cm/h) × 10 ⁻²	D (cm ² /h) × 10 ⁻⁴	ER _{sal}
T ₈ control ^a	198.52 ± 2.121	6.35 ± 0.212	52.79 ± 0.311	1.27 ± 0.071	3.83 ± 0.255	----
T ₈ (OA) ^a	320.81 ± 1.853†	9.14 ± 0.184	49.61 ± 0.834	1.82 ± 0.240	4.08 ± 0.212	1.43 ± 0.099
T ₈ (DMF) ^a	273.61 ± 3.677†	7.56 ± 0.775	49.69 ± 2.376	1.51 ± 0.240	4.07 ± 0.622	18 ± 0.198
T ₈ (NO) ^a	238.32 ± 5.968	7.3 ± 0.962	51.34 ± 0.962	1.46 ± 0.325	3.94 ± 0.382	1.15 ± 0.228
T ₁₅ control ^b	209.73 ± 3.224	5.41 ± 0.410	54.69 ± 1.725	1.08 ± 0.116	3.70 ± 0.438	----
T ₁₅ (OA) ^{bc}	245.47 ± 1.626	5.96 ± 0.071	55.39 ± 2.022	1.19 ± 0.057	3.65 ± 0.495	1.10 ± 0.3
T ₁₅ (DMF) ^{bd}	349.36 ± 1.202†	9.86 ± 0.212	49.38 ± 1.047	1.97 ± 0.057	4.10 ± 0.297	1.82 ± 0.269
T ₁₅ (NO) ^{bc}	301.84 ± 1.782†	8.26 ± 1.202	51.73 ± 2.786	1.65 ± 0.212	3.91 ± 0.297	1.52 ± 0.283

^aT₈: polymeric patch prepared using RS100 + 20% triacetin; ^bT₁₅: polymeric patch prepared using combination of RS100 and L100 in the ratio of 3:1 + 30% triacetin; ^cOA: 10% oleic acid; ^dDMF: 5% dimethyl formamide; ^eNO: 5% *n*-octanol.

Table 5. Demographic data, heart rate and respiratory rate for the recruited patients and their pulmonary function tests both before and after patch application

Category	T ₈		T ₁₅	
No. of patients (%)	15 (55.56)		12 (44.44)	
No. of males (%)	5 (30)		4 (30)	
Mean of age in years (SD) ^a	34.1 (7.82)		28.0 (4.55)	
Mean disease duration/year (SD)	5.6 (2.22)		4.75 (2.31)	
No. of wheezing patients (%)	6 (40)		6 (50)	
Mean of H.R (bpm) (SD)	93.0 (11.04)		104.13 (12.74)	
Mean of R.R (bpm) (SD)	23.95 (5.66)		26.56 (7.48)	
Pulmonary function tests	Before	After	Before	After
FVC% ^d	83.0 (5.40)	89.4 (7.00) ^e	84.0 (5.21)	87.0 (8.28)
FEV ₁ ^e	61.6 (3.91)	81.5 (17.0) ^b	64.75 (8.68)	78.63 (15.09)
FEV ₁ /FVC%	62.71 (3.91)	75.11 (10.34) ^c	62.56 (4.21)	75.23 (10.68) ^b

^aSD = Standard deviation; ^bStatistical Significant at $p < 0.05$, Wilcoxon signed ranks test; ^cStatistical Significant at $p < 0.01$, Wilcoxon signed ranks test; ^dFVC: Forced vital capacity; ^eFEV₁: Forced expiratory volume in one second.

effect of enhancers (viz OA, DMF and NO) on the steady-state flux (J_{ss}) and permeability coefficient of SS as well as the lag time, diffusion coefficient (D), and enhancement factor (ER). Moreover, the cumulative amounts of the drug at different diffusion times are shown in Figure 1. Among the various types of enhancers studied, OA for formulation T₈ and DMF for patch formulation T₁₅ provided a higher permeability coefficient and enhancement factor (ER).

An interesting finding is that OA interacts with and modifies the lipid domains of the stratum corneum because of its similar structure to these lipids (21). Electron microscopic studies have shown that OA in human stratum corneum exists as a separate phase (or as 'pools') within the bilayer lipids (38,39). The formation of such pools would result in permeability defects within the bilayer lipids, thus facilitating permeation of hydrophilic permeants through the membrane.

Considering the small, highly polar nature of DMF, it may interact with the head groups of some lipid bilayers to disrupt its backing geometry. Furthermore, DMF in skin may facilitate drug partitioning from the formulation into the skin; one study reported a 12-fold increase in the flux of caffeine permeating across human skin treated with DMF (40).

3.3. Determination of clinical efficacy of the selected formulations

The two finally selected patches, formulation T₈ containing 10% OA and T₁₅ containing 5% DMF, were

tried clinically on 30 acute asthmatic patients. These formulations were found to be the most appropriate with respect to drug content and all of the physical parameters evaluated, and they also exhibited superior *in-vitro* release behavior and a higher permeability coefficient and enhancement factor (ER).

Out of the 30 recruited patients, 27 completed the study and 3 dropped out because their condition was exacerbated and they required nebulizers. The 27 patients that completed the study had an average age of 31.4 ± 7.11 years, ranging from 23 to 50 years (median = 30.5 years). Patients' conditions were classified as mild to moderate bronchial asthma with average disease duration of 5.2 ± 2.24 years, ranging from 2 to 9 years (median = 5 years). Baseline characteristics are shown in Table 5. There was a preponderance of females (about 2:1) in both groups. The subjects' baseline demographic parameters, vital signs, and spirometric parameters were comparable ($p < 0.05$).

Twenty four hours after drug administration, all of the studied parameters (FEV₁%, FVC% and FEV₁/FVC) improved significantly ($p < 0.05$) in the first group (with patch T₈). Those patients treated with patch T₁₅ showed significant improvement ($p < 0.05$) in their FEV₁/FVC alone and showed non-significant improvement in both FEV₁% and FVC% (Table 5).

None of the recruited patients experienced any untoward effect or discomfort during and up to a week after the study period. No signs of skin reactions were seen at the site of application in any of the patients.

Quite clear from the reported results is the fact that patches prepared using RS100 and L100 in a ratio of

3:1 (T₁₅) with 30% triacetin with OA as a penetration enhancer had optimum physicochemical properties together with the greatest clinical improvement among all the tested patches.

4. Conclusion

The films of SS obtained by the solvent casting method had acceptable mechanical characteristics and satisfactory % drug release. The prepared films were transparent and had a smooth surface without any interactions between the drug and polymer.

The study demonstrates the feasibility of formulating transdermal drug delivery systems to deliver SS as part of asthma management. The transdermal formulations were found to be safe and non-reactive. Transdermal delivery of SS appears to be a better route for patients who respond well to β -agonists. In light of the present results, formulations for the transdermal delivery of SS should be further improved for durations up to several days. This is especially relevant in a country like Egypt, where inhalers are too expensive devices to be routinely used by asthmatic patients and where the inhalation technique is not adequately implemented.

Acknowledgement

The authors would like to thank Amoun Co., Cairo, Egypt, for their donation of salbutamol sulphate.

References

- Kelly HW, Murphy S. Beta-adrenergic agonists for acute, severe asthma. *Ann Pharmacother* 1992; 26:81-91.
- Sweetman SC. *Martindale: The complete drug reference*, 34th ed. Pharmaceutical Press, London, UK, 2005.
- Ahrens RC, Smith GD. Albuterol: an adrenergic agent for use in the treatment of asthma pharmacology, pharmacokinetics and clinical use. *Pharmacother* 1984; 4:105-121.
- Ranade VV. Drug delivery systems 6. Transdermal drug delivery. *J Clin Pharmacol* 1991; 31:401-418.
- Modamio P, Lastra CF, and Marino EL. A comparative *in vitro* study of percutaneous penetration of beta-blockers in human skin. *Int J Pharm* 2000; 194:249-259.
- Ke GM, Wang L, Xue HY, Lu WL, Zhang X, Zhang Q, Guo HY. *In vitro* and *in vivo* characterization of a newly developed clonidine transdermal patch for treatment of attention deficit hyperactivity disorder in children. *Biol Pharm Bull* 2005; 28:305-310.
- Audet MC, Moreau M, KoltunWD, Waldbaum AS, Shangold G, Fisher AC, Creasy GW, for the ORTHO EVRA/EVRA 004 Study Group. Evaluation of contraceptive efficacy and cycle control of a transdermal contraceptive patch vs. an oral contraceptive: A randomized controlled trial. *JAMA* 2001; 285:2347-2354.
- Arora P, Mukherjee B. Design, development, physicochemical, and *in-vitro* and *in-vivo* evaluation of transdermal patches containing diclofenac diethylammonium salt. *J Pharm Sci* 2002; 91:2076-2089.
- Eouani C, Piccerelle PH, Pinderre P, Bourret E, Joachim J. *In-vitro* comparative study of buccal mucoadhesive performance of different polymeric films. *Eur J Pharm Biopharm* 2001; 52:45-55.
- Ritthidej GC, Phaechamud T, Koizumi T. Moist heat treatment on physicochemical change of chitosan salt films. *Int J Pharm* 2002; 232:11-22.
- Baichwal RW. *Advances in drug delivery systems*. MSR foundation, Bombay, India, 1983; pp. 136-147.
- Lin SY, Chen KS, Chu LR. Organic esters of plasticizers affecting the water absorption, adhesive property, glass transition temperature and plasticizer permanence of Eudragit acrylic films. *J Control Release* 2000; 68:343-350.
- Donnelly RF, McCarron PA, Zawislak AA, Woolfson AD. Design and physicochemical characterisation of a bioadhesive patch for dose-controlled topical delivery of imiquimod. *Int J Pharm* 2006; 307:318-325.
- Radebaugh GW. Film coatings and film forming materials: Evaluation. In: *Encyclopedia of pharmaceutical technology*, Vol. 6 (Swarbrick J, Boylan JC, eds). Marcel Dekker, New York and Basel, 1992.
- Martin A. *Physical pharmacy: Physical and chemical principles of pharmaceutical sciences*. 4th ed. Lea & Philadelphia. 1993; pp. 575-578.
- Azarmi S, Roa W, Löbenberg R. Current perspectives in dissolution testing of conventional and novel dosage forms. *Int J Pharm* 2007; 328:12-21.
- Guide for the Care and Use of Laboratory Animals #86-23. Bethesda, MD: National Institutes of Health, 1985.
- Nicoli S, Penna E, Padula C, Colombo P, Santi P. New transdermal bioadhesive film containing oxybutynin: *In-vitro* permeation across rabbit ear skin. *Int J Pharm* 2006; 325:2-7.
- Babu RJ, Pandit JK. Effect of penetration enhancers on the release and skin permeation of bupranolol from reservoir-type transdermal delivery systems. *Int J Pharm* 2005; 288:325-334.
- Williams AC. *Transdermal and topical drug delivery*. Pharmaceutical Press, London, UK, 2003.
- Williams AC, Barry BW. Penetration enhancers. *Adv Drug Deliv Rev* 2004; 56:603-618.
- Sutariya VB, Mashru RC, Sankalia MG, Sankalia JM. Liquid chromatographic determination and pharmacokinetics study of salbutamol sulphate in rabbit plasma. *Ars Pharm* 2006; 47:185-197.
- Saha P, Kim KJ, Yamahara H, Crandall ED, Lee VHL. Influence of lipophilicity on beta-blocker permeation across rat alveolar epithelial cell monolayers. *J Control Release* 1994; 32:191-200.
- Tojo K, Chiang CC, Chien YW. Drug permeation across the skin: effect of penetrant hydrophilicity. *J Pharm Sci* 1987; 76:123-126.
- Williams AC, Barry BW. Essential oils as novel human skin penetration enhancers. *Int J Pharm* 1989; 57:R7-R9.
- Egyptian guidelines for asthma management. The Egyptian society of chest diseases and tuberculosis. *Egypt J Chest Diseases and Tuberculosis* 1999; 42 (suppl 2):1-37.
- The Pharmacopoeia of the United States of America 27, The National Formulary 22 (Asian ed). Pharmacopoeial Convention, Inc., Rockville, MD, USA, 2004; pp.

- 454-458.
28. Clearly GW. Transdermal controlled release systems. In: Medical Applications of Controlled Release. Vol 1 (Langer RS, Wise DS, eds). CRC Press, Boca Raton, FL, USA, 1984; pp. 204-251.
 29. Lim LY, Wan LSC. The effect of plasticizers on the properties of polyvinyl alcohol films. Drug Dev Ind Pharm 1994; 20:1007-1020.
 30. Gander B, Gurny R, Doelker E. Pharmaceutical Technology: Controlled Drug Release (Rubinstein MH, ed.) volume 1, Ellis Horwood Series. Wiley and Sons, New York, USA, 1987; p. 34.
 31. Lim LY, Wan LSC. Combined effects of heat treatment and plasticizers on polyvinyl alcohol films. Drug Dev Ind Pharm 1995; 21:369-373.
 32. Rowe RC, Sheskey PJ, Weller PJ. Handbook of Pharmaceutical Excipients, 4th ed. American Pharmaceutical Association, Pharmaceutical Press, London and Chicago. 2003.
 33. Lin SY, Lee CJ, Lin YY. The effect of plasticizers on compatibility, mechanical properties, and adhesion strength of drug-free Eudragit E films. Pharm Res 1991; 8:1137-1143.
 34. Guyot M, Fawaz F. Design and *in-vitro* evaluation of adhesive matrix for transdermal delivery of propranolol. Int J Pharm 2000; 204:171-182.
 35. Shah VP, Tymes NW, Yamamoto LA, Skelly JP. *In-vitro* dissolution profile of transdermal nitroglycerin patches using paddle method. Int J Pharm 1986; 32:243-250.
 36. O'Neill CT, Deasy PB. Development and evaluation using hairless mouse skin of a transdermal timolol product. Int J Pharm 1988; 48:247-254.
 37. Cevc G, Blume G. New, highly efficient formulation of diclofenac for the topical, transdermal administration in ultradeformable drug carriers. Bioch Biophys Acta 2001; 1514:191-205.
 38. Ongpipattanakul B, Burnette RR, Potts RO, Francoeur ML. Evidence that oleic acid exists in a separate phase within stratum corneum lipids. Pharm Res 1991; 8:350-354.
 39. Tanojo H, BosvanGeest A, Bouwstra JA, Junginger HE, Bodde HE. *In-vitro* human skin barrier perturbation by oleic acid: thermal analysis and freeze fracture electron microscopy studies. Thermochim Acta 1997; 293:77-85.
 40. Southwell D, Barry BW. Penetration enhancers for human skin: mode of action of 2-pyrrolidone and dimethylformamide on partition and diffusion of model compounds water, *n*-alcohols and caffeine. J Invest Dermatol 1983; 80:507-515.

(Received June 9, 2008; Revised September 5, 2008; Accepted September 13, 2008)

Original Article

Establishment of a cell-based assay to screen insulin-like hypoglycemic drugs

Li Zhang, Juan-juan Hu, Guan-hua Du*

Institute of Materia Medica, Chinese Academy of Medical Sciences/Peking Union Medical College, Beijing, China.

ABSTRACT: This study sought to establish a cell-based assay to screen insulin analogs. Previous studies have proposed that up-regulation of glucose consumption may have the same anti-diabetic effects as insulin. Here, the amount of glucose that disappeared in culture medium after incubation with insulin or drugs was determined and served as an indicator of the glucose consumption of the cells. In order to establish a cellular model to screen insulin analogs, the sensitivities of four cell lines - BALB/c 3T3, HepG2, NIH3T3, and Bel7402 - to insulin were evaluated by detecting glucose consumption after incubation with insulin (0-125 nM) for 24 h. BALB/c 3T3 was more sensitive to insulin than the other three cell lines. Insulin elevated glucose consumption of BALB/c 3T3 in a concentration- and time- manner. Glucose consumption of BALB/c 3T3 increased by 30% after incubation with insulin (30 nM) for 24 h. Insulin increased the proliferation of BALB/c 3T3 at 48 h. A model was established by detecting glucose consumption after treating BALB/c 3T3 with drugs for 24 h. Using the cell-based assay, we screened more than two thousand samples from Traditional Chinese Medicine (TCM). Five extracts exhibiting glucose absorbance in medium were identified, indicating a hit rate of 0.5%. Results suggested that a cell-based assay by detection of glucose consumption in BALB/c 3T3 was suitable for high-throughput screening and was feasible to identify insulin-like hypoglycemic drugs. Five hits were discovered from natural products. Further characterization of these active extracts could help to identify potential anti-diabetic drugs.

Keywords: BALB/c 3T3 cell, Insulin analogs, Glucose consumption, Drug screening

*Correspondence to: Dr. Guan-hua Du, Institute of Materia Medica, Chinese Academy of Medical Sciences /Peking Union Medical College, Beijing 100050, China;
e-mail: dugh@imm.ac.cn

1. Introduction

Diabetes is a chronic metabolic disorder affecting approximately five percent of the population of industrialized nations. Insulin is essential for maintaining glucose homeostasis and regulating carbohydrate, lipid, and protein metabolism. The pathogenesis of type II diabetes includes insulin resistance and a relative deficiency in insulin secretion. Insulin stimulates a variety of cellular metabolic changes, such as glucose uptake and glycogen and lipid synthesis. The main assays for activity of insulin analogs have been reported to use radioisotopes (1,2). In order to find leading compounds for new insulin-like hypoglycemic drugs, a simple and sensitive high-throughput screening model that does not require radioisotopes must be established.

This study established a cell-based screening method by assaying glucose consumption. More than 2,000 samples including compounds and natural products were screened using this cellular model. The samples were derived from Traditional Chinese Medicine (TCM). DF007, DF052, DF167, DF262, and DF432 (lab serial numbers) were identified as accelerating glucose consumption in a BALB/c 3T3 cell line. These active extracts may provide potential anti-diabetic drugs and warrant further study.

2. Materials and Methods

2.1. Reagents

Insulin, MTT (3-(4,5-dimethyl-2-thiazolyl)-2,5-diphenyl-2H tetrazolium bromide), Pluronic F68, and a Glucose detection kit were obtained from Sigma. Dulbecco's modified Eagle's minimum essential medium (DMEM), RPMI 1640 medium, and Fetal bovine serum (FBS) were purchased from GIBICO. Metformin hydrochloride was purchased from Beijing Liling pharmaceutical Co. and dissolved in distilled normal saline.

2.2. Cell lines

BALB/c 3T3 was purchased from the Cell Center of Wuhan University. HepG2, NIH3T3, and Bel7402 were purchased from the Cell Center of Institute of Basic Medical Sciences, Chinese Academy of Medical Sciences.

2.3. Maintenance of cells

BALB/c 3T3 and HepG2 were maintained in DMEM culture medium including 10% FBS, 2 mM glutamine, 100 kU/L penicillin, 100 mg/L streptomycin, and a high glucose concentration (4.5 g/L) at 37°C, 5% CO₂. NIH3T3 and Bel7402 were maintained in culture medium RPMI1640 including 10% FBS, 2 mM glutamine, 100 kU/L penicillin, and 100 mg/L streptomycin at 37°C, 5% CO₂. Cells cultures that became confluent in culture flasks were used in the glucose consumption assay.

2.4. Glucose consumption assay

Cells were detached from the culture flask with a solution of 0.25% trypsin and 1 mM EDTA. Trypsin digestion was stopped by the complete culture medium. The cells were washed twice and resuspended in low-glucose (1.0 mg/mL) detection medium supplemented with 0.05% Pluronic F68, 0.2% bactopectone, and 2 mM glutamine. The cell density was regulated to a concentration of 1×10^5 /mL and cells were spread onto 96-well microtiter plates (100 µL per well). The cells were cultured with serial insulin (final concentration 0 - 125 nM) or samples at 37°C, 5% CO₂ for 4-48 h. At the end of incubation, 10 µL suspension per well or glucose standard medium (0-1,000 mg/L) was moved to another 96-well plate well by well. The glucose concentration remaining in suspension was measured by illumination in a glucose assay. Briefly, the reaction lasted 30 min at room temperature. The absorbance at 495 nm was determined with a Polarstar Microplate Reader. The glucose concentration left in medium was calculated by the standard curve of glucose. The percent of glucose consumption (*R_{gc}*) was calculated using the following formula and IC₅₀ was determined graphically.

$$R_{gc} = (A-B)/(A-C) \times 100$$

A, concentration of glucose in medium for the control; B, concentration of glucose in medium for sample groups; C, a blank control without cells in the same medium with the control. The glucose concentration was given in µg/mL.

2.5. MTT assay

BALB/c 3T3 cells were seeded at a density of 1×10^4

cells per well in 96-well microtiter plates and cultured with insulin (30 nM) in detection medium for 24-48 h at 37°C in an atmosphere 5% CO₂. The cells were stained with MTT by a modification of the method of Mosmann (3). Briefly, the suspension medium was removed and 100 µL MTT (final concentration 5 mg/L) were added to each well 4 h before the end of incubation. After culturing for 4 h, the suspension was discarded and 150 µL dimethyl sulfoxide (DMSO) per well were added. Absorbance was read at 540 nm with a Polarstar microplate reader.

2.6. Natural product extracts

All samples were from the Sample Library of this institute. Each TCM (2 kg) was finely milled and extracted with petroleum ether, 95% alcohol, and water in turn. The samples were dissolved in DMSO and diluted with normal saline. The final DMSO concentration was less than 0.1%.

2.7. Statistical analysis

Data were given as the mean ± S.D. and the differences were calculated with a Student's two-tail *t*-test. Values of *P* < 0.05 were considered to be statistically significant.

3. Results

3.1. Sensitivity of the four cell lines to insulin

BALB/c 3T3, HepG2, NIH3T3, and Bel7402 cell lines were incubated with serial diluted insulin for 24 h. Glucose consumption in medium was compared in different cells stimulated by insulin. As shown in Figure 1, insulin lowered glucose concentration in suspensions of BALB/c 3T3 and HepG2 in a dose-dependent manner. Glucose concentration tended to decrease in the suspension of Bel7402, but there was no change in glucose uptake of NIH3T3 in comparison to the control. BALB/c 3T3, HepG2, and Bel7402 were found to be sensitive to insulin. Of the cell lines, BALB/c 3T3 in particular had a high level of sensitivity, indicating its potential for use in a cell assay to screen hypoglycemic drugs.

3.2. Effect of insulin on glucose consumption in the BALB/c 3T3 cell line

Highly sensitive to insulin, the BALB/c 3T3 cell line was used to observe the dose-response and linear response curve of insulin on glucose consumption. As shown in Figure 2, insulin-accelerated glucose consumption in BALB/c 3T3 in a concentration- and time-dependent manner. Insulin of 31.25 nM was able to accelerate glucose consumption by 30% (Figure

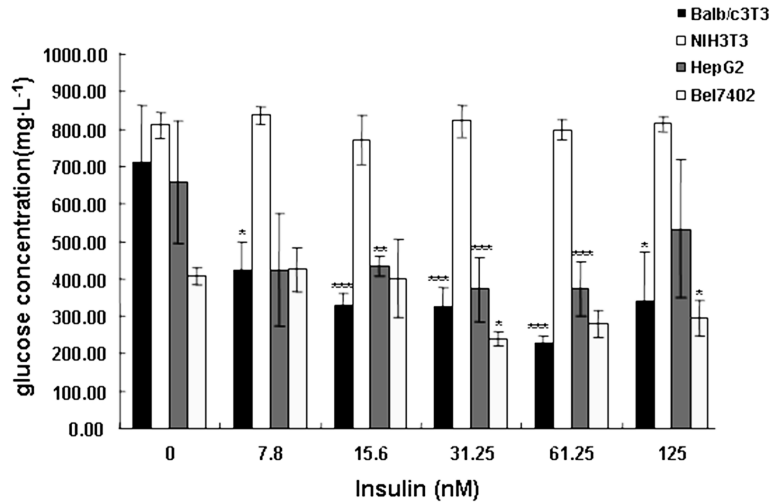


Figure 1. Sensitivity of different cells to insulin. BALB/c 3T3, NIH3T3, HepG2, and Bel7402 were treated with or without different concentrations of insulin for 24 h. Then, the glucose concentration remaining in suspension was measured as described in the Methods. All data are expressed as mean ± S.D. (n = 8). *P < 0.05, **P < 0.01, ***P < 0.001 vs. control cells without insulin treatment.

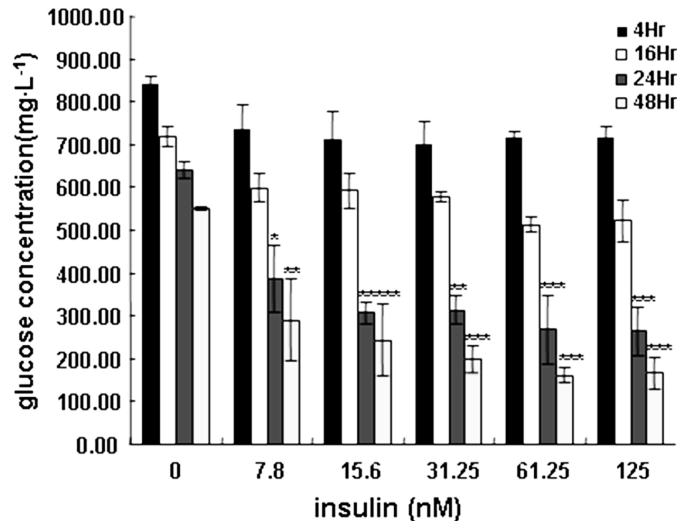


Figure 2. Dose-effect and time-dose relationships for insulin-induced glucose consumption in BALB/c 3T3. BALB/c 3T3 cells were treated with or without different concentrations of insulin for 24 h. The glucose concentration remaining in suspension was measured as described in the Methods. Values are expressed as mean ± S.D. (n = 8). **P < 0.01 compared to control cells without insulin treatment.

2). Glucose consumption at 24 h or 48 h was higher than that at 4 h and 16 h. In order to test the glucose consumption of BALB/c 3T3, the cells should be cultured with insulin for at least 24 h.

3.3. Effect of insulin on cell proliferation of the BALB/c 3T3 cell line

Because the glucose consumption was related to the number of cells, an experiment was performed to test cell proliferation. As shown in Table 1, insulin increased the proliferation of BALB/c 3T3 in time-dependent manner. There was marked difference between 31.25 nM insulin and the control at 48 h, and there was no significant difference at 24 h. An incubation time of 24 h proved suitable at eliminating the influence of cell numbers on glucose consumption.

Table 1. Effect of insulin on proliferation of BALB/c 3T3. BALB/c 3T3 cells were treated with or without insulin for 24 h or 48 h. Then, cell viability was determined by MTT assay. All data are presented as the mean ± S.D. of at least three independent experiments, n = 8

Insulin (nM)	24 h (OD)	48 h (OD)
0	0.89 ± 0.06	0.94 ± 0.05
7.8	0.87 ± 0.03	1.04 ± 0.08
15.6	0.92 ± 0.05	1.19 ± 0.04
31.25	0.94 ± 0.06	1.29 ± 0.05 ^a
62.5	0.96 ± 0.09	1.29 ± 0.09 ^a
125	0.99 ± 0.08	1.35 ± 0.06 ^a

^a P < 0.05 compared to the control.

3.4. Effect of metformin hydrochloride on glucose consumption in the BALB/c 3T3 cell line

Metformin hydrochloride accelerated glucose consumption in the BALB/c 3T3 cell line in a

Table 2. Effect of metformin hydrochloride on glucose consumption in BALB/c 3T3. BALB/c 3T3 cells were treated with or without insulin or metformin for 24 h. The glucose concentration remaining in suspension was measured as described in the Methods. Values are expressed as mean \pm S.D. ($n = 8$)

Group	Dose (M)	Glucose (mg/L)	% ^a
Control	-	644.56 \pm 55.79	
Insulin	3×10^{-8}	423.95 \pm 31.04 ^b	34.99
Metformin hydrochloride	7.55×10^{-4}	443.43 \pm 18.5 ^b	31.90
Metformin hydrochloride	7.55×10^{-5}	479.07 \pm 22.63 ^b	26.24
Metformin hydrochloride	7.55×10^{-6}	484.33 \pm 20.95 ^b	25.41
Metformin hydrochloride	7.55×10^{-7}	536.34 \pm 47.33	17.16
Metformin hydrochloride	7.55×10^{-8}	753.14 \pm 32.67	17.22

^a Glucose uptake (% of control) = (A-B)/(A-C) \times 100. A, control; B, sample; C, blank.

^b $P < 0.01$ compared to the control.

Table 3. Effect of test samples on glucose consumption in BALB/c 3T3 ($n = 8$)

Serial number of sample	Materia	Extract	IC ₅₀ (mg/L)
Control			-
DF007	<i>Alpinia oxyphylla</i> Miq.	Ether	84.48
DF052	<i>Croton tiglium</i> L.	Ether	53.72
DF167	<i>Angelica sinensis</i> Diels.	Ethanol	36.60
DF262	<i>Fructus trichosanthis</i>	Ethanol	58.50
DF432	<i>Polygonatum cyrtonea</i>	Ethanol	13.12

concentration-dependent manner. At a concentration of 7.55×10^{-6} M, metformin hydrochloride accelerated consumption at a rate of about 25.41% (Table 2).

3.5. Effect of test samples on glucose consumption in the BALB/c 3T3 cell line

There were more than 2,000 samples for screening using the model. DF007, DF052, DF167, DF262, and DF432 were identified as significantly accelerating glucose consumption and warranting further investigation. These samples exhibited an IC₅₀ at 84.48, 53.72, 36.60, 58.50, and 13.12 mg/L (Table 3). These samples were extracted from TCM. DF007 and DF052 were petroleum ether extracts from *Alpinia Oxyphylla* and *Croton Tiglium*, respectively. DF167, DF262, and DF432 were EtOH extracts from *Angelica Sinensis Diels*, *Fructus Trichosanthis*, and *Polygonatum*, respectively.

4. Discussion

Type II diabetes accounts for the vast majority of cases of diabetes (4). Discovery of oral insulin-mimetic agents has been a long-standing goal of pharmaceutical research. The target cells of insulin include fat cells, hepatic cells, muscle cells, and fibrosis cells. Several reports showed that 3T3-L1 (a prefat cell) provided a cell model to study the mechanism of insulin resistance or effects of anti-hyperglycemic agents (5,6). In the current study, the

four cell lines of BALB/c 3T3 (a fibrosis cell line), HepG2 (a hepatic cell line), Bel7402 (a hepatic cell line), and NIH3T3 (a fibrosis cell line) were used to develop a high-throughput screening model by metabolic assay. BALB/c 3T3 is a fibroblast cell line that has been used to quantify insulin-like growth factor (IGF) bioactivity with stimulation of cell proliferation and glucose consumption (7). HepG2 is a hepatic embryo tumor cell line and has the same morphology and function of hepatic cells (8). Bel7402 was from a human hepatic tumor. The current study found that NIH3T3 was not sensitive to insulin, and glucose concentration in remaining medium tended to decrease for HepG2 and Bel7402. NIH3T3 was not sensitive to insulin because it had no endogenous insulin receptors. However, the results did indicate that BALB/c 3T3 had a high level of sensitivity to insulin, making it the best candidate cell line for use in the screening model. MTT assay revealed that insulin (31.25 nM) did not cause a change in the number of BALB/c 3T3 cells after 24 h of culturing. Results demonstrated that the effect of cell proliferation on glucose consumption was minimized by incubating BALB/c 3T3 cells with insulin or samples for 24 h.

Results showed that in BALB/c 3T3 cells metformin hydrochloride reduced levels of glucose remaining in medium. This suggests that the cell-based assay is appropriate and consistent. TCMs have historically been a prolific source of therapeutically useful drugs. Results also identified five active samples that were petroleum ether extracts or EtOH extracts from TCMs; the glucose consumption of these samples was evaluated using high-throughput screening. In order to identify leading compounds, these samples must be further separated and purified and subjected to structure-activity analysis and structural modification.

Of course, active samples identified by this model may have many potential effects, such as activating insulin and insulin growth factor (IGF) receptors, stimulating Glut4 transporter, or activating tyrosine kinase (IRTK) activity. In order to identify the mechanism at work, positive samples should be tested for activation of insulin receptor signaling. Phosphorylation of insulin receptor substrate-1 could be tested by using SDS-PAGE and Western blotting analysis. If they activate IRS-1 phosphorylation, the samples may be insulin-mimetic agents.

The indicator used by the cell-based assay was glucose consumption. Traditional methods of detecting glucose metabolism included measuring glucose absorbance or detecting hepatic products and fatty acids. These assays require radiolabeled metabolites. In the current study, however, glucose consumption was assayed colorimetrically with no need for radioisotopes. In conclusion, this cell-based assay is simple, inexpensive, and suitable for screening of insulin-like hypoglycemic drugs.

Acknowledgments

This work was supported by the International Science and Technology Cooperation Project (Project No. 2006DFA31420).

References

1. Du HJ, Shi JH, Cui DF, Zhang Y. Insulin analogs with B24 or B25 phenylalanine replaced by biphenylalanine. *Acta Biochim Biophys Sin* 2008; 40:133-139.
2. Romero R, Casanova B, Pulido N, Suarez AI, Rodriguez E, Rovira A. Stimulation of glucose transport by thyroid hormone in 3T3-L1 adipocytes: increased abundance of GLUT1 and GLUT4 glucose transporter proteins. *J Endocrinol* 2000; 164:187-195.
3. Mosmann T. Rapid colorimetric assay for cellular growth and survival application to proliferation and cytotoxicity assays. *J Immunol Method* 1983; 65:55-63.
4. Shinkai H. Novel antidiabetic agents. *Exp Opin Ther Patents* 2000; 10:59-66.
5. Ross SA, Chen X, Hope HR, Sun S, McMahon EG, Broschat K, Gulve EA. Development and comparison of two 3T3-L1 adipocyte models of insulin resistance: increased glucose flux vs glucosamine treatment. *Biochem Biophys Res Commun* 2000; 273:1033-1041.
6. Luan WW, Deng LY, Dong RN, Qiang H, Li L, Li W, Dai RJ, Yu YH. Optimization and application of Mice's Adipocyte Model for DM Drug Screening. *Life Science Instrument* 2006; 4:3-8.
7. Okajima T, Nakamura K, Zhang H, Ling N, Tanabe T, Yasuda T, Rosenfeld RG. Sensitive colorimetric bioassays for insulin-like growth factor (IGF) stimulation of cell proliferation and glucose consumption: use in studies of IGF analogs. *Endocrinology* 1992; 130:2201-2212.
8. Simpson AM, Tuch BE, Swan MA, Tu J, Marshall GM. Functional expression of the human insulin gene in a human hepatoma cell line (HepG2). *Gene Ther* 1995; 2:223-231.

(Received June 16, 2008; Revised July 29, 2008; Accepted August 1, 2008)

Original Article**Inhibition of *in vivo* angiogenesis by *Anacardium occidentale* L. involves repression of the cytokine VEGF gene expression**

Sheela M. Lingaraju, Kaveri Keshavaiah, Bharathi P. Salimath*

Department of Studies in Applied Botany and Biotechnology, University of Mysore, Manasagangotri, Mysore, India.

ABSTRACT: Lethal tumor growth and progression cannot occur without angiogenesis, which facilitates cancer cell proliferation, survival, and dissemination. Among the many growth factors and cytokines engaged in angiogenesis, the cytokine vascular endothelial growth factor (VEGF) is regarded as the most potent and specific. Angiogenesis inhibitors are recognized as potentially useful agents for treating angiogenesis-associated diseases and VEGF represents a promising and well-studied target for antiangiogenic agents. In this study, we have tested the crude ethanolic extract of the leaves of *Anacardium occidentale* Linn, on Ehrlich ascites tumor cells (EAT) *in vivo* and *in vitro*. *Anacardium occidentale* extract (AOE) was able to suppress VEGF-induced angiogenesis *in vivo* in the chorioallantoic membrane, rat cornea, and tumor-induced angiogenesis in the peritoneum of EAT-bearing mice. The extract inhibited cell proliferation of different tumor cells such as EAT, BeWo, and MCF-7 *in vitro* in a dose-dependent manner and it reduced the VEGF level in the ascites of treated mice. A decrease in the microvessel density count and CD31 antigen staining of treated mice peritoneum provide further evidence of its antiangiogenic activity. Our results from Northern blot analysis and ELISA demonstrate that AOE can downregulate endogenous VEGF gene expression at the mRNA and protein level. Furthermore, results of our gene analysis of VEGF-promoter luciferase reporter indicated that this effect is mediated by transcriptional repression of VEGF promoter activity in EAT cells treated with AOE. Taken together, the data suggest that the VEGF system of angiogenesis is the molecular target for the antiangiogenic action of AOE.

Keywords: Angiogenesis, Ehrlich ascites tumor cells, VEGF, *Anacardium occidentale*

*Correspondence to: Dr. Bharathi P. Salimath, Department of Applied Botany and Biotechnology, University of Mysore, Manasagangotri, Mysore-570006, India; e-mail: salimathuom@rediffmail.com

1. Introduction

Tumor angiogenesis is a critical component of tumor growth and metastasis, and the targeting of the vascular supply of tumors is an intense field of interest, with many promising preclinical trials highlighting the potential effectiveness of this form of therapy (1). Increased vascularity may allow not only an increase in tumor growth but also greater enhancement of hematogenous tumor embolization. Thus, inhibiting tumor angiogenesis may halt tumor growth and decrease the metastatic potential of tumors. Generated from a variety of tumors, the cytokine vascular endothelial growth factor (VEGF) is the most important angiogenic factor associated closely with induction and maintenance of the neovasculature in tumors (2), so the inhibition of VEGF expression by tumor cells is known to have an impact on angiogenesis-dependent tumor growth and metastasis.

A balance between angiogenic and anti-angiogenic factors has given rise to a significant interest in the use of exogenous anti-angiogenic agents for the treatment of solid tumors, and research has demonstrated that anti angiogenic treatment retards tumor growth (3). Although new chemotherapeutic drugs of both synthetic and natural origin are occasionally discovered, there is no satisfactory cure for a disease like cancer. Thus, an important step is to screen antineoplastic compounds from plants either in the form of crude extract or as a component isolated from them (4). Anticancer agents from medicinal plants appear to be satisfactory for the control of diseases and prolonging the life of the patient. There has been a continuous search for compounds to use in the prevention or treatment of cancer, and especially for agents with reduced toxicity.

Oriental herbal medicine has been used since ancient times to treat malignancies. Systematic characterization of active phytochemicals in medicinal herbs and their mechanisms of action are important for providing the rationale for their efficacy and for transforming herbal practices into evidence-based medicine. Several studies have shown that extracts from a number of herbal medicines or mixtures have anticancer potential *in vitro*, *in vivo*, or both (5-8). For example, alcohol extracts of

Ganoderma lucidum can induce apoptosis in MCF-7 human breast cancer cells (6). An aqueous extract of *Paeonia lactiflora* can inhibit growth of Hep G₂ and Hep 3B hepatoma cells (8) whereas aqueous extracts of Bu-Zhong-Yi-Qi Tang (a mixture of 10 herbs) have also suppressed growth of hepatoma cells (7). The water soluble ingredients of Sho-saiko-To (a mixture of 7 herbs) inhibit proliferation of KIN-1 human hepatoma cells and KMC-1 cholangiocarcinoma cells (9). Finally, PESPEs (a mixture of 8 herbs) was developed for clinical treatment of prostate cancer and has been shown to inhibit growth of colon cancer cells (10). The crude methanolic extracts obtained from *Hypericum caprifoliatu* and *Hypericum myrianthum* have shown an antiproliferative effect on HT-29 human colon carcinoma cells and H-460 non-small cell lung carcinoma (11). A crude aqueous *Sutherlandia frutescens* whole plant extract has been found to induce cytotoxicity in neoplastic cells (cervical carcinoma) and CHO (Chinese Hamster Ovary cells) cell lines (12). The antiangiogenic and pro-apoptotic effect of the hexane fraction of *Tinospora cordifolia* on Ehrlich ascites tumor (EAT) cells has also been investigated (13).

The cashew, *Anacardium occidentale* Linn., is a multipurpose tree that provides numerous resources and products. The bark and leaves of the tree are used medicinally and the cashew nut has international appeal and market value as a food. Clinical studies have documented this tree's action as an antiseptic, antidysenteric, antibacterial, antiulcerative, antidiabetic, cough suppressant, decongestant, diuretic, febrifuge, refrigerant, and astringent (14). The active principles are thought to be tannins, anacardic acid, and cardol. Research has shown that these chemicals curb the darkening effect of aging by inhibiting tyrosinase activity and that they are toxic to certain cancer cells. Anacardol and anacardic acid have shown some activity against Walker carcinosarcoma. Anacardic acid isolated from the nut shell liquid of *A. occidentale* L. has been found to have antibacterial activity against *Streptococcus mutans* ATCC 25175 (15). The hydroethanolic extract of *A. occidentale* leaves has been shown to have an antiulcerogenic effect (14). *Semecarpus anacardium* Linn of the family *Anacardiaceae* has been tested for its antitumor activity against mammary carcinoma in animals (16). The mechanism of antitumor activity of *Semecarpus anacardium* seems to be through the suppression of hypoxic and angiogenic factors (17). *Semecarpus anacardium* nut oil has been shown to have an apoptotic effect on the following human tumor cell lines: acute myeloblastic leukemia (HL-60), chronic myelogenous leukaemia (K-562), breast adenocarcinoma (MCF-7), and cervical epithelial carcinoma (HeLa) (18). The current study attempts to identify whether the leaf extract of *Anacardium occidentale* L. inhibits tumor growth *in vivo*. This is the first report of the antiproliferative effect of *Anacardium occidentale* L. extract (AOE) on different tumor cell lines *in vitro*

and the antiangiogenic effect of AOE *in vivo* through propagation of ascetic transplantable tumors like EAT that grow as cell suspensions in the intraperitoneal cavity of mice.

2. Materials and Methods

Swiss albino mice (6-8 weeks old) were obtained from the animal house, Department of Zoology, University of Mysore, Mysore, India. EAT (mouse mammary carcinoma) cells are maintained in our laboratory and are routinely used for *in vivo* transplantation. BeWo (Choriocarcinoma), MCF-7 (Breast cancer) and HEK 293 (Human embryonic kidney) cell lines were from the National Center for Cell Science, Pune, India. [³H]thymidine and α-[³²P]ATP were from the Baba Atomic Research Center, Mumbai, India. DMEM, FBS and penicillin-streptomycin were from Invitrogen, USA. DMEM/Ham's nutrient mixture F-12 and poly-2-hydroxyl ethylmethacrylate were from Sigma Aldrich, USA. Fertilized eggs were from a government poultry farm in Bangalore, India. Anti-CD31 antibody was from Santa Cruz Biotechnology, CA, USA. A mammalian transfection kit and β-galactosidase assay kits were from Stratagene, USA. A luciferase reporter assay kit was from BD Bioscience, USA. An RNeasy kit was procured from Qiagen, USA. All other reagents were of the highest analytical grade.

2.1. Plant material

The leaves of *Anacardium occidentale* L were collected from the campus of the University of Mysore, Manasagangotri, Mysore, Karnataka, India, in April 2007 and identified by a taxonomist. Identification was confirmed by depositing the voucher specimens in the Herbarium of the Department of Botany, University of Mysore, Mysore (voucher specimen number: UOM. BOT.0133) and by comparing them with available voucher specimens. The leaves were dried in the shade and powdered. The dried leaf material (1 g) was extracted exhaustively with 100 mL of 50% ethanol at room temperature for a period of seven days. Ethanol removal was done by evaporation in order to obtain crude ethanolic AOE of the leaves at a concentration of 1 mg/0.05 mL. The sample was further diluted in saline to obtain the required concentrations for each assay.

2.2. *In vitro* culture of EAT, BeWo, MCF-7, and HEK 293 cells

EAT, MCF-7, and HEK 293 cells were cultured in Dulbecco's modified Eagle's medium (DMEM) supplemented with 10% fetal bovine serum (FBS), 100 units/mL penicillin and 100 µg/mL streptomycin. BeWo cells were cultured in DMEM/Ham's nutrient mixture F-12 medium with 10% FBS, 100 units/mL penicillin,

100 µg/mL streptomycin, and 250 µg/mL amphotericin. All cell lines were incubated in a humidified atmosphere of 37°C and 5% CO₂. When cells reached confluency, they were passaged by trypsinizing with trypsin/EDTA and were then used for the experiments.

2.3. Tumor and normal cell proliferation assay

A proliferation assay was carried out as described previously (19) in tumor and normal cells. To verify the *in vitro* effect of AOE on proliferation of EAT, BeWo, MCF-7, and HEK 293 cells, 50,000 cells/well were seeded in 12-well plates in their respective media and grown in 5% CO₂ at 37°C for 2 days. The sample was filter sterilized and diluted with cell culture medium (1 µg/µL). On the 3rd day, [³H]thymidine (1 µCi/mL medium) was added and AOE was tested at the concentrations of 0.0, 1.0, 5.0, 10.0, and 50 µg/mL. After 48 h, the cells were trypsinized and washed with phosphate buffered saline (PBS); high molecular weight DNA was precipitated using 10% ice-cold trichloroacetic acid. Scintillation fluid (5 mL) was added to all of the samples and radioactivity was determined with a liquid scintillation counter. Each concentration of AOE was then plotted against the percentage cell survival. A dose-response curve was thus generated and the IC₅₀, *i.e.* the concentration of the extract required to inhibit cell growth by 50%, was determined.

2.4. *In vivo* angiogenesis assays

2.4.1. Chorioallantoic membrane (CAM) assay

Chorioallantoic membrane (CAM) assay was carried out in accordance with the method described previously (20). In brief, fertilized eggs were incubated at 37°C in a humidified and sterile atmosphere for 10 days. Under aseptic conditions, a window was made on the eggshell to check for proper development of the embryo. The window was resealed and the embryo was allowed to develop further. On the 12th day, saline, recombinant cytokine VEGF (50 ng per egg) or AOE (100 µg per egg) was air dried on sterile glass cover slips. The window was reopened and the cover slip was inverted over the CAM. The window was closed again, and the eggs were returned to the incubator for another 2 days. The windows were opened on the 14th day and inspected for changes in the vascular density in the area under the coverslip and photographed at 40 × magnification.

2.4.2. Corneal micropocket assay/Rat cornea assay

A corneal micropocket assay was performed in accordance with the method described previously (21). In brief, for the pellet preparation, hydron polymer poly-2-hydroxyethylmethacrylate was dissolved in ethanol to a final concentration of 12%. An aliquot of the Hydron/

EtOH solution was added to VEGF (1 µg/pellet) with or without AOE (100 µg/pellet). Aliquots of 10 µL of 12% Hydron/EtOH alone (Group 1), with cytokine VEGF (Group 2), and with VEGF and AOE (Group 3) were placed onto a teflon surface and allowed to air dry for at least 2 h. Male Wister rats weighing 300-350 gms were anesthetized with a combination of xylazine (6 mg/kg, IM) and ketamine (20 mg/kg, IM). The eyes were topically anesthetized with 0.5% proparacaine and gently proptosed and secured by clamping the upper eyelid with a non-traumatic hemostat. A corneal pocket was made by inserting a 27-gauge needle, with the pocket's base 1 mm from the limbus. A single pellet was advanced into the lamellar pocket to the limbus using corneal forceps. The rats were observed for 24-72 h for the occurrence of non-specific inflammation and localization of the pellets. On day 7, the rats were anesthetized and the corneas were photographed using a CCD camera (40 ×).

2.4.3. *In vivo* growth of EAT cells and peritoneal angiogenesis assay

EAT cells or mouse mammary carcinoma cells (5×10^6) were injected intraperitoneally into mice and growth was recorded every day until the 12th day. These cells grow in the mice peritoneum, forming an ascites tumor with massive abdominal swelling. The animals show a dramatic increase in body weight over the growth period and animals succumbed to the tumor burden 14-16 days after transplantation.

To verify whether the AOE extract inhibited tumor growth and angiogenesis mediated by EAT cells *in vivo*. Leaf extract 133 mg/kg body weight was injected into the peritoneum of the EAT-bearing mice every day after the 6th day of transplantation. The body weight of the mice was monitored from the 1st day till the 12th day. The animals were sacrificed on the 7th to 12th day, 2ml of saline was injected (*i.p.*), and a small incision was made in the abdominal region to collect the tumor cells along with ascites fluid. The EAT cells and ascites fluid were harvested into a beaker and centrifuged at 3,000 rpm for 10 min. The ascites volume was measured by subtracting the volume of saline injected while harvesting the EAT cells from the total ascites volume measured. The pelleted cells were counted by trypan blue dye exclusion using a hemocytometer. The animals were dissected to observe the effect of the extract on peritoneal angiogenesis. All experiments were conducted according to the guidelines of the Committee for the Purpose of Control and Supervision of Experiments on Animals (CPCSEA), Government of India, India.

2.4.4. Mouse survivability assay

A mouse survival assay was performed on EAT mice treated with AOE (133 mg/kg body weight) or not every day after the 6th day of transplantation. About 20 EAT-

bearing animals were used in this study; 10 served as a control and the remaining 10 were treated with AOE. The mice were weighed every day starting after the 1st day of tumor transplantation and weighing continued for the duration of their life span. Mice were assessed for mortality twice daily, in the early morning and late afternoon. Mice were euthanized upon reaching the criteria for morbidity. Deaths occurring overnight were recorded the next morning.

2.5. Immunohistological analysis (H and E staining) for microvessel density scoring

To determine whether AOE inhibits microvessel density, the effect of the extract on the angiogenic response induced by the cytokine VEGF was verified in EAT-bearing mice. EAT-bearing mice were treated regularly with the extract after the 6th day of transplantation. On the 12th day, the animals were sacrificed and the peritoneum from treated or untreated mice was fixed in 10% formalin. Sections (5 µm) were made from paraffin embedded peritoneum and stained with hematoxylin and eosin. Microvessel counts were done using a Leitz-DIAPLAN microscope with attached CCD camera and photographs were taken at 40 × magnification.

2.6. CD31 immunostaining for proliferating endothelial cells in peritoneal blood vessels

The effect of the extract on proliferating blood vessel endothelial cells was determined by staining the paraffin sections with anti-CD31 antibody as described previously (22). Peritoneum sections were processed as per the protocol supplied by the manufacturer. In brief, sections were dewaxed in xylene, rehydrated in descending concentrations of ethanol, and washed in distilled water. Antigen retrieval was done by heating the sections at 95°C for 15 min. The sections were treated with 3% H₂O₂ in PBS to block endogenous peroxidase activity. They were blocked in blocking serum for 30 min to reduce non-specific binding and were incubated with anti-CD31 (PECAM-1) antibodies overnight at 4°C. Following PBS washing, slides were incubated with secondary antibody (biotinylated rabbit anti-mouse IgG) for 1h at room temperature followed by ABC reagent for 45 min. Antigen and antibody complex was detected using a substrate (DAB, 100 µL/section) for 5 min. Subsequently, the slides were counter-stained with 2% hematoxylin for 5-7 min and washed again in tap water thrice for 5 min each. The slides were washed successively for 2 min each in 50% ethanol, 80% ethanol, and absolute alcohol. After a xylene wash, the slides were mounted using Entellan mountant solution and the sections were evaluated using a DIAPLAN light microscope and photographed (40 ×).

2.7. Northern blot analysis

Total RNA was extracted from untreated EAT cells and EAT cells treated with AOE (1 mg/mL of cells) at regular time intervals starting at 0-4 h using an RNeasy kit according to the instructions from the manufacturer. Total RNA (20 µg) was separated by 1.2% agarose-formaldehyde gel electrophoresis and blotted onto a nylon membrane that was baked and hybridized with α [³²P]-dATP-labeled VEGF₁₆₅. The hybridized blot was processed and transferred to IP, and the image was scanned with a phosphoimage analyzer. After scanning, the blots were stripped and reprobed for expression of GAPDH as an internal control using labeled GAPDH cDNA.

2.8. VEGF-enzyme linked immunosorbent assay (VEGF-ELISA)

VEGF-ELISA was done using ascites fluid collected from treated or untreated mice as described previously (23). In brief, 100 µL of ascites sample from AOE-treated or untreated mice were coated onto 96-well microplates using a coating buffer at 4°C overnight. Wells were washed and blocked with blocking buffer (5% skimmed milk powder in PBS) for 2 h at 37°C, followed by incubation with anti-VEGF₁₆₅ antibodies (1:1,000). Recombinant anti-mouse VEGF₁₆₅ was used to set up the standard curve. After incubation for 2 h, the wells were washed before they were treated with 100 µL/well of goat anti-rabbit IgG conjugated to alkaline phosphatase (1:2,000). Incubation was continued for another 2 h at room temperature, and plates were washed prior to addition of 100 µL of the substrate *p*-nitro-phenyl phosphate (*p*-NPP). After incubation for 30 min at room temperature, the reaction was terminated by adding 0.1 N NaOH and the absorbance at 405 nm was measured with a Medispec ELISA reader.

2.9. Transient transfection and luciferase assay

To determine the effect of AOE on tumor or normal cells, EAT and HEK 293 cells were respectively transfected with 2 µg of VEGF promoter-luciferase reporter constructs containing the 5' flanking region (-2068 bp) of the human VEGF gene promoter coupled to the promoterless luciferase reporter gene vector pCDNA3 and 2 µg of the β-galactosidase expression vector β-Gal. Transient transfection assays were performed using a calcium phosphate transfection kit according to the manufacturer's instructions. In brief, 2 × 10⁵ cells were seeded in 6-well plates and cultured to 60-70% confluency. The transfected cells were cultured further for 20 h followed by incubation with or without AOE (0.0, 1.0, 5.0, 10.0, and 50 µg/mL). Cells were washed once with PBS and lysed with reporter lysis buffer. Luciferase (Luc) activity of

the cell extract was determined using the luciferase assay system. β -Galactosidase (β -Gal) activity was determined by measuring hydrolysis of *O*-nitrophenyl β -D-galactopyranoside using 50 μ L of cell extract at 37°C for 2 h. Absorbance was measured at A_{405} . Luciferase activity was determined using 50 μ L of cell extract. The reaction was initiated by injection of 100 μ L of luciferase assay substrate. Relative Luc activity (defined as VEGF reporter activity) was calculated as Luc (relative light units per 50 μ L cell extract)/ β -Gal activity (A_{405} per 50 μ L cell extract per 2 h).

2.10. Plant extraction

To further verify the chemical nature of the specific fraction, the dried plant powder of *A. occidentale* was extracted sequentially from non-polar to polar solvents, namely petroleum ether-hexane-benzene-chloroform-ethylacetate-acetone-methanol and ethanol. The solvents were evaporated with a rotary evaporator and all of the fractions (100 μ g/dose) were tested for antiangiogenic activity *in vivo* in the EAT model.

2.11. Statistical analysis

Effects of various groups on various biological outcomes were statistically evaluated using analysis of variance and by use of a Student's *t*-test; levels of significance were evaluated with the *p* value. All experiments were repeated at least three times to ensure reproducibility. The results are expressed as means \pm SE, with *p* < 0.05 considered to be statistically significant.

3. Results

3.1. AOE inhibits *in vitro* proliferation of tumor cells

EAT, BeWo, MCF-7, and untransformed HEK 293 tumor cells were used to verify if AOE inhibits the proliferation of tumor or normal cells *in vitro*. AOE inhibited proliferation of different tumor cell lines in a dose-dependent manner. As shown in Figures 1 A, B, C and D, a maximum of 80%, 85%, 70%, and 20% inhibition of proliferation was seen in EAT, BeWo, MCF-7, and HEK 293 cells, respectively. When compared to the effect of AOE on tumor cells, little or no effect was seen with untransformed normal HEK 293 cells. The IC_{50} of the extracts are shown in Table 1. The IC_{50} of AOE on EAT, BeWo, and MCF-7 cells was at concentrations between 1-20 μ g/mL. AOE had a very similar inhibitory effect on all three cell lines. The IC_{50} shows 50% inhibition of growth of cells at a given concentration. Here, a higher IC_{50} value means a less toxic extract. The IC_{50} of AOE on HEK -293 cells was significantly greater than that on other cell lines, indicating that AOE was less toxic to normal cells than to cancer cell lines.

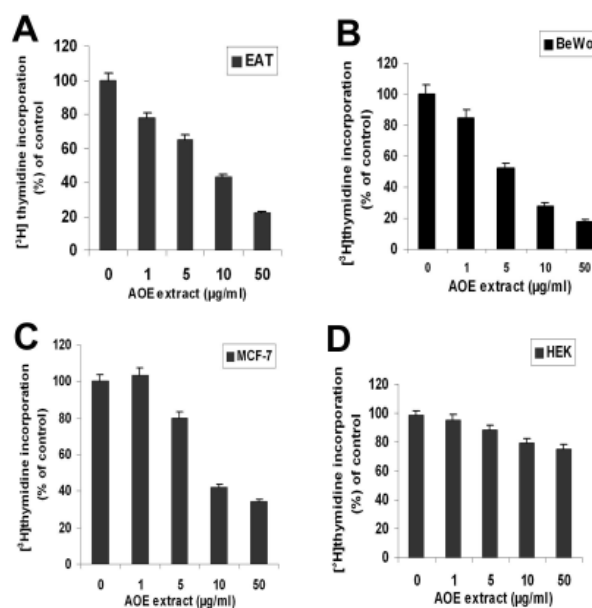


Figure 1. Effect of AOE on proliferation of normal and tumor cell lines. EAT (A), BeWo (B), MCF-7 (C), and HEK 293 cells (D); cells (50,000/well) were treated with AOE or left untreated in the presence of [3 H] thymidine (1 μ Ci/mL). After 48 h of incubation, the incorporated [3 H] thymidine into the cells was quantified by scintillation counting. All data are presented as the mean from three different experiments with triplicates and means of \pm S.E.M.

Table 1. Antiproliferative activity (IC_{50} value, μ g/mL) of the crude ethanolic extract of *Anacardium occidentale* L

Sample	EAT	BeWo	MCF-7	HEK-293
AOE	8.11469	5.54608	15.85254	597.36224

3.2. Angioinhibitory effect of AOE

The CAM assay and rat cornea assay are commonly used for *in vivo* validation of the angioinhibitory activity of antiangiogenic molecules. Results shown in Figures 2A and B indicate that AOE has a direct effect on inhibition of angiogenesis in an *in vivo* model system. When compared to the extensive angiogenesis seen in VEGF-treated CAM and rat cornea, angiogenesis at the site of the application of AOE was significantly reduced.

3.3. *In vivo* treatment of AOE inhibits growth of EAT cells and extends the survival period

The result in Figure 3A indicates that control EAT-bearing mice had a gradual increase in body weight of about 8-10 gms when 5×10^6 cells were injected on day zero. When compared to the body weight of control EAT-bearing mice on day 12, the body weight of the treated mice decreased significantly by about 50%, indicating the effect of the extract in preventing the growth of tumor cells. In a fully grown ascites tumor, a volume of 8-9 mL of ascites is usually generated during the tumor growth period of 12 days. In AOE-treated mice, the volume of ascites was about 1-2 mL (Figure 3B). The number of viable cells in full-grown EAT-bearing mice is about 48×10^6 /mouse while this number was reduced in AOE-

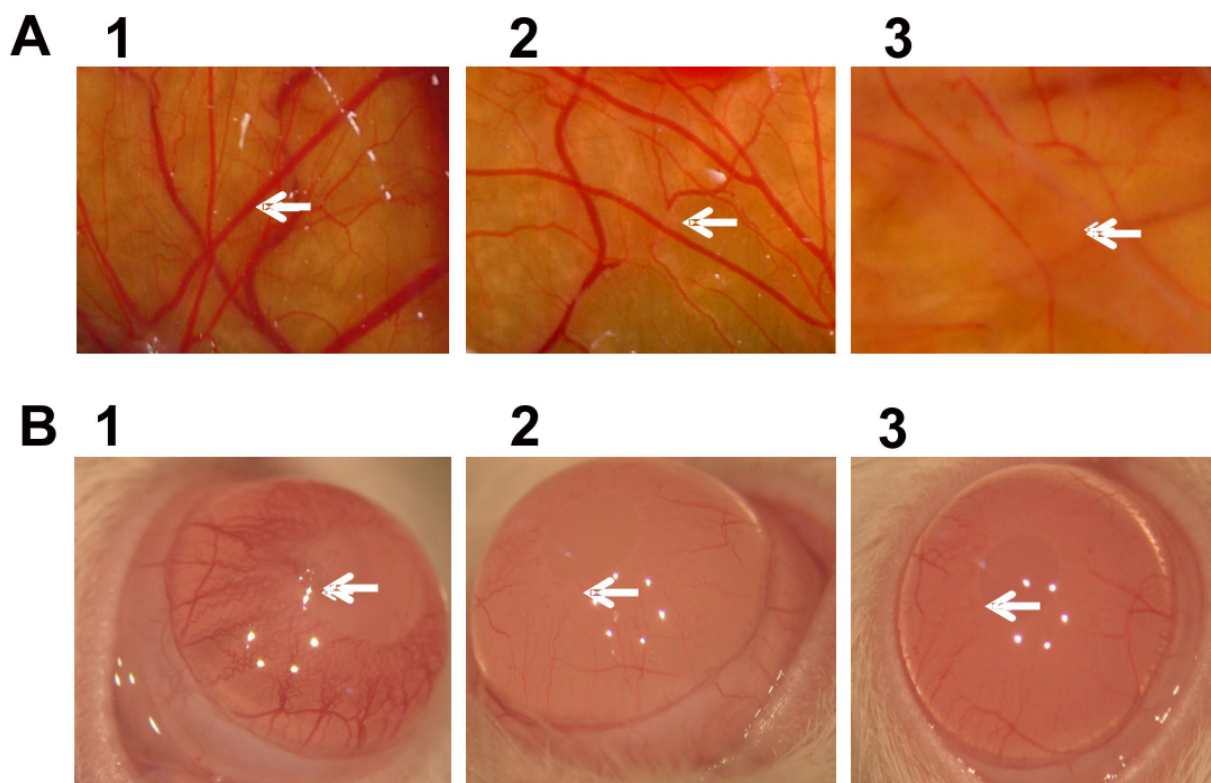


Figure 2. Effect of AOE on blood vessel regression in the chick CAM and rat cornea assays. A) VEGF alone (1) (+ control), saline (2) (– control), or VEGF + AOE (100 μ g) (3) was applied to the CAM of 11-day-old chicken embryos. After 48 h of incubation, the treated area was inspected for changes in neovascularization. The arrows indicate the treated area. The data shown represent the result of an experiment that was done using a maximum of six eggs in each group. All photographs were taken at 40 \times magnification. B) Photographs of VEGF-induced neovascularization observed in rat corneas: 1) hydon polymer + VEGF (1 μ g) (+ control), 2) hydon polymer alone (– control), and 3) hydon polymer + VEGF + AOE (100 μ g). Details of the experiments are described in the Materials and Methods. After 7 days of incubation, the corneas were photographed at 40 \times magnification.

treated mice to 6×10^6 /mouse (Figure 3C), indicating an 8-fold reduction when compared to the control. These results indicate the antitumor activity of AOE. In a fully grown ascites tumor *in vivo*, there is extensive peritoneal angiogenesis, as shown in Figure 3D. In AOE-treated mice, a significant decrease in peritoneal angiogenesis was observed *in vivo*.

Further, the effect of AOE on survival of EAT-bearing animals was tested. Upon intraperitoneal transplantation of 5×10^6 cells/mice, the EAT-bearing mice survived for 15 days, with tumor cells increasing in number to 15×10^9 cells/mice. The animals succumbed to the tumor burden 15 days after tumor transplantation. AOE treatment (133 mg/kg body weight/dose, every day for 10 doses) extends the survival time of EAT-bearing mice from 15 days up to two months (data not shown).

3.4. H & E and CD31 immunostaining

Histological examination of the peritoneal sections of both groups revealed a relative reduction in the number of newly formed microvessels in the AOE-treated peritoneum compared to the control (Figure 4A). CD31 is used as a marker to indicate the proliferation of endothelial cells. The current results of CD31 staining indicate that there is a reduction in the number of

proliferating endothelial cells in the peritoneum of AOE-treated EAT-bearing mice (Figure 4B), corroborating the results shown in the inhibition of peritoneal angiogenesis *in vivo*.

3.5. Inhibition of VEGF mRNA levels by AOE

In order to investigate the effect of AOE on the VEGF gene, levels of mRNA synthesis were determined in untreated EAT cells or EAT cells treated with AOE and incubated for 30 min to 4 h. As shown in Figure 5, VEGF mRNA levels decreased considerably over a period of 4 h in AOE-treated EAT cells as compared to untreated cells. The decrease in VEGF gene expression was corroborated by the reduction in the amount of VEGF protein as estimated by VEGF-ELISA in the ascites of EAT cells treated with AOE.

3.6. AOE inhibits VEGF production in EAT cells

In control EAT-bearing mice, over the 0-12 day tumor growth period quantification of VEGF in the ascites secreted by the growing tumor indicated that there is a gradual production and secretion of VEGF by EAT cells. These results indicate that 1,716 ng of VEGF is present in the ascites of a fully grown tumor whereas 49 ng of

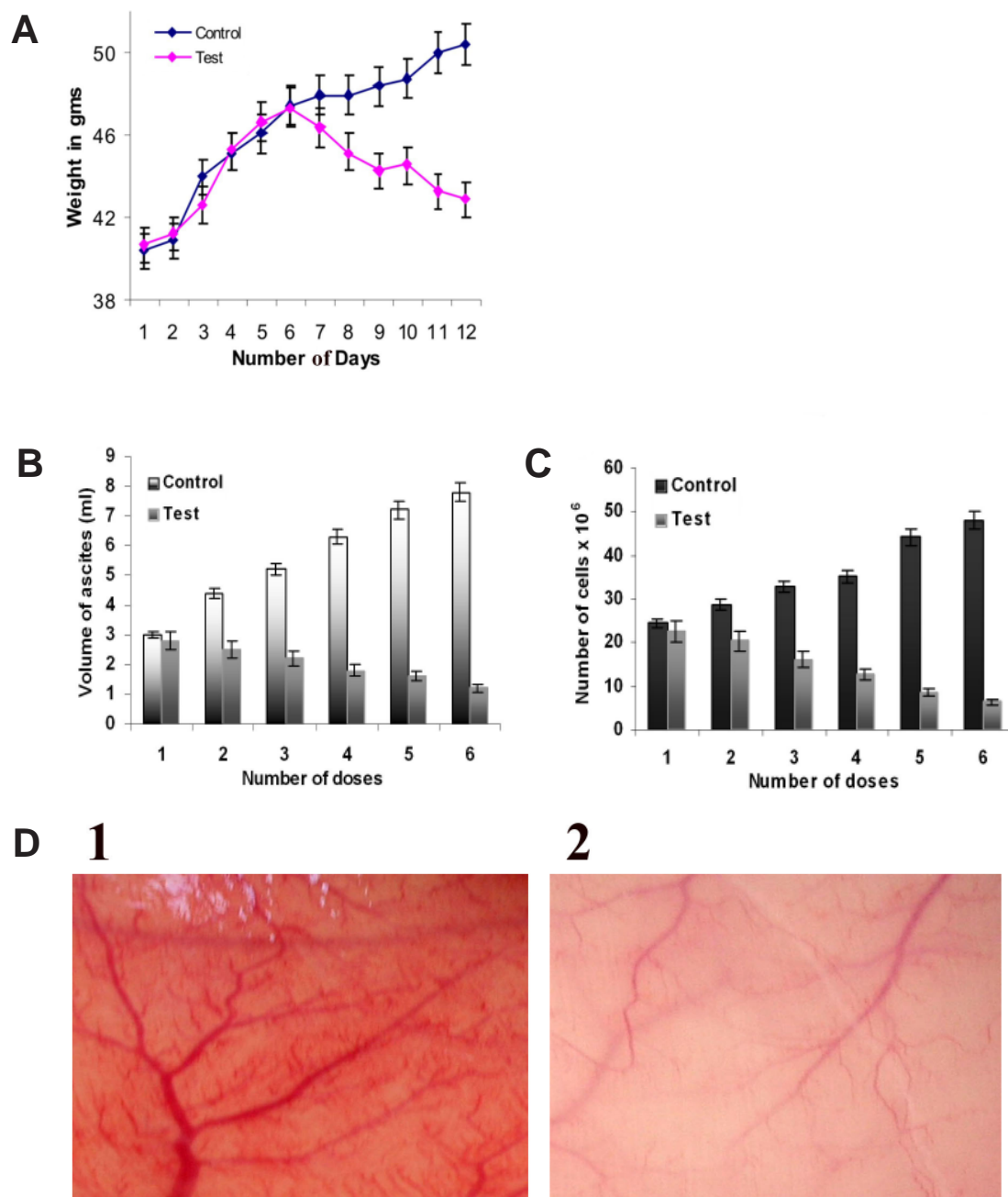


Figure 3. *In vivo* inhibition of tumor growth and angiogenesis by AOE. Body weights of EAT-bearing untreated mice or mice treated with AOE were recorded. From the 6th day onwards, AOE (133 mg/kg body weight) was administered (*i.p*) for six doses every day (A), The animals were sacrificed on the 7th-12th day. EAT cells were collected along with ascites fluid and measured (B), Cells were counted with a haemocytometer (C), The peritoneum of the animal was photographed (D), At least five mice were used in each group and the results obtained are an average of three individual experiments and means of \pm S.E.M. $n = 5$ per group.

VEGF per mouse was detected in AOE-treated mice, suggesting the inhibition of VEGF secretion (Figure 6).

3.7. Down regulation of VEGF gene expression by AOE

To determine whether AOE modulates VEGF gene expression, the effect of AOE on VEGF promoter luciferase reporter gene analysis was tested. When compared to normal untransformed HEK 293 cells, the activity of VEGF gene expression was 50-60% higher

in EAT cells than in normal cells. A dose-dependent inhibition of VEGF gene expression was seen with increasing concentrations of AOE, with a maximum of 80% inhibition with 50 μ g/mL of AOE in EAT cells (Figure 7), while a maximum of 25% inhibition of VEGF gene expression was seen in HEK 293 cells.

3.8. Fractionation and identification of the specific antiangiogenic fraction of *A. occidentale*

The dried leaf powder of *A. occidentale* was

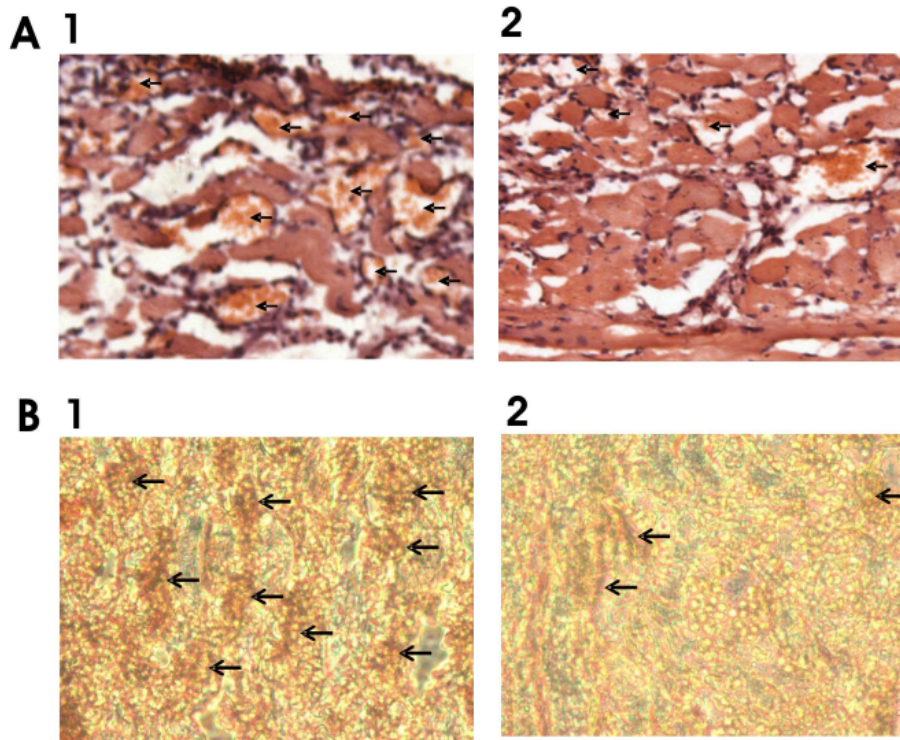


Figure 4. AOE inhibits MVD and proliferation of endothelial cells in mouse peritoneum. A) The peritoneums of control (1) as well as AOE-treated (2) EAT-bearing mice were embedded in paraffin and 5 μ m sections were made using a microtome. The sections were stained with hematoxylin and eosin and observed for microvessel density (40 \times). Arrows indicate the microvessels. B) Paraffin sections (5 μ m) of peritoneum of control (1) and AOE (2) mice were immunostained with anti-CD31 (PECAM) antibodies. Arrows indicate the stained activated endothelial cells.

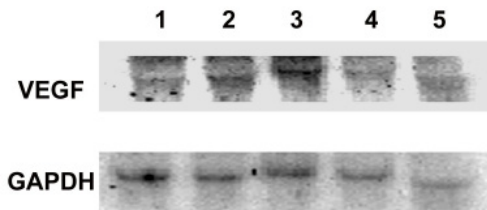


Figure 5. Effect of AOE on expression of mRNA in EAT cells. Total RNA from untreated EAT cells or EAT cells treated with AOE was isolated for varying time periods (Lane 1: Control, Lanes 2-5: 30 min – 4 h) and Northern blot analysis was performed using a VEGF₁₆₅ cDNA probe. GAPDH was used as an internal control. The experiment was performed three times.

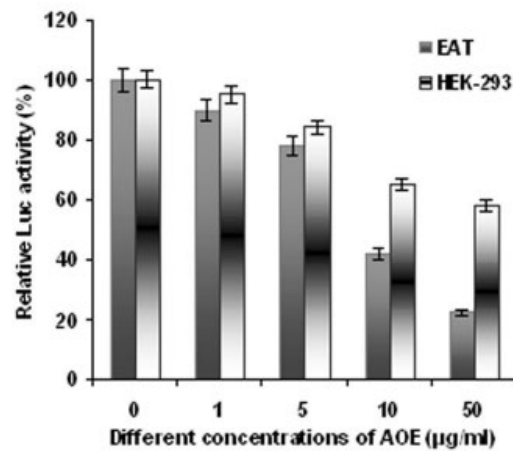


Figure 7. Effect of AOE on VEGF promoter activity. EAT and HEK 293 cells were transiently transfected with 2 μ g of pLuc 2068. Forty eight hours later, cells were assayed for luciferase activity. AOE extract repressed VEGF promoter activity in a dose-dependent manner in EAT cells.

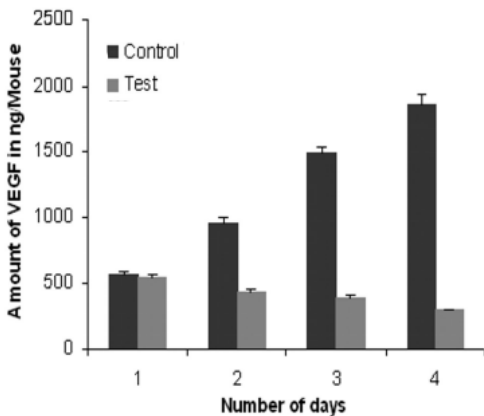


Figure 6. Effect of AOE on VEGF levels in ascites fluid *in vivo*. EAT-bearing mice were injected with AOE (133 mg/kg body weight) for four doses or left untreated, and ascites fluid was collected every day after each dose of treatment. ELISA was carried out after sacrificing the animal to quantify the VEGF in ascites fluid using anti-VEGF₁₆₅ antibodies. Strong inhibition of VEGF expression in AOE-treated mice is evident.

sequentially extracted with petroleum ether, hexane, benzene, chloroform, ethyl acetate, acetone, methanol, and ethanol, and all of the extracts were tested for their angioinhibitory effect using the EAT model. Results indicated a decrease in the body weight, ascites volume, cell number, and neovascularization in the peritoneum of EAT-bearing mice treated with an ethanolic fraction of *A. occidentale* (Table 2).

Table 2. Effect of different solvent fractions of *Anacardium occidentale* leaves on EAT growth *in vivo*

Solvent	Body weight		Ascites volume	Cell number	Peritoneal angiogenesis
	Day 1	Day 12			
Petroleum ether	32.6 g	40.1 g	5.0 ml	7.2×10^8 /mouse	No inhibition
Hexane	33.0 g	40.6 g	5.2 ml	8.4×10^8 /mouse	No inhibition
Benzene	31.9 g	41.3 g	5.5 ml	8.8×10^8 /mouse	No inhibition
Chloroform	32.0 g	42.8 g	7.5 ml	8.8×10^8 /mouse	No inhibition
Ethyl acetate	33.2 g	39.6 g	5.0 ml	8.8×10^8 /mouse	No inhibition
Acetone	33.8 g	40.3 g	5.0 ml	6.8×10^8 /mouse	No inhibition
Methanol	33.4 g	43.0 g	7.5 ml	8.96×10^8 /mouse	No inhibition
Ethanol	31.5 g	32.0 g	0.2 ml	0.8×10^8/mouse	Inhibition
Tumor bearing	32.6 g	43.6 g	7.0 ml	14×10^8 /mouse	Extensive angiogenesis

4. Discussion

Tumor growth and metastasis are dependent on the formation of new blood vessels. The most elegant investigation of the correlation between the onset of angiogenesis and tumor growth was carried out by Folkman *et al.* (24). The clinical usage of herbal medicine could have an impact on therapy for cancer. The present study was the first to provide direct evidence that an ethanolic extract of *Anacardium occidentale* L. has potent antiangiogenic activity *in vitro* and *in vivo*, corroborating the tumor-preventing action of AOE. The current authors have already reported the effect of a methanolic fraction of *Glycyrrhiza glabra* on EAT cells in screening for antiangiogenic medicinal plants (25). Given that angiogenesis is essential for tumor growth, the antitumor effects of AOE may correlate with its antiangiogenic activity. The antiangiogenic activities of AOE *in vivo* may be explained by its inhibitory action on proliferation of tumor cells *in vitro* in a dose-dependent manner as compared to the little effect, if at all, it has on the untransformed normal cell line. The IC_{50} of AOE on tumor cell lines was between concentrations of 1-20 $\mu\text{g/mL}$ while it was significantly greater in normal cells. The lower the IC_{50} value, the more potent the extract is as an inhibitor of tumor cell growth. The current results show that there is inhibition of neovascularization by AOE in the CAM and rat cornea. Inhibition of fluid accumulation, tumor growth, and microvessel density by neutralization of VEGF has been demonstrated, underlining the importance of VEGF in malignant ascites formation (26-28). Since there is inhibition of neovascularization by AOE, this supports the view that AOE may repress the expression of VEGF-like factors or inhibit the secretion of such factors, thereby inhibiting the accumulation of ascites fluid and formation of new blood vessels. Further evidence for the antiangiogenic potential of AOE comes from the current results on inhibition of the extent of proliferating endothelial cells in the peritoneal lining of tumor-bearing mice. A significant decrease in peritoneal angiogenesis and levels of stained PECAM in sections of peritoneal wall confirm the antiangiogenic activity of AOE. Research has demonstrated that the density of microvessels was almost doubled in tumors from

patients with metastasis (29). Further, the role of AOE with regard to the regulation of VEGF expression was investigated at the mRNA, protein, and gene level. This finding is in agreement with the effect AOE has at repressing endogenous VEGF expression, where VEGF is downregulated on an mRNA as well as on a protein level in a time-dependent manner. Moreover, transient transfection assays revealed that AOE downregulated VEGF promoter activity in EAT cells in a dose-dependent manner. This result suggests that transcriptional repression of the VEGF gene represents the mechanism by which AOE downregulates VEGF expression. As in normal angiogenesis, tumor angiogenesis appears to rely heavily on VEGF. In addition to producing VEGF themselves, tumors may induce the production of VEGF in their surrounding tissue; therefore, high levels of VEGF production in a wide variety of tumors and tumor-associated cells suggest that VEGF plays a pivotal role in tumor angiogenesis. Thus, an antiangiogenic agent could conceivably block the paracrine action of tumor cells and hence suppress the proliferation and survival of tumor cells. Inhibition of VEGF gene expression by AOE should also be reflected by the levels of VEGF in the ascites secreted by the EAT cells. In an EAT model, mice produced about 8-9 mL of ascites fluid over a growth period of 12-14 days; this fluid contained 230 ng of VEGF/mL (30). The current results on quantification of the cytokine in the ascites of EAT-bearing mice have clearly indicated that AOE efficiently decreases the level of VEGF in an *in vivo* model system. A decrease in ascites formation *in vivo* and in VEGF levels in ascites bears significant importance in terms of a clinical correlation with inhibited ascites formation in human tumors. In conclusion, the present data indicate a possible role AOE has in preventing cancer from becoming malignant, presumably *via* selective curbing of neovessel formation at the tumor site. AOE may hold potential as a pharmaceutical drug and its antiangiogenic activity may contribute to its well-documented clinical activity. Although this study investigated the antiangiogenic activity of the crude ethanolic extract of *A. occidentale*, the leaf powder of this plant has also been fractionated using different solvents based on polarity. An ethanolic fraction

produced a drastic decrease in body weight, ascites volume, cell number, and peritoneal angiogenesis on the 12th day of tumor transplantation as compared to untreated control EAT mice and EAT-bearing mice treated with other solvent fractions. Together, these data confirm that the ethanolic fraction had the maximum antiangiogenic activity. Further purification and characterization of this active compound is in progress.

Acknowledgements

The authors appreciate the financial support of the Department of Science and Technology, Women Scientists Scheme A (DST WOS-A) (No. SR/WOS-A/LS-177/2006), University Grants Commission, New Delhi and the Board of Research in Nuclear Sciences, Department of Atomic Energy, Mumbai, India. The authors wish to thank Dr. H.N. Yajurvedi of the Animal facility, Department of Zoology, University of Mysore, Mysore, India, for the timely supply of animals for these experiments.

References

1. Veikkola T, Alitalo K. VEGF's, receptors and angiogenesis. *Semin Cancer Biol* 1999; 9:211-220.
2. McMahon G. VEGF Receptor signaling in tumor angiogenesis. *Oncologist* 2000; 5:3-10.
3. Liekens S, De Clercq E, Neyts J. Angiogenesis: regulators and clinical applications. *Biochem Pharmacol* 2001; 61:253-270.
4. Lee IS, Nishikawa A, Furukawa F, Kasahara K, Kim SU. Effects of *Selaginella tamariscina* on *in vitro* tumor cell growth, p53 expression, G1 arrest and *in vivo* gastric cell proliferation. *Cancer Lett* 1999; 144:93-99.
5. Bonham M, Arnold H, Montgomery B, Nelson PS. Molecular effects of the herbal compound PC-SPES: identification of activity pathways in prostate carcinoma. *Cancer Res* 2002; 62:3920-3942.
6. Hu H, Ahn NS, Yang X, LeeYS, Kang KS. *Ganoderma lucidum* extract induces cell cycle arrest and apoptosis in MCF-7 human breast. *Int J Cancer* 2002; 102:250-253.
7. Kao ST, Yeh CC, Hsieh CC, Yang MD, Lee MR, Liu HS. The Chinese medicine Bu-Zhong-Yi-Qi-Tang inhibited proliferation of hepatoma cell lines by inducing apoptosis via G0/G1 arrest. *Life Sci* 2001; 69:1485-1496.
8. Lee SM, Li ML, Tse YC, Leung SC, Lee MM, Tsui SK. Paeoniae Radix, a Chinese herbal extract, inhibits hepatoma cell growth by inducing apoptosis in a p53 independent pathway. *Life Sci* 2002; 71:2267-2277.
9. Yano H, Mizoguchi A, Fukuda K, Haramaki M, Ogasawara S, Momosaki S. The herbal medicine sho-saiko-to inhibits proliferation of cancer cell lines by inducing apoptosis and arrest at the G0/G1 phase. *Cancer Res* 1994; 54:448-454.
10. Huerta S, Arteaga JR, Irwin RW, Ikezo T, Heber D, Koeffler HP. PC-SPES inhibits colon cancer growth *in vitro* and *in vivo*. *Cancer Res* 2002; 62:5204-5209.
11. Ferraza A, Fariab DH, Bennetib MN, Brondani da Rochab A, Schwartzmann G, Henriquesa A, von Posera GL. Screening for antiproliferative activity of six southern Brazilian species of *Hypericum*. *Phytomedicine* 2005; 12:112-115.
12. Tai J, Cheunga S, Chanb E, Hasmanb D. *In vitro* culture studies of *Sutherlandia frutescens* on human tumor cell lines. *J Ethnopharmacol* 2004; 93:9-19.
13. Thippeswamy G, Salimath BP. Induction of caspase-3 activated DNase mediated apoptosis by hexane fraction of *Tinospora cordifolia* in EAT cells. *Env Tox Pharmacol* 2007; 23:212-220.
14. Konan NA, Bacchi EM. Antiulcerogenic effect and acute toxicity of a hydroethanolic extract from the cashew (*Anacardium occidentale* L) leaves. *J Ethnopharmacol* 2007; 112:237-242.
15. Green IR, Tocoli FE, Lee SH, Nihei KI, Kubo I. Design and evaluation of anacardic acid derivatives as anticavity agents. *Eur J Med Chem* 2008; 43:1315-1320.
16. Sujatha V, Sachdanandam P. Recuperative effect of *Semecarpus anacardium* linn. Nut milk extract on carbohydrate metabolizing enzymes in experimental mammary carcinoma-bearing rats. *Phytother Res* 2002; 1:14-18.
17. Mathivadani P, Shanthi P, Sachdanandam P. Hypoxia and its downstream targets in DMBA induced mammary carcinoma: protective role of *Semecarpus anacardium* nut extract. *Chem Biol Interact* 2007; 167:31-40.
18. Chakraborty S, Roy M, Taraphdar AK, Bhattacharya RK. Cytotoxic effect of root extract of *Tiliacora racemosa* and oil of *Semecarpus anacardium* nut in human tumor cells. *Phytother Res* 2004; 18:595-600.
19. Giridharan P, Somasundaram ST, Perumal K, Vishwakarma NP, Velmurugan R, Balakrishnan A. Novel substituted methylenedioxy lignan suppresses proliferation of cancer cells by inhibiting telomerase and activation of c-myc and caspases leading to apoptosis. *Br J Cancer* 2002; 87:98-105.
20. Gururaj AE, Belakavadi M, Salimath BP. Antiangiogenic effects of butyric acid involves inhibition of VEGF/KDR gene expression and endothelial cell proliferation. *Mol Cell Biochem* 2003; 243:107-112.
21. Sarayba MA, Li L, Tungsiripat T, Liu NH, Sweet PM, Patel AJ, Osann KE, Chittiboyina A, Benson SC, Pershadsingh HA, Chuck RS. Inhibition of corneal neovascularization by a peroxisome proliferators-activated receptor- γ ligand. *Exp Eye Res* 2005; 80:435-442.
22. Deepak AV, Salimath BP. Antiangiogenic and proapoptotic activity of a novel glycoprotein from *U. indica* is mediated by NF-kappaB and Caspase activated DNase in ascites tumor model. *Biochimie* 2006; 88:297-307.
23. Belakavadi M, Salimath BP. Mechanism of inhibition of ascites tumor growth in mice by curcumin is mediated by NF-kB and caspase activated DNase. *Mol Cell Biol* 2005; 273:57-67.
24. Folkman J, Shing Y. Angiogenesis. *J Biol Chem* 1992; 267:10931-10934.
25. Sheela ML, Ramakrishna MK, Salimath BP. Angiogenic and proliferative effects of the cytokine VEGF in Ehrlich ascites tumor cells is inhibited by *Glycyrrhiza glabra*. *Int Immunopharmacol* 2006; 6:494-498.
26. Mesiano S, Ferrara N, Jaffe RB. Role of vascular endothelial growth factor in ovarian cancer. Inhibition of ascites formation by immunoneutralization. *Am J Pathol* 1998; 153:1249-1256.
27. Kim KJ, li B, Winer J, Armanini M, Gillett N, Philips

- HS, Ferrara N. Inhibition of vascular endothelial growth factor induced angiogenesis suppresses tumor growth *in vivo*. *Nature* 1993; 362:841-844.
28. Borgstrom P, Hillan KJ, Sriramarao P, Ferrara N. Complete inhibition of angiogenesis and growth of microtumors by antivascular endothelial growth factor neutralizing antibody, novel concept of angiostatic therapy from intravital videomicroscopy. *Cancer Res* 1996; 56:4032-4039.
29. Weidner N, Carroll PR, Flax J, Blumenfeld W, Folkman J. Tumor angiogenesis correlates with metastasis in invasive prostate carcinoma. *Am J Pathol* 1993; 143:401-409.
30. Prabhakar BT, Khanum SA, Shashikanth S, Salimath BP. Antiangiogenic effect of 2-benzoyl-phenoxy acetamide in EAT cell is mediated by HIF-1 α and down regulation of VEGF *in vivo*. *Invest New Drugs* 2006; 24:471-478.

(Received June 25, 2008; Revised August 20, 2008; Accepted August 23, 2008)

Original Article**Production of a human antibody fragment against the insulin-like growth factor I receptor as a fusion protein**Yu Kusada¹, Toru Morizono¹, Keiko Sakai^{2,3}, Atsushi Takayanagi^{3,4}, Nobuyoshi Shimizu⁴, Yoko Fujita-Yamaguchi^{1,2,3,*}¹ Department of Applied Biochemistry, Tokai University School of Engineering, Kanagawa, Japan;² Institute of Glycotechnology, Tokai University, Kanagawa, Japan;³ Core Research for Evolutional Science and Technology (CREST), Japan Science and Technology Agency (JST), Japan;⁴ Department of Molecular Biology, Keio University School of Medicine, Tokyo, Japan.

ABSTRACT: The aim of this study was to isolate single-chain variable fragments (scFvs) against human insulin-like growth factor I receptor (IGF-IR) from a phage library displaying human scFvs. Isolated scFvs-displaying phages showed affinity for IGF-IR in comparison to the control. Expression of scFv proteins in *Escherichia coli* for further characterization, however, proved extremely difficult. Alternatively, the scFv protein was expressed as a fusion protein with a maltose-binding protein (MBP) that is a highly soluble *E. coli* protein. The MBP-scFv fusion protein expressed in a soluble form in *E. coli* was purified to homogeneity by two-step affinity chromatography. The resulting MBP-scFv exhibited affinity for IGF-IR and structurally-related insulin receptor (IR). These results suggest both that MBP-scFv fusion proteins are practical alternatives to isolating scFv proteins for further characterization and that successful isolation of human scFvs against a specific protein of interest requires vigorous screening in the early stages. Such screening is accomplished by using two independent screening methods such as measuring binding to IGF-IR but not to IR by ELISA or measuring competitive binding by IGF-I in addition to binding to IGF-IR alone.

Keywords: Therapeutic antibody, Single-chain antibody, Insulin-like growth factor I receptor, Phage display, Maltose-binding protein fusion

1. Introduction

Insulin-like growth factor I receptor (IGF-IR) plays

an essential role in cancer growth, progression, and metastasis (1-3). IGF-IR is overexpressed in a variety of malignant tumors and also plays a role in hormone-independent growth of breast and prostate cancers (4,5). IGF-IR is therefore considered to be a good target molecule for cancer therapy. Several anti-cancer strategies have been developed such as anti-sense RNA (6), tyrosine kinase inhibitors (7), and mAbs (8), but anti-IGF-IR mAbs are probably the best anti-tumor therapeutics for several reasons. First, the antibodies bound to the receptor result in inhibition of ligand-induced phosphorylation of β subunits followed by silencing of down-stream signal molecules. Secondly, antibodies induce receptor clustering due to their bivalency. The antibody-receptor complex is then internalized into endosomes and then to lysosomes, where the receptors are thought to degrade. This process, down-regulation of IGF-IR, was first demonstrated in breast cancer cells (9,10) and is responsible for causing the refractoriness of cancer cells to IGF-I stimulation and inducing apoptosis. Thirdly, IGF-IR antibodies can recruit effector functions, including ADCC through FC γ R and complement fixation (11).

Several approaches to producing therapeutic antibodies are now available, that is, CDR grafting from the mouse variable region to a human frame (12), immunizing transgenic mice carrying human antibody gene loci (13), and screening of phage display libraries *in vitro* (14). Of these approaches, the phage display screening method is a powerful tool for producing scFv or Fab fragments *in vitro* in a short period of time. The major drawback associated with this method is, however, difficulty in readily producing soluble scFv proteins in *E. coli* transfected with original phages. For example, previous studies reported aggregations of scFvs in the periplasmic space of *E. coli* (15,16). Several methods of improving solubility have been evaluated such as use of different *E. coli* strains

*Correspondence to: Dr. Yoko Fujita-Yamaguchi, 1117 Kitakaname, Hiratsuka, Kanagawa 259-1292, Japan; e-mail: yamaguch@keyaki.cc.u-tokai.ac.jp

(17), changes in the vector construction (18), and introduction of a new tag (19).

The current authors previously reported that 1H7 scFv-Fc consisting of scFv derived from anti-IGF-IR mAb 1H7 and a human IgG1 Fc domain had an inhibitory effect on tumor growth *in vivo* (9,10). In an attempt to obtain more effective as well as humanized anti-IGF-IR Abs, a phage library displaying human scFvs was screened in this study using a human recombinant IGF-IR extracellular domain as an antigen. Since difficulties in expressing scFv proteins from phage-infected *E. coli* were encountered as anticipated, a scFv gene was fused to the gene for maltose-binding protein (MBP) in order to produce scFv proteins of interest in a soluble form (20). MBP-scFv expressed was purified by two-step affinity chromatography and was shown to bind to the antigen in a dose-dependent manner. Therefore, MBP fusion protein can be used to characterize scFv in *in vivo* experiments. The purified MBP-scFv protein was also found to bind to the insulin receptor, which indicated the presence of common epitopes for isolated scFvs.

2. Materials and Methods

2.1. Materials

E. coli strains used were the suppressor strain TG1, and the nonsuppressor strain TOP10F' from Invitrogen (CA, USA). *E. coli* JM109 was the suppressor strain from Takara Bio (Shiga, Japan). *E. coli* XL1-Blue was the suppressor strain from STRATAGENE (CA, USA). Recombinant human extracellular IGF-IR (rhIGF-IR) and IR (rhIR) were purchased from R&D Systems Inc. (MN, USA). Helper phage M13KO7, HRP/anti-M13 conjugate, HRP/anti-E tag conjugate, and His MicroSpin Purification Module were from GE Healthcare Bio-Sciences Corp. (NJ, USA). The plasmid vector pMAL-p2E that encodes MBP, anti-MBP mAb, and Amylose Resin High Flow were purchased from New England Biolabs (MA USA). All DNA primers used in this study were designed accordingly and ordered from Nihon Gene Research Laboratories, Inc. (Sendai, Japan). A control phage named 1H7 displaying mouse scFv specific for IGF-IR was constructed as previously described (21).

2.2. Selection of IGFIR-binders from a phage library displaying human scFvs by panning

A phage library representing over 10^{11} independent clones that displayed human scFvs was constructed and used to screen anti-IGF-IR scFvs as previously described (22). Phage clone selection was basically carried out according to previously published procedures with some modifications (22,23). For the first panning, 24 wells of a 96-well plate were coated

with rhIGF-IR 50 ng/50 μ L in 20 mM Tris-HCl buffer, pH 7.4, containing 0.15 M NaCl (TBS) and incubated at 4°C overnight. The wells coated with rhIGF-IR were blocked by incubation with 150 μ L of 3% bovine serum albumin (BSA) in TBS at room temperature (RT) for 2 h. After removal of blocking solution, the phage library was added to the wells and incubated at RT for 2 h. Unbound phages were washed away by incubation with TBS containing 0.2% Tween 20 (TBST) and TBS. For elution, 100 mM triethyl amine (TEA) solution was added to each well and the plate was incubated at RT for 10 min. TEA solution containing eluted phages was neutralized by adding 0.7 M Tris-HCl buffer, pH 7.4, containing 1.5% BSA solution. This elution step was repeated. *E. coli* TG1 cells were added to collected phage solutions and incubated at 37°C for 1 h to allow phages to infect TG1 cells. Infected TG1 cells were spread out on LB (1% tryptone, 0.5% yeast extract, 1% NaCl, and 1 mM NaOH) supplemented with 2% glucose and 50 μ g/mL carbenicillin (LBGC) in plates and allowed to grow at 25°C for 2 d until independent colonies formed. All resulting colonies were pooled and stored in SBS medium (3% tryptone, 2% yeast extract, 0.5% NaCl, and 20 mM Tris-HCl buffer, pH 7) supplemented with 16% glycerol at -80°C. For the second round of panning, this phage-infected *E. coli* stock was used to enrich IGF-IR reactive scFvs. Five hundred μ L of this stock were added to SBS supplemented with 50 μ g/mL of carbenicillin (SBSC) and cultured at 37°C for 2 h followed by infection with 8.8×10^{10} pfu of M13KO7 helper phage by culturing at 37°C for 1 h. To select double-infected and scFv-producing *E. coli*, 100 μ g/mL chloramphenicol and 50 μ g/mL kanamycin were added to the *E. coli* solution followed by culturing at 25°C for 2 d. The resulting phage preparation was precipitated in 4% polyethylene glycol/0.5 M NaCl (PEG precipitation) and resuspended in TBS containing 1.5% BSA and 0.2% Tween 20 followed by treatment with Benzonaze (Novagen) to digest any unnecessary DNA. The prepared phages were subjected to the second round of panning following the above procedure with some modifications. For the second to fourth round of panning, a longer elution time and fewer antigen-coated wells were used as the panning process advanced. Furthermore, *E. coli* cells infected with phages eluted after the second and third rounds of panning were directly added to SBSC medium and then subjected to the helper phage-rescuing procedure as described above.

2.3. Screening for phages displaying human scFvs against IGF-IR

After four rounds of panning, the concentrated phages were subjected to dilution and infection to logarithmically growing *E. coli* XL1-Blue strain.

a third antibody, respectively. For detection of scFv proteins, HRP/anti-E-tag conjugate (1:2,000 dilution) was used as a second antibody. The wells were washed 7 times with TBST and then 3 times with TBS. Peroxidase activity was detected by reaction with 100 μ L of ABTS/ H_2O_2 for 30 min and termination with 1% oxalic acid. The absorbance at 415 nm was measured by a BIO-RAD plate-reader.

2.8. Characterization of phage antibodies by surface plasmon resonance (SPR)

SPR analysis was carried out at 25°C using 10 mM HEPES, pH 7.4, containing 150 mM NaCl, and 0.005% surfactant P20 (HBS-P buffer) as a running buffer. Binding properties of phage antibodies were determined using a Biacore X (Pharmacia Biosensor AB, Uppsala, Sweden). A CM3 sensor chip was equilibrated overnight with the running buffer before use. Immobilization of the antigen on the sensor chip was achieved by injecting 50 μ L of 10 mM sodium acetate buffer, pH 3.8, containing 500 μ g/mL of rhIGF-IR *via* amine groups using the Amine Coupling Kit (Pharmacia Biosensors) as previously described (25). Binding of phage antibodies displaying 2A1, 3E2, 3H5, and 4C5 scFv was analyzed at two or three different concentrations as indicated in the figure legend. M13KO7 helper phage, which does not display scFv, served as a negative control.

3. Results

3.1. Panning and screening of anti-IGF-IR human scFv-displaying phages

A phage display library consisting of more than 10^{11} independent clones was subjected to four rounds of panning against rhIGF-IR as an antigen (Figure 1). Of 419 independent clones screened by ELISA, twenty-three positive clones were found to show ELISA positivity with S/N of > 2 . Typical results of ELISA are shown in Figure 2A. ScFv genes, amplified from 23 clones by PCR as indicated by the examples in Figure 2B, were subjected to DNA sequencing analyses, which revealed that 4 clones were identical. Thus, 20 independent clones were obtained as candidate phages presenting anti-IGF-IR scFvs. Amino acid sequence alignments of VH and VL of all 20 scFvs are shown in Tables 1A and B, respectively. These scFvs were clearly derived from different clones with diverse origins.

3.2. Initial characterization of phage antibodies by SPR

SPR analyses were carried out to determine whether or not phages displaying "anti-IGF-IR" scFvs have binding affinities for IGF-IR. Figures 3A, B, C, and D

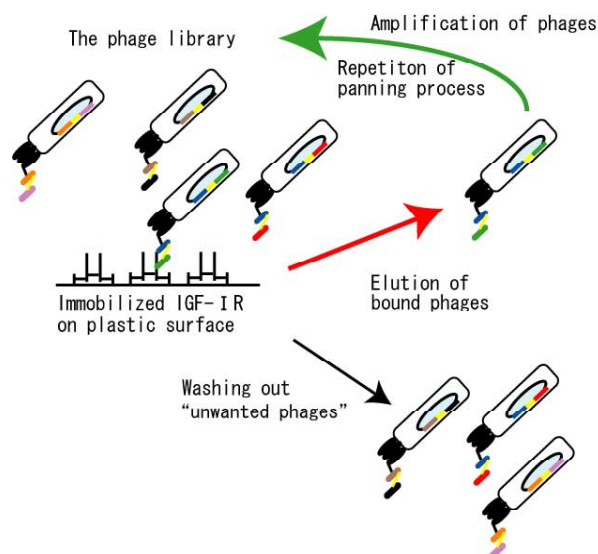


Figure 1. Schematic panning procedure for isolation of human scFvs displayed on phages. Phage antibodies were added onto wells coated with rhIGF-IR. After washing, bound phages were eluted and amplified in *E. coli*. This process was repeated four times to concentrate antigen-specific phage clones.

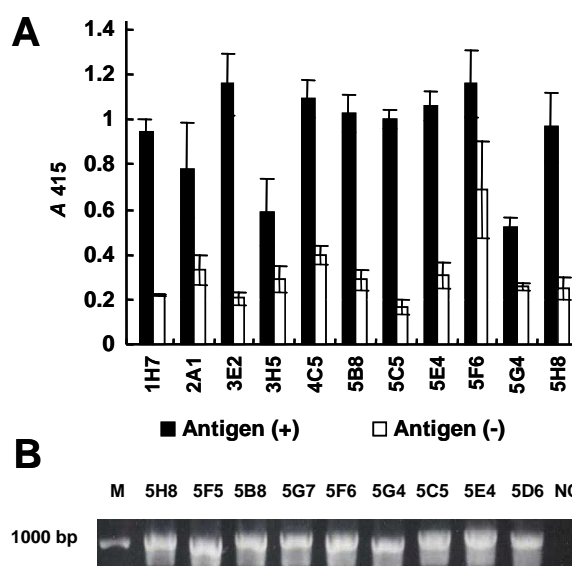


Figure 2. Analyses of candidate phage antibodies screened by human IGF-IR from a phage library displaying scFvs. (A) Binding of isolated phage antibodies to IGF-IR as measured by ELISA. Each phage clone (1×10^{12} cfu/mL) was assayed for its affinity against immobilized rhIGF-IR (Antigen +) or BSA only (Antigen -) as described in the Methods. 1H7 is a control phage displaying mouse scFv prepared from anti-IGF-IR mAb 1H7-producing hybridoma as described (27). The error bars represent the standard deviation calculated from replicates ($n = 3$). (B) PCR amplification of scFv genes in the isolated clones. ScFv genes were amplified by colony PCR using specific primers as described in the Methods. PCR products were analyzed by 1% agarose gel electrophoresis.

show sensorgrams at different concentrations of phages displaying 2A1, 3E2, 3H5, and 4C5 scFv, respectively. Although these data are merely qualitative, the resulting sensorgrams clearly indicated that the phage antibodies bound to immobilized IGF-IR in a dose-dependent manner. In addition, M13KO7 helper phage, which served as a negative control, displayed no signal (data not shown), indicating that all phage antibody affinity

Table 1A. Multiple alignment for deduced amino acid sequences of 20 anti-IGF1R scFv VH fragments

2A1	QVQLVESGPDVKKPGASVKVCKTSGYFTFD--HYIHWVRQAPGQGLEWVGWVTPQASASTNYADKFSRVTMTRDTSINTAYMELSGLTSDDTAIYYCAR-GERT-----PLERW-LDPWGQGLTVTVSS-----
2A7	QVQLVQSGGGGLEPQGGSLRLSCAASGLTFSS--YAMSWARQAPGKGLEWVSSISSGGTTYADPVKGRFTISRDNKNTLYLQMNLSRAEDTALYYCASQKSVCTDGICYKDYIYYGMDVWVGQTTTVTVSS-----
2D9	QVQLLETGGGVVQGRSLRLSCEASGSSFSH--YAIQWVRQAPGKGLEWVAVISFDGRERYADSVKGRFAVSRDNSKNTLHLQMNLSRPEDTAVYYCAREMYPSTTVL----SPD GMDVWVGLGTTTVTVSSASTKGPSS
2G5	QVQLVESGGGVVQPGESLRLSCAASGFIFSR--YGMQWVRQAPGKGLEWVAFIPYDGSNKYYVDSVKGRFTVSRDNSKNTLYLQMNLSRLEDTAVYHCAICRDG-----YNPL DHWGQGLTVAVSSASTKGPSS
3A5	QVQLVESGGGLVQPGGSLRLSCVASGFSFSP--YSMNWVRQAPGKGLEWLSYISGSSGTYIAESVKGRFTISRDNKNSLYLQMNRLTVDDTALYYCARESGTG-----PTHYYSH GMAVWVGQTTTVTVSS-----
3A6	QVQLVESGGDLIQPGGSLRLSCAASGFIVSS--KYMTWVRQAPGKGLEWVSVIDS-GGTTYANSVKGRFTISRDNKNTLYLQMNLSRAEDTAVYYCVRDSSS-----SGLDY WGGQTRVTVSSGASAPT-
3C5	QVQLVESGGALVKPQGGSLRLSCTASGFLSD--YNINWVRQAPGKGLEWVSSFSGGKTKMYANSVGRFTVSRDSAKNSLFLQMNLSLADDTAMYYCASPIYRG-----IVAYYF HYWGHGTLTVTVSS-----
3C10	QVQLLETGAEVKKSGASVKASGFLSD--YFMHWVRQAPGQGLEWGMWINPNNGGAKYAQKQGRVMTTRDTSINTVYEMELTRLPDDTAIYYCAREGQEG-----YGG DW-FDPWGQGLTVTVSS-----
3E2	QVQLQSGPGLVRPSETLSLCTVSEGSFRS--YLSWIRQASAGKLEWIGRMYL-NGKTYNPSLRSRVMSVDTSKKQFSLNLSVTAADTAVYYCATDRGW-----ATSSQG-M DVWGQTTTVTVSS-----
3G5	QVQLQESGGGLVQPGGSLRLSCAASGFKFSD--YWMHWVRQAPGKGLMWVRSINDGSSTFAESVKGRFSMSRDNAKNTLYLQMNLSRGDDAAVYYCVR--DS-----FTA LDLWGQGLTVTVSSASTKGPSS
3G8	QVQLVESGAEVKRPQGGSLRLSCKAFGGSSFS--YAFSWLRQAPGQPEWGRHPIVGLPTYTSNFQGRISISADTSTRVFMDLNSLSDAAVYFCARESSRN-----SGVGYFD LWGQGLTVTVSS-----
3H5	QVQLVESGGGVVQGRSLRLSCEASGFTFSR--HEMHWVRQAPGKGLEWVALISNDGGSNYADSVKGRFTISRDNKNTLHLQMNLSRPDDTAIYYCARDTVG-----VGM DVWGQTTTVTVSS-----
4C5	QVQLQSGPGLLKPSQTLTSLCTVSDGSISSGSHYWSWIRQAPGKLEWIGHIFY-SGVTYITPSLRSKRLTMSADTSKNQFSLRLTSVTAADTAVYYCARQICF-----GASCS--FDS WGQGLTVTVSS-----
5B8	QVQLVQSGAEVKKPGSSVKVCKASGGTFSS--YAISWVRQAPGQGLEWGMGIPIFGTANYAQKQGRVTTITADESTSTAYMELSSLRSEDVAVYYCARANYDF-----WSGYTSG GPWGQGLTVTVSS-----
5C5	QVQLVESGGDLVQPGGSLRLSCAASGFTFRD--YAMSWVRQAPGKGLEWVSTSSGSGSNYADSVKGRFTISRDNKNTLYLQMNLSRADDATAYYCVKGG-----YYYH MDVWGQTTTVTVSS-----
5D6	QVTLKESGPVLVKTETLTLCTVSGFSLNARMGVSWIRPPGKALEWLAHIFS-NDEKSYSTLSKRLTISKDTSKSQVVLTMNDMPVDATAYYCGV-----ASRE--YDYW GQGLTVTVSS-----
5E4	QVQLVETGAEVKKPGASVVRCKPSGYNFSD--YFLHWVRQAPGQGLEWGMWINPRSGDTTYAQFLGRVTLTSDTSINTAYMELSSLTSDAAVYYCARDIITG-----ALYYA MDVWGQTTTVTVSS-----
5F6	QVQLVESGAEVKPKGSSVKVCTASGTFRS--YVFSWVRQAPGQGLEWGMGIPIVFGTPKYAQKYQGRVSTADESTSTAYMELSSLRSEDVAVYCAVALLP-----PTYYYGM DVWGQTTTVTVSS-----
5G4	QVQLVESGGGLVQPGGSLRLSCAASGFTFSD--YYMSWVRQAPGKLEWVFSISAGSISYADSVKGRFTVSRDDAKNSLYLQMNLSRAEDTAVYYCFG-----DYGVVDV WGRGTTTVTVSS-----
5H8	QVQLQSGPGLVLPSETLSLCTIVSGDSMSSDYIYWSWLRQPPGKLEWIGNVFH-SGFPYYNPSLHNRTISIDTSESRFSLKLTSTVAADNAVYYCARSLHE-----YGDYVGV LDLPWGQGLTVTVSS-----

Table 1B. Multiple alignment for deduced amino acid sequences of anti-IGF1R scFv VL fragments

2A1	QSVLTQPP-SVSGTPGQRTVITSCGSSSNGSST---VNWYHQLPGAAPKLLIYNNDQRPSGVPDRFSGSK--SGTSASLAISGLQSEDEADYYCAAWDGLSGR--VFGGKTLTVL
2A7	NFMLTQPH-SVSESPGKTVTMSCTGSGGSIATSY---VQWYQQRPGSVPTVIYEDDQRPSGVPDRFSGSVSDSSNSASLTISGLKSEDEADYYCQSYDG-SNVI--FGGKTKVTVL
2D9	QTVVTVQEP-SLTVSPGGVTTLTCAASSTAATYAY---PNWFQKQKTAQPTLIYSTDNKHSHWTPARFSGSL--LGGKAALTLRSVQPDDEADYYCCLWFG-GAWV--FGGKTKLTVL
2G5	QSVLTQPP-SASGTPGQRTVITSCGSSSNGSNIY---VYWYQQLPGTPPKLIYRNNRPSGVPDRFSGSK--SGTSASLAISGLRSEDEADYYCAAWDDLSGR--LFGGKTLTVL
3A5	QPGLTQPP-SVSLSPGQTASITCSGDK--LEEKY---VSWYQKPGQSPVLVIYQDNRNRPSTPERFSGSN--SGNTATLITGTQAIDEADYYCQAWDT--FTVG--FGGKTKLTVL
3A6	NFMLTQPH-SVSESPGKTTITCRSSGNIVSNY---VQWYQQRPGSAPTTVIYEDDRRPSGVPDRFSGSIDSSNSASLTISGLKTEDEADYYCQSSHT-SYVV--FGGKTKLTVL
3C5	QSVVTVQPP-SVSGAPGQRTVITSCGSSNIGTYD---VQWYQQLPGTAPKLLIYDNNRPSGVPDPQFSGSK--SGTSASLAITGLQAEDEADYYCQSYDSSLSGHNYVFGTKLTVL
3C10	NFMLTQPH-SVSESPGKTVTISCSGISGDIG-DY---VQWYQQRPGSAPTTVIYENDQRASGVPDRFSGSIDRTSKSASLTISGLKTDDEADYYCQSYAGDTLWV--FGGKTKLTVL
3E2	EIVLTQSPATLSLQGERATLSCRASQNFSGS---YLLAWYQKPGQAPRLLIYGASTRATGIPDRFSGSG--SETDFTLTISGLDPEDSATYCHQYAG--PPGTFGQGTKEIK
3G5	EIVLTQSPDRAVSLGEGATIDCKSSQLLKSSNNKYLWYQKPGQPPKLLIYWASTRESGVPDRFSGSG--SGTDFLTISLQAADVAVYYCHQYNN--TP-YTFGQGTKEIK
3G8	EIVLTQSPDRLSLSPGERATLSCRASQVTD-----TYLAWYQKPGQAPRLLIYGASSRATGIPDRFSGSG--SGTDFLTISRLEPEDFAVYYCQHQG---TSPFTFGPGTKVDIK
3H5	DIVMTQSPSSLASVEDRVTITCRASQGIHN-----DLGWYQKPGKAPRLLIYAASSLQSGVPSRFSGSG--SGTEFTLAISLQPEDFATYCCQYSY--TP-ITFGQGTREIK
4C5	DIVLTQSPATLSLSPGERATLFCRASQVSG-----SYLAWYQKPGQAPRLLIYDASNRAATGIPARFSGNG--SGTDFLTISLQPEDFALYYCQQP-----TMGVSFPGTKVDIK
5B8	DIVMTQTPDLSAVSLGETATITCKSSRSVYFRNSGDFLAWYQKQGPQPKLLIYWASTRESGVPDRFSGSG--SGTDFLTISRLEQSEDAVYFCQYQYD--TP-PTFGPGTKEDIK
5C5	DIRVTQSPDLSAVPLGERATINCKSSQILYSPNNKYLWGFQKPGQPPKLLIYWASTRESGVPDRFSGSG--SGTDFLTISLQAEADVAVYYCQYQY--SPPIYGGQGTREIK
5D6	DIRVTQSPSSLASVGDRTVITCRASQSIHR-----YLNWYQKPGKAPKLLIYAASSLQSGVPSRFSGSG--SGTEFTLAISLQPEDFATYCCQYSY--TP-ITFGQGTREIK
5E4	QPVLTVQPP-SASGTPGQRTVITSCGSSSNGSNT---VNWYQQLPGTAPKLLIYSNIQPSGVPDRFSGSK--SGTSAALASGLQSEDEAEYYCAAWDDLSLNL--LFGGKTKLTVL
5F6	NFMLTQPP-SASGTPGQRTVITSCGSSSNGITNF---VYWYQVPGAAPRLLIYRNDQRPSGVPDRFSGSK--SGTSASLAISGLRSEDKADYYCSAWDDRLDGP--MFGGKTKLTVL
5G4	DIRVTQSPSSLASVGDRTVITCRASQSIIT-----YLNWYQKPGKAPKLLIYATSSLQSGVPSRFSGSG--SGTDFLTISLQPEDFATYCCQHLHS---YP-ITFGQGTREIK
5H8	SSELSQDP-AVSVALGQTVKICQGDS--LRTFY---AGWYQKPGQAPTLVYVDKNNRPSGIPDRFSGSK--SGNTAFLTITGAQAEDEADYYCISRDISGNHWV--FGGKTKLTVL

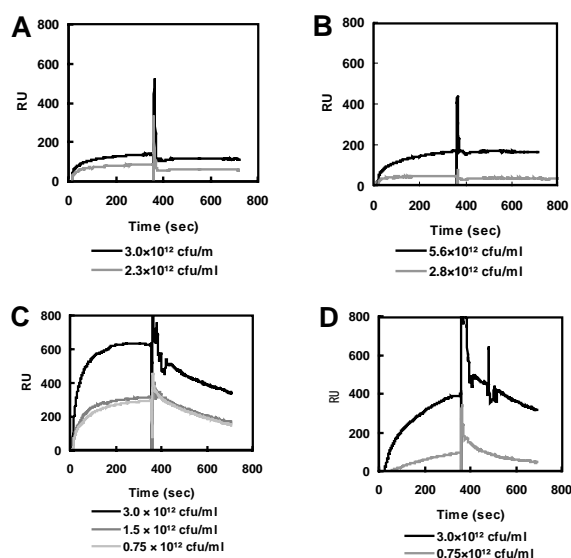


Figure 3. SPR analyses of scFv-presenting phage antibodies. Phage antibodies at indicated concentrations were passed over the IGF-IR-immobilized CM3 chip at a flow rate of 5 μ L/min as described in the Methods. The sensorgrams are 2A1 (A), 3E2 (B), 3H5 (C), and 4C5 (D) phage antibodies, respectively.

is attributable to the scFv portions and not due to the phage itself.

3.3. Expression of a soluble scFv protein from a phage-displaying human scFv

Although different *E. coli* strains transfected with phages derived from the original phage library were subjected to induction of scFv protein expression by IPTG, levels of expression of scFv proteins in this modified system were much lower than in the conventional system (21). SDS-PAGE/CBB staining (Figure 4A) and Western blotting/anti-E tag Ab immunostaining (Figure 4B) revealed an expression profile typical of scFv proteins produced from TOP10F'-FS infected with phages. The immunostaining did not reveal any apparent bands with \sim 30 kDa scFvs, indicating that respective scFv proteins were not produced.

3.4. Expression, purification and evaluation of MBP-scFv

To thus produce and purify scFv proteins, one of the isolated scFvs was expressed as a MBP-fused protein in *E. coli* and was expected to be a highly soluble and stable protein (20). The 5E4 scFv gene, selected as a model scFv gene encoding a typical scFv sequence, was inserted into pMAL-p2E vector as illustrated in Figure 5A. *E. coli* JM109, transformed with pMAL-p2E-5E4, was cultured with IPTG to induce the 5E4 MBP-scFv. Periplasm fractions were collected and subjected to two step-affinity chromatography purification. Each purification step was monitored

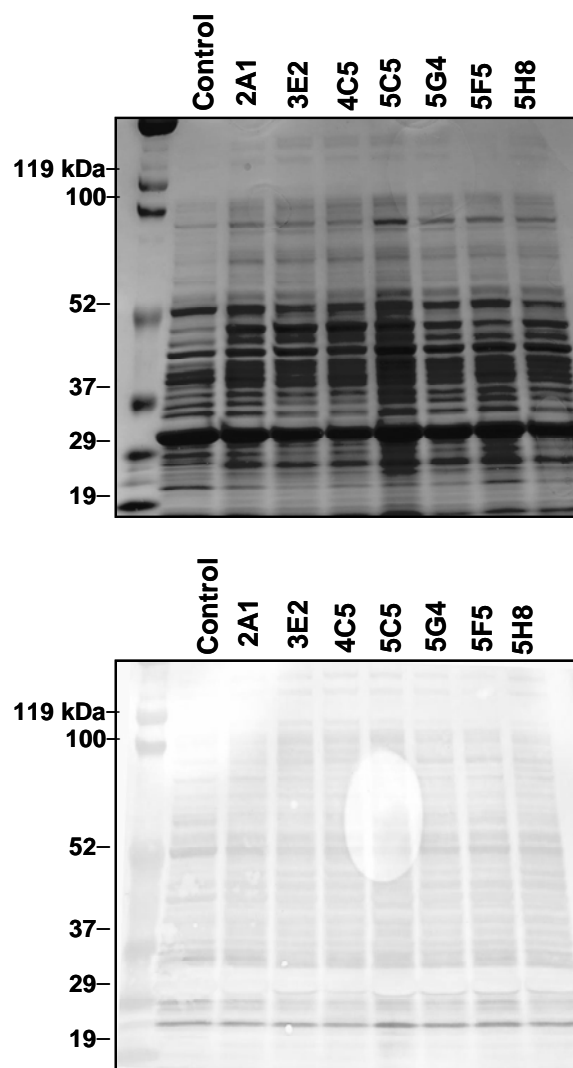


Figure 4. SDS-PAGE/Western blotting analysis of expression levels of isolated scFv proteins. Periplasm fractions (10 μ g/lane) extracted from *E. coli* infected with phages were subjected to SDS-PAGE/CBB stain (Figure 4A) or blotted onto a PVDF membrane that was immunostained with HRP-anti-E tag Ab (Figure 4B).

by SDS-PAGE (Figure 5B). Both MBP and MBP-scFv proteins were recovered after the first affinity chromatography step (Figure 5B, lane 3), but only the MBP-scFv fusion protein was purified to apparent homogeneity by the second affinity chromatography step (Figure 5B, lane 5). The yield of purified MBP-scFv was 0.3 mg from 1L culture. As a control, MBP protein was expressed, purified, and analyzed by SDS-PAGE (Figure 5A, lane 6). The binding affinity of MBP-scFv for IGF-IR was evaluated by ELISA. As seen in Figure 6A, the purified MBP-scFv bound to IGF-IR in a dose-dependent manner whereas the purified MBP protein did not bind to IGF-IR, indicating that the binding of MBP-scFv to IGF-IR was *via* its scFv domain. Further analysis of MBP-scFv revealed cross-reactivity to rhIR (Figure 6B), which shares sequence and structural similarities. This result implied that the scFv recognizes the epitopes that are shared by IGF-IR and IR.

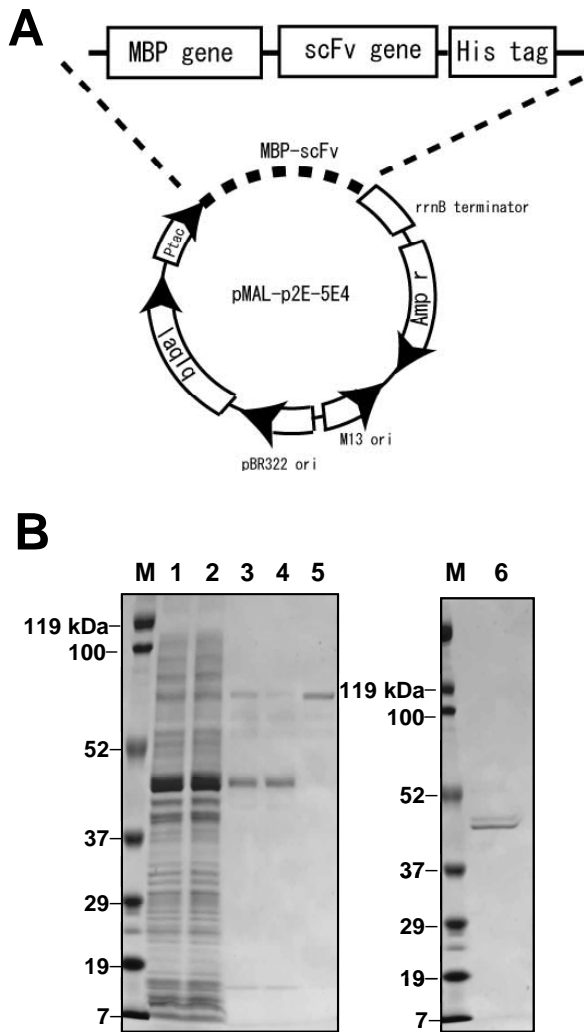


Figure 5. Construction, expression, and purification of anti-IGF-IR MBP-scFv. (A) Schematic representation of the pMAL-scFv vector into which the scFv gene (5E4) with a His tag sequence was inserted. (B) SDS-PAGE analysis of purification steps. The MBP-scFv protein expressed in the periplasm of *E. coli* was first applied to an amylose resin column. The eluates were further purified with a Ni²⁺-column. SDS-PAGE gel stained with Coomassie Brilliant Blue shows: lane 1, periplasmic fraction; lane 2, flow-through fraction of the amylose resin column; lane 3, the eluted fraction from the amylose resin column, lane 4, flow-through fraction of Ni²⁺-column; lane 5, the eluted fraction from Ni²⁺-column (purified MBP-scFv), and lane 6, purified MBP. Five μ g of protein were loaded in lanes 1 and 2 whereas 2 μ g of protein were loaded in lanes 3-6.

4. Discussion

This study achieved successful isolation of phage antibodies bearing human scFvs against IGF-IR. As anticipated, expression of scFv proteins in the periplasmic space of phage-infected *E. coli* was so difficult that one of scFv proteins was fused with MBP. The resulting fused protein was successfully produced and purified by two-step affinity chromatography. MBP-scFv clearly exhibited binding affinity for IGF-IR whereas MBP did not bind to the antigen, which suggested that the IGF-IR binding affinity of MBP-scFv protein was attributable to the scFv domain. Further experiments, however, revealed that MBP-scFv cross-reacted to rhIR, implying that the scFv recognizes

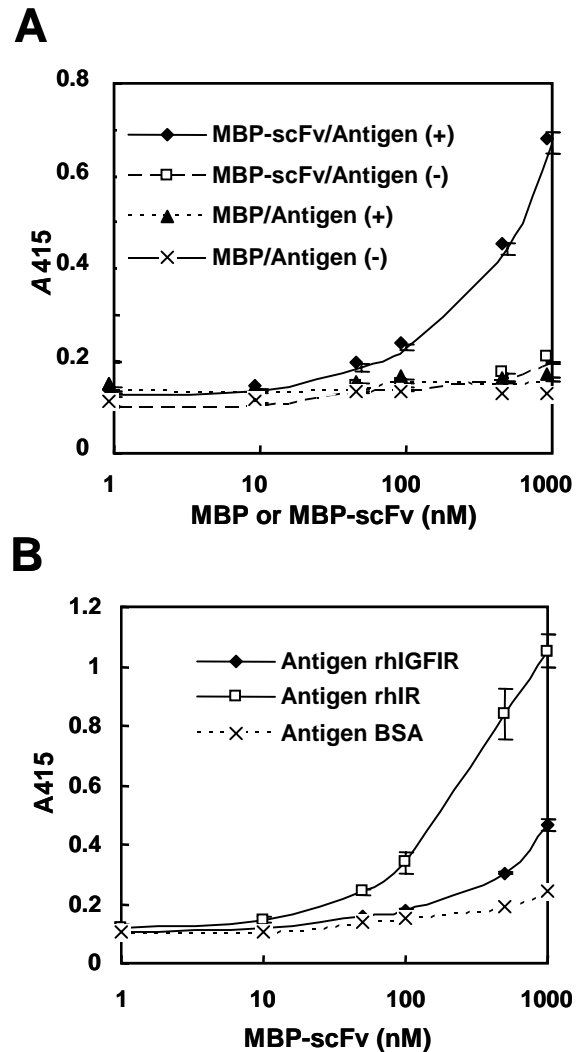


Figure 6. Binding of purified MBP-scFv and MBP to IGF-IR or IR. (A) Binding of the purified MBP-scFv and MBP to immobilized rhIGF-IR (antigen +) or BSA (antigen -) measured by ELISA. Binding of MBP-scFv and MBP at indicated concentrations was detected by an anti-MBP mAb followed by an anti-mouse IgG/HRP. (B) Binding of the purified MBP-scFv at indicated concentrations to immobilized rhIGF-IR (antigen IGF-IR), rhIR (antigen IR), or BSA (antigen BSA) was measured by ELISA as described above. The error bars represent the standard deviation calculated from replicates ($n = 3$).

the epitopes that are shared by IGF-IR and IR. This result highlights the importance of vigorous screening with the use of two or more independent approaches during isolation of candidate clones from a phage display library.

Since phage display technology provides genes that encode scFvs with specificity of interest, recombinant antibodies including completely human IgGs for therapeutic applications can readily be produced. However, the best clones must be chosen after completing initial characterization of scFv proteins from isolated phage clones by examining whether scFvs have high specificity and affinity for the antigen of interest. Usually, this can be achieved by inducing the production of scFv protein in phage-infected *E. coli*. Although scFvs that can be expressed in the

cytoplasm of cells have considerable biotechnological and therapeutic potential, the reducing environment of the cytoplasm inhibits the formation of disulfide bonds that are essential for correct folding and functionality of the antibody fragments. Thus, scFvs expressed in the cytoplasm are mostly insoluble and inactive. Alternatively, scFv proteins are often expressed in the periplasmic space, though this process is not always successful, as indicated by the current results (Figure 4). As a general approach to stabilizing scFvs for efficient functional expression in the cell cytoplasm, scFvs were expressed as C-terminal fusions with the *E. coli* MBP (24). A previous study demonstrated that MBP-fused scFvs are expressed at high levels in the cytoplasm of *E. coli* as soluble and active proteins regardless of the redox state of the bacterial cytoplasm, suggesting that MBP seems to function as a molecular chaperone that promotes the solubility and stability of scFvs. In this study, MBP-scFv protein was expressed in the periplasm, which should further facilitate stability of the expressed protein. In conclusion, this study demonstrated that MBP-scFv can be expressed as a recombinant human scFv in the periplasm of *E. coli*, which can be easily purified for further characterization.

References

1. LeRoith D, Roberts CT Jr. The insulin-like growth factor system and cancer. *Cancer Lett* 2003; 195:127-137.
2. Haddad T, Yee D. Targeting the insulin-like growth factor axis as a cancer therapy. *Future Oncol* 2006; 2:101-110.
3. Hartog H, Wesseling J, Boezen HM, van der Graaf WT. The insulin-like growth factor I receptor in cancer: old focus, new future. *Eur J Cancer* 2007; 43:1895-1904.
4. Maor S, Mayer D, Yarden RI, Lee AV, Sarfstein R, Werner H, Papa MZ. Estrogen receptor regulates insulin-like growth factor-I receptor gene expression in breast tumor cells: involvement of transcription factor Sp1. *J Endocrinol* 2006; 191:605-612.
5. Pandini G, Mineo R, Frasca F, Roberts CT Jr, Marcelli M, Vigneri R, Belfiore A. Androgens up-regulate the insulin-like growth factor-I receptor in prostate cancer cells. *Cancer Res* 2005; 65:1849-1857.
6. Neuenschwander S, Roberts CT Jr, Leroith D. Growth inhibition of MCF7 breast cancer cells by stable expression of an insulin-like growth factor I receptor antisense ribonucleic acid. *Endocrinology* 1995; 136:4298-4303.
7. Mitsiades CS, Mitsiades NS, McMullan CJ, Poulaki V, Shringarpure R, Akiyama M, Hideshima T, Chauhan D, Joseph M, Liberman TA, Garcia-Echeverria C, Pearson MA, Hofman F, Anderson KC, Kung AL. Inhibition of the insulin-like growth factor receptor 1 tyrosine kinase activity as a therapeutic strategy for multiple myeloma, other hematologic malignancies, and solid tumors. *Cancer Cell* 2004; 5:221-230.
8. Hofmann F, Garcia-Echeverria C. Blocking the insulin-like growth factor-I receptor as a strategy for targeting cancer. *Drug Discov Today* 2005; 10:1041-1047.
9. Kusada Y, Fujita-Yamaguchi Y. An overview of currently available anti-insulin-like growth factor I receptor antibodies. *BioScience Trends* 2007; 1:128-133.
10. Hwang WY, Almagro JC, Buss TN, Tan P, Foote J. Use of human germline genes in a CDR homology-based approach to antibody humanization. *Methods* 2005; 36:35-42.
11. Lonberg N. Human antibodies from transgenic animals. *Nat Biotechnol* 2005; 23:1117-1125.
12. Hoogenboom HR. Human antibodies from transgenic animals. *Nat Biotechnol* 2005; 23:1105-1116.
13. Bothmann H, Pluckthun A. The periplasmic *Escherichia coli* peptidylprolyl cis,trans-isomerase FkpA. I. Increased functional expression of antibody fragments with and without cis-prolines. *J Biol Chem* 2000; 275:17100-17105.
14. Ramm K, Pluckthun A. The periplasmic *Escherichia coli* peptidylprolyl cis,trans-isomerase FkpA. II. Isomerase-independent chaperone activity *in vitro*. *J Biol Chem* 2000; 275:17106-17113.
15. Dueñas M, Vázquez J, Ayala M, Söderlind E, Ohlin M, Pérez L, Borrebaeck CA, Gavilondo JV. Intra- and extracellular expression of an scFv antibody fragment in *E. coli*: effect of bacterial strains and pathway engineering using GroES/L chaperonins. *Biotechniques* 1994; 16:476-477, 480-483.
16. Martin CD, Rojas G, Mitchell JN, Vincent KJ, Wu J, McCafferty J, Schofield DJ. A simple vector system to improve performance and utilisation of recombinant antibodies. *BMC Biotechnol* 2006; 6:46.
17. Oh MS, Kim KS, Jang YK, Maeng CY, Min SH, Jang MH, Yoon SO, Kim JH, Hong HJ. A new epitope tag from hepatitis B virus preS1 for immunodetection, localization and affinity purification of recombinant proteins. *J Immunol Methods* 2003; 283:77-89.
18. Sachdev D, Li SL, Hartell JS, Fujita-Yamaguchi Y, Miller JS, Yee D. A chimeric humanized single-chain antibody against the type I insulin-like growth factor (IGF) receptor renders breast cancer cells refractory to the mitogenic effects of IGF-I. *Cancer Res* 2003; 63:627-635.
19. Ye JJ, Liang SJ, Guo N, Li SL, Wu MA, Giannini S, Sachdev D, Yee D, Brunner N, Ikle D, Fujita-Yamaguchi Y. Combined effects of tamoxifen and a chimeric humanized single chain antibody against the type I IGF receptor on breast tumor growth *in vivo*. *Horm Metab Res* 2003; 35:836-842.
20. Kapust RB, Waugh DS. *Escherichia coli* maltose-binding protein is uncommonly effective at promoting the solubility of polypeptides to which it is fused. *Protein Sci* 1999; 8:1668-1674.
21. Kusada Y, Morizono T, Matsumoto-Takasaki A, Sakai K, Sato S, Asanuma H, Takayanagi A, Fujita-Yamaguchi Y. Construction and characterization of single-chain antibodies against human insulin-like growth factor-I receptor from hybridomas producing 1H7 or 3B7 monoclonal antibody. *J Biochem* 2008; 143:9-19.
22. Sakai K, Shimizu Y, Chiba T, Matsumoto-Takasaki

- A, Kusada Y, Zhang W, Nakata M, Kojima N, Toma K, Takayanagi A, Shimizu N, Fujita-Yamaguchi Y. Isolation and characterization of phage-displayed single chain antibodies recognizing non-reducing terminal mannose residues. 1. A new strategy for generation of anti-carbohydrate antibodies. *Biochemistry* 2007; 46:253-262.
23. Marks JD, Hoogenboom HR, Bonnet TP, McCafferty J, Griffiths AD, Winter G. By-passing immunization. Human antibodies from V-gene libraries displayed on phage. *J Mol Biol* 1991; 222:581-597.
24. Bach H, Mazor Y, Shaky S, Shoham-Lev A, Berdichevsky Y, Gutnick DL, Benhar I. Escherichia coli maltose-binding protein as a molecular chaperone for recombinant intracellular cytoplasmic single-chain antibodies. *J Mol Biol* 2001; 312:79-93.
25. Bachhawat K, Thomas CJ, Amutha B, Krishnasastri MV, Khan MI, Surolia A. On the stringent requirement of mannosyl substitution in manno oligosaccharides for the recognition by garlic (*Allium sativum*) lectin. *J Biol Chem* 2001; 276:5541-5546.

(Received July 18, 2008; Revised July 28, 2008; Accepted July 29, 2008)

Original Article**The effects of dietary obesity on protein expressions of insulin signaling pathway in rat aorta**Sameer H. Fatani¹, Ebrahim K. Naderali^{1,*}, Sunil Panchiani², Feisal Shah³, Chris Wong⁴¹ Neuroendocrine and Obesity Biology Unit, School of Clinical Science, University of Liverpool, Liverpool L69 3GA, UK;² Royal Liverpool Hospital, Prescott Street, Liverpool, L7 8XP, UK;³ Countess of Chester Hospital NHS Foundation Trust, Liverpool Road, Chester CH2 1UL, UK;⁴ Aintree University Hospital NHS Foundation Trust, Longmoor lane, Liverpool, L9 7AL, UK.

ABSTRACT: The deleterious effects of obesity on insulin response in vasculature may be due to changes in various components of insulin signaling pathway. Therefore, this study was designed to investigate effects of dietary-obesity, removal of palatable diet, and fenofibrate treatment on protein expressions of insulin signaling pathway in rat aorta. Adult male Wistar rats were fed either standard chow or a palatable diet (untreated obese animals) for 15 weeks. Another group of rats were fed the palatable diet for 8 weeks followed by standard chow for further 7 weeks, while a further group were fed the palatable diet for 15 weeks and were dosed with fenofibrate (50 mg/kg/day) for the last 7 weeks. Untreated obese animals had significantly higher body weight than other three groups ($p < 0.05$ for all). There were no significant differences between IR- β , IRS1 and IRS2, Akt, Shc, and ERK1/2 levels in chow-fed and untreated obese animals, while PI 3-kinase level were significantly ($p < 0.0001$) decreased in untreated obese animals. Chronic removal of palatable diet completely reversed the levels of PI 3-kinase to the normal while, fenofibrate treatment further reduced PI 3-kinase levels. On the other hand, there was a significant ($p < 0.05$) increase in eNOS in untreated obese animals compared with chow-fed controls. This effect was reversed by removal of palatable diet and fenofibrate treatment. These data suggest that dietary-obesity selectively inhibits PI 3-kinase while, removal of obesity-inducing diet improves PI 3-kinase levels which may have a role in vascular reactivity.

Keywords: Obesity, Insulin resistance, Insulin signaling pathway, Vascular function, PI 3-kinase, Fenofibrate

*Correspondence to: Dr. Ebrahim K. Naderali, Neuroendocrine and Obesity Biology Unit, School of Clinical Science, University of Liverpool, Daulby Street, Liverpool L69 3GA, UK; e-mail: naderali@liv.ac.uk

1. Introduction

Obesity, characterized by excess adipose tissue is now becoming a worldwide epidemic (1,2). Various studies have suggested that obesity *per se* is an independent cardiovascular risk factor (3), as well as predisposing to type 2 diabetes, hypertension and dyslipidaemia (4). Furthermore, obesity induces insulin resistance which is associated with development of cardiovascular diseases that include hypertension (5), and reduced endothelial function (6). Insulin has a protective role in vascular function. It stimulates nitric oxide (NO) production, leading to vasorelaxation. Insulin-induced NO-dependent vasorelaxation is markedly decreased in obesity (7), however, the mechanism(s) of decrease in insulin-induced vasorelaxation is not fully understood. Insulin has other major physiological roles that include facilitation and increase of amino acid transport, glycogen synthesis, DNA synthesis and gene expression (8). Moreover, it specifically enhances release of nitric oxide (9,10), regulates mRNA matrix proteins (11) and constitutive endothelial NO synthase (12) activity in vasculature.

In vascular cells, the effects of insulin are initiated through binding to the insulin receptor alpha subunit (IR- α), which activates the intrinsic receptor tyrosine kinase (13), resulting in autophosphorylation of insulin receptor beta subunit (IR- β) and tyrosine phosphorylation of intracellular adaptor proteins - insulin receptor substrates (IRS-1 and IRS-2) (14) and Shc (15). Tyrosine phosphorylated IRS-1 or IRS-2 then binds to src-homology 2 (SH2) domains of intracellular proteins, including the p85 regulatory subunit of phosphatidylinositol (PI) 3-kinase (16). The interactions of IRS and p85 subunit of PI 3-kinase results in the activation of p110 catalytic subunit of PI 3-kinase. Activation of PI 3-kinase increases serine phosphorylation of Akt which in turn, directly phosphorylates eNOS on serine 1177 and activates the enzyme, leading to increased NO production and thus providing vascular protection (17). Tyrosine

phosphorylated Shc and IRS proteins can also bind to SH2 domain of Growth factor Receptor-protein Bound 2 (GRB2), leading to the activation of the Ras-Raf-MAP kinase signal pathway that is associated with gene expression and cell growth (18). PI 3-kinase expression and activation has been linked to NO production, whereas, Raf-MAP kinase pathway is associated with the growth of vascular cells and the expression of extracellular matrix proteins (10). Furthermore, various studies (7-12) have shown attenuation of insulin-induced vasorelaxation in obesity, however, there is little information on the mechanism(s) of diet-induced changes in insulin signaling pathway in vasculature. Therefore, it is possible that changes in any component of insulin signaling pathway may alter vasorelaxant property of insulin. Furthermore, the level of protein expression of these kinases could fluctuate and respond differently to any pathological, physiological, or pharmacological conditions, such as dietary obesity and its treatment. Therefore, investigating the protein expression of these kinases under certain obesity-related experimental conditions could provide vital information about obesity-induced insulin resistance in vascular tissues. Consequently, we aimed in this study to investigate the protein expression of insulin signaling components in aorta of four different experimental groups, namely, 1) control chow-fed lean animals, 2) untreated diet-induced obese animals, 3) obese animals following chronic withdrawn of palatable diet, and 4) obese animals treated with fenofibrate. Fenofibrate has been shown to improve lipid profiles, reduce adiposity, and may have a role in correction of vascular function in obesity.

2. Materials and Methods

2.1. Animal and experimental protocol

All procedures used in this study were approved by the institutional committee and accord with current UK legislations. Adult male Wistar rats ($n = 28$, 190 ± 3 g) were randomized and assigned to a control group ($n = 7$) and a test group ($n = 21$). All animals had free access to water and were housed individually under controlled environmental conditions ($19-22^{\circ}\text{C}$; 30-40% humidity) and a 12 h light-dark cycle (lights on at 07:00 h). Controls were fed standard laboratory pelleted diet (Chow-fed; CRM Biosure, Cambridge, UK), while test group had free access to a highly-palatable diet consisting of (by weight) 33% ground pellet diet, 33% Nestlé condensed milk, 7% sucrose and 27% water. The energy content of chow was: 60% as carbohydrate, 30% as protein, and 10% as fat, and that of palatable diet was 65% as carbohydrate, 19% as protein and 16% as fat. Chow-fed controls remained on their prospective diet for 15 weeks, while after 8 weeks palatable-diet-fed animals were subdivided into three subgroups (each group 7 animals). In the first subgroup, palatable diet was

removed and the standard chow diet was re-introduced (diet-to-chow), while the second subgroup remind on palatable diet and were given fenofibrate (fenofibrate-treated, 50 mg/kg/day) by oral gavage for further 7 weeks and the third subgroup (diet-fed) was given vehicle (1% carboxymethyl cellulose at 1 mL/kg body weight; Sigma, UK), by oral gavage daily for 7 weeks. On the day of experiment (after 15 weeks), the rats were killed by CO_2 inhalation after 2 h of fasting and the aorta was dissected and snap frozen in liquid nitrogen for molecular studies.

2.2. Protein extraction

Fifty milligram of aorta was homogenized at 4°C in 500 μL buffer containing 120 mM NaCl, 10% glycerol, 2 mM Na_3VO_4 , 1% Nonidet-P40, 1 mM PMSF, 10 mM $\text{Na}_4\text{P}_2\text{O}_7$, 100 mM NaF, 20 mM Tris (pH 7.6) and a complete mini[®] protease inhibitor cocktail with polytron homogenizer. The homogenates were then incubated on a rocking platform at 4°C for 30 min. After 3×10 sec bursts of sonication, tubes were subsequently centrifuged for 45 min at $13,000 \times g$ at 4°C . Supernatants were collected, and protein concentrations were determined by the BCA method kit.

2.3. Western-immunoblotting

2.3.1. SDS-PAGE

A discontinuous acrylamide gel system was used. A stacking gel (5%) was set above a 10% (depending on protein of interest) resolving gel. Samples were standardized to 4 mg/mL with lysis buffer. 20 μL of sample protein was boiled in 20 μL $2 \times$ electrophoresis sample buffer, for 10 min and then subjected to SDS-PAGE (Tris-glycine buffer, 100 V). Resolved proteins were electro blotted onto nitrocellulose membranes in buffer containing 25 mM Tris, 190 mM glycine, 1% SDS (w/v) and 20% (v/v) methanol (100 V for 1 h). Staining immobilized proteins on nitrocellulose with Ponceau S assessed successful transfer. Nitrocellulose blots were sub-merged in 0.2% Ponceau S for 15 min with agitation. Blots were then washed with $1 \times$ PBS with 1% Tween, until proteins could be visualized. Blots were then washed until protein bands had disappeared.

2.3.2. Immunoblotting

Non-specific binding proteins were prevented by incubating the blot with blocking buffer (5% milk powder, $1 \times$ PBS) at room temperature for one hour, followed by immunoblotting with appropriate primary antibody (1:500 dilution) made up in blocking buffer, left overnight at 4°C . Blots were then washed in $1 \times$ PBS with 1% Tween and incubated with secondary antibody (1:1,000), a HRP linked anti-rabbit for 1 h at room temperature. Proteins were detected using enhanced

chemiluminescence method. Positive controls were included for standardization of samples between blots and molecular weights markers were used for sizing bands. Densitometry was used to quantify protein bands.

2.4. Chemicals and antibodies

SDS-PAGE and immunoblotting equipments were obtained from Bio-Rad (Richmond, Calif., USA). Tris, phenylmethylsulfonyl fluoride (PMSF), aprotinin, dithiothreitol, Tween-20 and glycerol were obtained from Sigma Chemicals (Sigma Ltd., UK). Complete mini[®] protease inhibitor cocktail was obtained from Roche Diagnostics Ltd. (East Sussex, UK). BCA (Bicinchoninic acid) method kit for protein determination was obtained from (Sigma Ltd., UK). Secondary antibody, an HRP-linked anti-rabbit was purchased from (Serotec, Oxford, UK). Molecular weight marker was obtained from (BioRad Laboratories Ltd., Hertfordshire, UK) Polyclonal antibodies against beta subunit of insulin receptor (C-19, sc-711), IRS-1 (C-20, sc-559), IRS-2 (A-19, sc-1556), eNOS (NOS3, C-20, sc-654), Akt1 (C-20, sc-1618), Shc (C-20, sc-288: specific for Shc p46, p52 and p66) and ERK1 (C-16, sc-93: reactive with ERK1 p44 and, to lesser extent, ERK2 p42) and PI 3-kinase were purchased from Santa Cruz Biotechnology (Santa Cruz, Calif., USA).

2.5. Data interpretation and statistical analysis

Changes in body weights of each group were collected weekly and are expressed as absolute total body weight respectively. For Western blotting, the data from chow-fed (control) animals were expressed as 100% response, and the results from other three groups were normalized and subsequently expressed as the percentage of their respective controls. Data are expressed as mean \pm S.E.M. Data have normal distribution (Shapiro Wilk W test). Statistical significance was tested using Student 't-test' or repeated-measures (ANOVA; Bonferroni *t*-test) or the Mann-Whitney test, as appropriate. Results were considered statistically significant at the $p < 0.05$ levels.

3. Results

3.1. Changes in total body weight

Animals given palatable diet progressively gained more weight than their chow-fed counterparts. A significant difference in total body weight was observed after 5th week of feeding and further increased after 8th week where diet-fed animals had significantly ($> 10\%$, $p = 0.0041$) higher total body weight than chow-fed controls. At the end of the experiment, body weight of diet-to-chow and fenofibrate treated animals were significantly ($p < 0.01$) lower than untreated diet-fed animals (Figure 1).

3.2. Protein expression studies

3.2.1. IR- β

There were no significant differences in IR- β protein levels in aorta from chow-fed, untreated diet-fed and diet-to-chow animals, while aorta from fenofibrate-treated animals had significantly (up to 30%, $p < 0.001$) higher IR- β protein levels than chow-fed group (Figure 2).

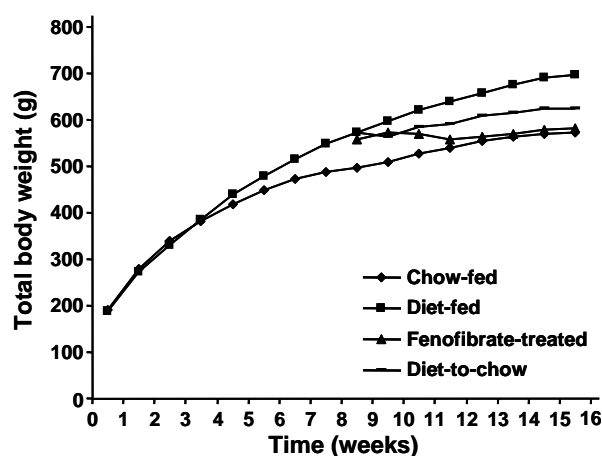


Figure 1. The effect of palatable diet, its removal, and fenofibrate treatment on total body weight in the rat. Animals were fed either standard chow (chow-fed) or a palatable diet (diet-fed) for 15 weeks. Fenofibrate treated group was fed palatable diet for 15 weeks and received fenofibrate (50 mg/Kg/day) for the last 7 weeks, while diet-to-chow group was fed palatable diet for the first 8 weeks and chow for the last 7 weeks of the experiment. At the end of the experiment (15 weeks) diet-fed animals weighed significantly greater than the chow-fed, fenofibrate-treated, and diet-to-chow groups ($p < 0.0002$, 0.002 , and 0.02 , respectively). The body weight of diet-to-chow group was significantly greater ($p < 0.02$) than the chow-fed group, while that of the fenofibrate-treated group was not significantly ($p < 0.66$) different from the chow-fed group. Data are expressed as mean \pm S.E.M.

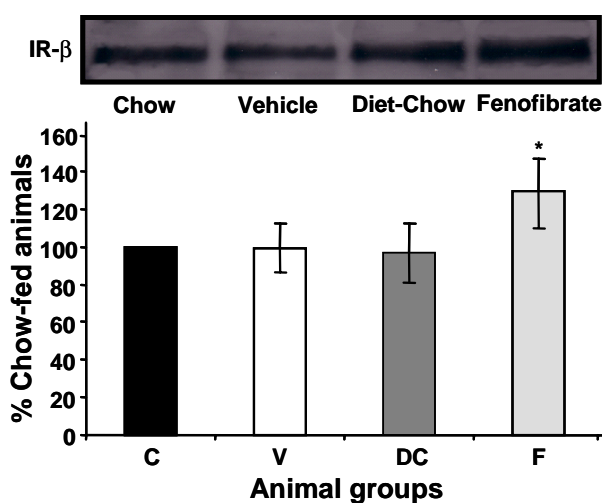


Figure 2. Protein expression of IR- β in the rat aorta. Equal amounts (40 μ g/well) of protein were separated by SDS-PAGE and immunoblotted with IR- β antibody. The animal groups are: C) chow-fed lean control, V) Vehicle group (untreated dietary obese), DC) Diet-to-Chow group, and F) fenofibrate treated group. Data (mean \pm SEM; $n = 7$) are normalised to that of control group and expressed as a percentage of the chow fed (control) rats. * $p < 0.05$ vs chow fed.

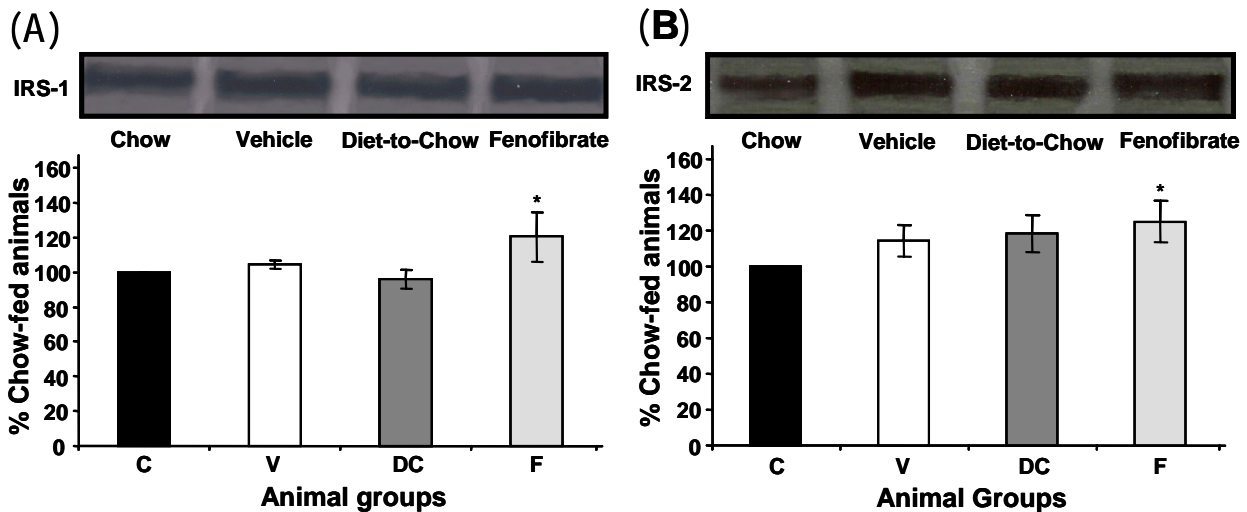


Figure 3. Protein expression of IRS-1 and IRS-2 in the rat aorta. Equal amounts (40 $\mu\text{g/well}$) of protein were separated by SDS-PAGE and immunoblotted with IRS-1 (A) or IRS-2 (B) antibody. The animal groups are: C) chow-fed lean control, V) Vehicle group (untreated dietary obese), DC) Diet-to-Chow group, and F) fenofibrate treated group. Data (mean \pm SEM; $n = 7$) are normalised to that of control group and expressed as a percentage of the chow fed (control) rats. * $p < 0.05$ vs chow fed.

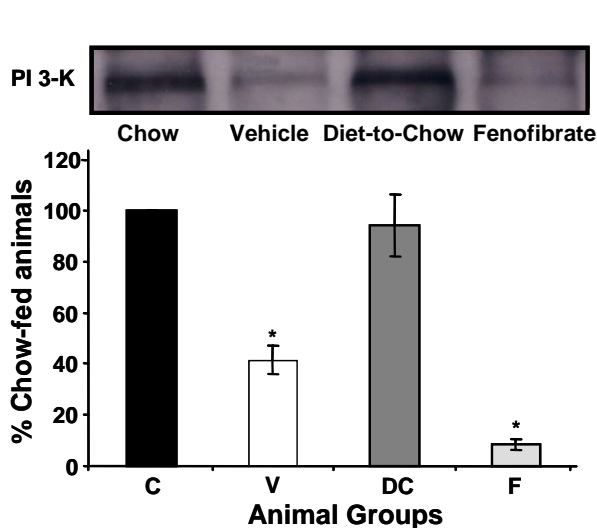


Figure 4. Protein expression of PI 3-K in the rat aorta. Equal amounts (40 $\mu\text{g/well}$) of protein were separated by SDS-PAGE and immunoblotted with PI 3-kinase antibody. The animal groups are: C) chow-fed lean control, V) Vehicle group (untreated dietary obese), DC) Diet-to-Chow group, and F) fenofibrate treated group. Data (mean \pm SEM; $n = 7$) are normalised to that of control group and expressed as a percentage of the chow fed (control) rats. * $p < 0.0001$ vs chow fed.

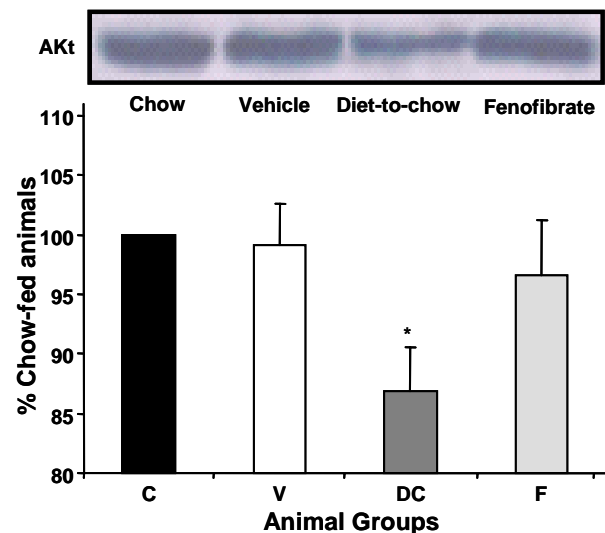


Figure 5. Protein expression of Akt in the rat aorta. Equal amounts (40 $\mu\text{g/well}$) of protein were separated by SDS-PAGE and immunoblotted with Akt antibody. The animal groups are: C) chow-fed lean control, V) Vehicle group (untreated dietary obese), DC) Diet-to-Chow group, and F) fenofibrate treated group. Data (mean \pm SEM; $n = 7$) are normalised to that of control group and expressed as a percentage of the chow fed (control) rats. * $p < 0.05$ vs chow fed.

3.2.2. IRS-1 and IRS-2

As with IR- β , the IRS-1 and IRS-2 levels in chow-fed, untreated diet-fed and diet-to-chow fed groups were comparable, while aorta from fenofibrate-treated animals had significantly higher levels of both IRS-1 (26%, $p < 0.05$) and IRS-2 (25%, $p < 0.05$) compared to chow-fed group (Figure 3).

3.2.3. PI 3-kinase

Compared with chow-fed animals, there was a marked reduction in PI 3-kinase levels in untreated diet-fed

animals (59%, $p < 0.001$). PI 3-kinase levels were further reduced by fenofibrate-treatment (92%, $p < 0.0001$), while removal of palatable diet completely reversed the reduction in PI 3-kinase levels seen in diet-fed group (Figure 4).

3.2.4. Akt

The protein levels of Akt were similar in chow-fed, untreated diet-fed and fenofibrate-treated animals, while aorta from diet-to-chow group had significantly lower (13%, $p < 0.01$) levels of Akt protein (Figure 5).

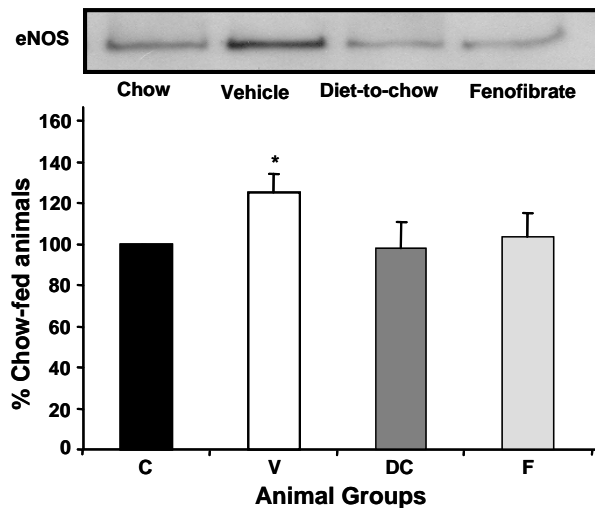


Figure 6. Protein expression of eNOS in the rat aorta. Equal amounts (40 $\mu\text{g}/\text{well}$) of protein were separated by SDS-PAGE and immunoblotted with eNOS antibody. The animal groups are: C) chow-fed lean control, V) Vehicle group (untreated dietary obese), DC) Diet-to-Chow group, and F) fenofibrate treated group. Data (mean \pm SEM; $n = 7$) are normalised to that of control group and expressed as a percentage of the chow fed (control) rats. * $p < 0.05$ vs chow fed.

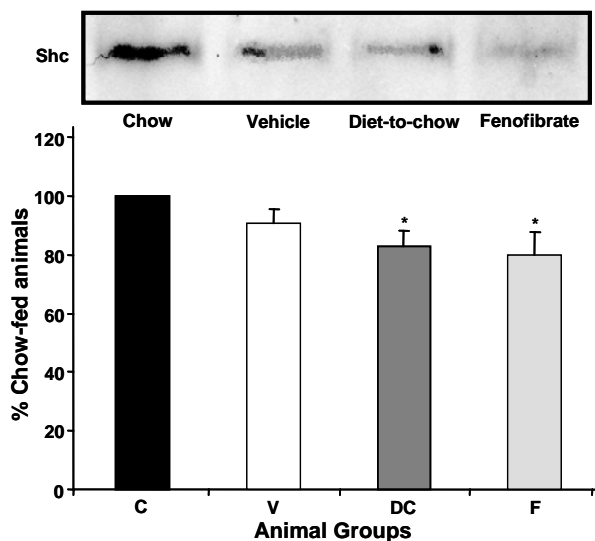


Figure 7. Protein expression of Shc in the rat aorta. Equal amounts (40 $\mu\text{g}/\text{well}$) of protein were separated by SDS-PAGE and immunoblotted with Shc antibody. The animal groups are: C) chow-fed lean control, V) Vehicle group (untreated dietary obese), DC) Diet-to-Chow group, and F) fenofibrate treated group. Data (mean \pm SEM; $n = 7$) are normalised to that of control group and expressed as a percentage of the chow fed (control) rats. * $p < 0.05$ vs chow fed.

3.2.5. eNOS

There was a significant (25%, $p < 0.001$) elevation of eNOS levels in aorta from untreated diet-fed animals compared with that of chow-fed control, while removal of diet or fenofibrate-treatment markedly reduced the elevation of eNOS protein concentration seen in untreated diet-fed animals (Figure 6).

3.2.6. Shc

Although, Shc protein levels were not significantly altered by diet feeding but removal of the diet or

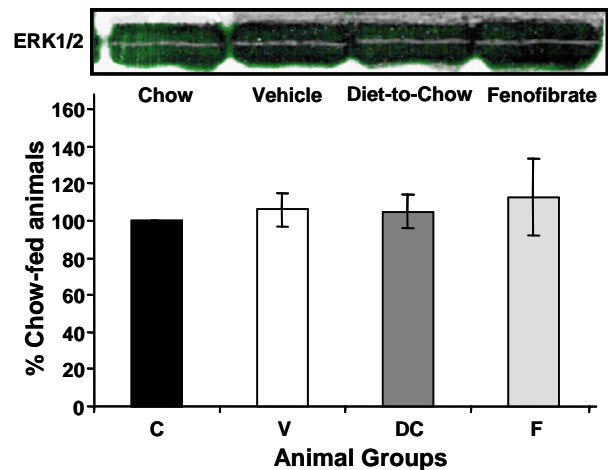


Figure 8. Protein expression of ERK1/2 in the rat aorta. Equal amounts (40 $\mu\text{g}/\text{well}$) of protein were separated by SDS-PAGE and immunoblotted with PERK1/2 antibody. The animal groups are: C) chow-fed lean control, V) Vehicle group (untreated dietary obese), DC) Diet-to-Chow group, and F) fenofibrate treated group. Data (mean \pm SEM; $n = 7$) are normalised to that of control group and expressed as a percentage of the chow fed (control) rats.

fenofibrate-treatment significantly (by up to 20%, $p < 0.05$) attenuated Shc levels in comparison to that of chow-fed controls (Figure 7).

3.2.7. ERK1/2

Immunoblotting analysis of ERK1/2 (MAP kinase pathway) protein in all four groups was remarkably similar to each other. Palatable-diet feeding in the presence or absence of fenofibrate had no effect on ERK1/2 levels nor did the removal of the palatable diet altered ERK1/2 levels in aorta (Figure 8).

4. Discussion

Interactions between insulin, IR- β , IRS-1, and IRS-2 activates PI 3-kinase pathway that results in vasorelaxation. Therefore, the integrity of protein levels and activation of the cascade in insulin signaling pathway in vasculature is a crucial factor in mediating normal vascular functions. In the present study, dietary-obesity did not adversely alter the concentrations of IR- β , IRS-1, and IRS-2, suggesting that reduced vasorelaxation to insulin seen in dietary-obesity (7,19) may not be due to the changes in protein levels of IR- β , IRS-1, and IRS-2. This raises possibility that attenuated insulin responses seen in obesity (7,19) may be due to changes in protein levels beyond membrane receptors. In fact, the present study indicates a marked decrease in PI 3-kinase levels in aorta from dietary-obese rats, suggesting that dietary-obesity adversely affects PI3-kinase protein level and thereby reducing insulin-induced vasorelaxation. Studies on genetically obese animals have reported similar observation. Jiang and colleagues have shown reductions in IRS-1, and IRS-2 but not IRS- β protein levels in obese Zucker rats in comparison with lean animals (20). Moreover, the

same study reported a marked inhibition of PI 3-kinase activation in aorta of fatty-Zucker rats. Although, in this study we did not measure insulin-induced phosphorylation of signaling components, however, low level of PI 3-kinase seen in our study together with reduced functionality of PI 3-kinase reported on Zucker rats (20) may play an important role in integrity of endothelial function. A similar finding has also been reported in human umbilical vein endothelial cells where inhibition of PI 3-kinase markedly attenuated insulin-stimulated NO production (21), further arguing for a significant role of PI 3-kinase-changes in endothelial dependent insulin-induced vasorelaxation.

We have reported that, in obese animals, removal of obesity-inducing diet completely restores endothelial function (22) suggesting that reversal of adiposity might be of benefit in correcting obesity-induced attenuation of PI 3-kinase. In fact, in our present study, PI 3-kinase levels were restored in diet-to-chow group, further strengthening the hypothesis that PI 3-kinase levels may determine the magnitude of endothelial function in obesity. Therefore, it is possible that any deficiency in the concentrations of PI 3-kinase may participate in inducing insulin resistance in vascular system accompanied with reduced NO production, leading to endothelial dysfunction.

In this study, fenofibrate-treatment further reduced PI3-kinase. Peroxisome proliferator-activated receptor (α) (PPAR- α) plays a crucial role in the control of mitochondrial β -oxidation of fatty acids (23,24). Moreover, PPAR- α expressed in the vascular tissue, mainly the endothelial cells (25). Therefore, it is plausible to assume that the increased intracellular fatty acids and the presence of abundant amount of PPAR- α agonist (fenofibrate) may enhance fatty acid oxidation leading to increase in the intracellular fatty acid metabolites. Fatty acid metabolites such as fatty acyl-CoA, diacylglycerols, and ceramides shown to alter insulin signaling and induce insulin resistance (26) thus causing reduction in PI3 kinase levels in these animals.

Functionally active PI 3-kinase stimulates Akt, which in turn activates eNOS, leading to production of NO and subsequent vasorelaxation (21). In our study, protein levels of Akt were similar between dietary-obese and lean aorta while removal of palatable diet caused marked decrease in Akt levels. On the other hand, to our surprise there was a significant increase of eNOS levels in the obese group, whereas, removal of palatable diet or fenofibrate treatment restored eNOS levels to that of lean control group. Although, increased eNOS level in this study is suggestive of augmented endothelial-dependent vasorelaxation, but numerous human and animal studies have shown attenuated endothelial function in obesity (6,19,27). There are several possibilities on increased level of eNOS in obese animals. One possible explanation, is activation of a compensatory mechanism to overcome the decrease

in NO production or increase inactivation of NO seen in arteries of dietary obese rats as a result of increased oxidative stress (28). Moreover, in obese animals there are elevation of insulin concentration and endothelial dysfunction (22). Furthermore, insulin is a potent enhancer of reactive oxygen species (ROS) synthesis in endothelial and vascular smooth muscle cells, and superoxide is known to reduce NO and subsequently increased vasoconstriction (29,30), thus, the elevation of eNOS could compensate this reduction. Insulin is also shown to induce eNOS expression in endothelial cells (31,32) and therefore, insulinaemia which observed in obese rats could directly be responsible for the enhancement of eNOS expression. Similar results and hypothesis have also been reported by others indicating an increase in eNOS levels in Zucker obese coronary (28) and cerebral (33) arteries. However, the function of eNOS maybe regulated by the PI 3-kinase or MAP-kinase pathway (34), and thus decrease in PI 3-kinase seen in untreated obese rats may cancel any beneficial effects of increased eNOS. Furthermore, activated VEGF stimulates eNOS expression at both mRNA and protein levels in a dose-dependent manner (34), suggesting that the elevated levels of eNOS in dietary-obese group seen in the present study maybe due to increased level of VEGF through MAP-kinase pathway, correlating positively with the dietary-obese subjects (35). Therefore, restoration (*i.e.* reduction) of total body fat seen in diet-to-chow and fenofibrate-treated animals, may have resulted in reduced effect of VEGF on eNOS expression (35) and thus improved vascular function (22,36). Inhibition of PI 3-kinase pathway enhances the mitogenic actions of insulin through MAP kinase pathway (37). Hence, it is possible that inhibition of PI 3-kinase pathway seen in both untreated dietary-obese and fenofibrate treated groups may cause over activation of other signaling pathway such as MAP kinase, resulting in the genesis of atherosclerosis and cardiovascular disease.

In conclusion, the present study demonstrates for the first time that long term feeding (15 weeks) of animals with an obesity-inducing palatable diet causes selective changes in protein levels of PI 3-kinase-dependent signaling pathway in aorta. Chronic withdrawal of obesity-inducing diet causes a complete normalization of PI 3-kinase, while fenofibrate treatment failed to improve PI 3-kinase concentrations in dietary-obese animals. A reduction in PI 3-kinase levels may have a role in inducing insulin resistance in vasculature, contributing to increased incidence of cardiovascular events seen in obese subjects. Furthermore, we also postulate that, the inhibition of PI 3-kinase pathway may result in increased activation of MAP kinase pathway leading to an increased proliferation and migration of endothelial cells, thereby increasing the risk of cardiovascular events. However, this hypothesis merits further investigation. Furthermore, the adverse

effects of dietary obesity on insulin transduction in vasculature are post receptor, on the level of PI3-kinase and downstream, and reversible, mainly by removal of obesity-inducing diet, which may have a role in combating diet-induced obesity-related cardiovascular dysfunction.

Acknowledgments

This study was supported by a grant from British Heart Foundation (FS/02/002).

References

- James PT, Leach R, Kalamara E, Shayeghi M. The worldwide obesity epidemic. *Obes Res* 2001; 4:228-233.
- Staels B, Dallongeville J, Auwerx J, Schoonjans K, Leitersdorf E, Fruchart JC. Mechanism of action of fibrates on lipid and lipoprotein metabolism. *Circulation* 1998; 98:2088-2093.
- Dufflou J, Vrmani R, Rabin I, Farb A, Smialek J. Sudden death as a result of heart disease in morbid obesity. *Am Heart J* 1995; 130:306-313.
- Reaven GM. Role of insulin resistance in human disease. *Diabetes* 1988; 37:1595-1607.
- Reaven GM. Role of insulin resistance in human disease (syndrome x): an expanded definition. *Annu Rev Med* 1993; 44:121-131.
- Steinberg HO, Chaker H, Leaming R, Johnson A, Brechtel G, Baron AD. Obesity/insulin resistance is associated with endothelial dysfunction. Implications for the syndrome of insulin resistance. *J Clin Invest* 1996; 97:2601-2610.
- Walker AB, Savage MW, Doros J, Williams G. Insulin-induced attenuation of noradrenaline-mediated vasoconstriction in resistance arteries from Wistar rats is nitric oxide dependent. *Clin Sci* 1997; 93:147-152.
- Obata T, Kashiwagi A, Maegawa H, Nishio Y, Ugi S, Hidaka H, Kikkawa R. Insulin signaling and its regulation of system A amino acid uptake in cultured rat vascular smooth muscle cells. *Circ Res* 1996; 79:1167-1176.
- Mancini FP, Lanni A, Sabatino L, Moreno M, Giannino A, Contaldo F, Colantuoni V, Goglia F. Fenofibrate prevents and reduces body weight gain and adiposity in diet-induced obese rats. *FEBS Lett* 2001; 491:905-908.
- Zeng G, Quon MJ. Insulin-stimulated production of nitric oxide is inhibited by wortmannin. Direct measurement in vascular endothelial cells. *J Clin Invest* 1996; 98:894-898.
- Tamaroglio TA, Lo CS. Regulation of fibronectin by insulin-like growth factor-1 in cultured rat thoracic smooth muscle cells and glomerular mesangial cells. *Exp Cell Res* 1994; 21:338-346.
- Kuboki K, *et al.* Mechanism of insulin's effect on endothelial nitric oxide synthase (eNOS) *in vivo* and *in vitro*. *Diabetes* 1998; 47:A24. (Abstr.)
- Kasuga MF, Karlsson A, Kahn CR. Insulin stimulates the phosphorylation of the 95,000-dalton subunit of its own receptor. *Science* 1982; 215:185-186.
- Sun XJ, Rothenberg P, Kahn CR, Backer JM, Araki E, Wilden PA, Cahill DA, Goldstein BJ, White MF. The structure of insulin receptor substrate IRS-1 defines a unique signal transduction protein. *Nature* 1991; 352:73-77.
- Skolnik EY, Lee CH, Batzer A, Vicentini LM, Zhou M, Daly R, Myers MJ. Jr, Backer JM, Ullrich A, White MF, Schlessinger J. The SH2/SH3 Domain-containing protein GRB2 interacts with tyrosine phosphorylated IRS1 and Shc: implications for insulin control of ras signalling. *EMBO J* 1993; 12:1929-1936.
- Myers MG Jr, Backer JM, Sun XJ, Shoelson S, Hu P, Schlessinger J, Yoakim M, Schaffhausen B, White MF. IRS-1 activates phosphatidylinositol 3'-kinase by associating with src homology 2 domains of p85. *Proc Natl Acad Sci USA* 1992; 89:10350-10354.
- Dimmeler S, Fleming I, Fisslthaler B, Hermann C, Busse R, Zeiher AM. Activation of nitric oxide synthase in endothelial cells by Akt-dependent phosphorylation. *Nature* 1999; 399:601-605.
- Skolnik EY, Batzer A, Li N, Lee CH, Lowenstein E, Mohammadi M, Margolis B, Schlessinger J. The function of GRB2 in linking the insulin receptor to Ras signaling pathways. *Science* 1993; 260:1953-1955.
- Naderali EK, Brown MJ, Pickavance LC. Dietary obesity in the rat induces endothelial dysfunction without causing insulin resistance: a possible role for triacylglycerols. *Clin Sci* 2001; 101:499-506.
- Jiang ZY, Lin YW, Clemont A, Feener EP, Hein KD, Igarashi M, Yamauchi T, White MF, King GL. Characterization of selective resistance to insulin signaling in the vasculature of obese Zucker (fa/fa) rats. *J Clin Invest* 1999; 104:447-457.
- Zeng G, Nystrom FH, Ravichandran LV, Cong LN, Kirby M, Mostowski H, Quon M. Roles for insulin receptor, PI3-kinase and Akt in insulin-signaling pathways related to production of nitric oxide in human vascular endothelial cells. *Circulation* 2000; 101:1539-1545.
- Naderali EK, Fatani S, Williams G. Chronic withdrawal of a high-palatable obesity-inducing diet completely reverses metabolic and vascular abnormalities associated with dietary-obesity in the rats. *Atherosclerosis* 2004; 172:63-69.
- Eringa EC, Stehouwer CD, van Nieuw Amerongen GP, Ouwehand L, Westerhof N, Sipkema P. Vasoconstrictor effects of insulin in skeletal muscle arterioles are mediated by ERK1/2 activation in endothelium. *Am J Physiol Heart Circ Physiol* 2004; 287:H2043-H2048.
- Pyorala M, Miettinen H, Laakso M, Pyorala K. Plasma insulin and all-cause, cardiovascular, and noncardiovascular mortality: the 22 year follow-up results of Helsinki policemen study. *Diabetes Care* 2000; 23:1097-1102.
- Marx N, Sukhova GK, Collins T, Libby P, Plutzky J. PPARalpha activators inhibit cytokine-induced vascular cell adhesion molecule-1 expression in human endothelial cells. *Circulation* 1999; 99:3125-3131.
- Schmitz-Peiffer C. Protein kinase C and lipid induced insulin resistance in skeletal muscle. *Ann NY Acad Sci* 2002; 967:146-157.
- Naderali EK, Pickavance LC, Widling JPH, Doyle PJ, Williams G. Troglitazone corrects metabolic changes but not vascular dysfunction in dietary-obese rats. *Eur J Pharmacol* 2001; 416:133-139.
- Katakam PV, Tulbert CD, Snipes JA, Erdos B, Miller AW, Busija DW. Impaired insulin-induced vasodilation in small coronary arteries of Zucker obese rats is mediated by reactive oxygen species. *Am J Physiol Heart*

- Circ Physiol 2005; 288:H854-H860.
29. Cai H, Harrison DG. Endothelial dysfunction in cardiovascular diseases: the role of oxidant stress. *Circ Res* 2000; 87:840-844.
 30. Griendling KK, FitzGerald GA. Oxidative stress and cardiovascular injury: Part I: basic mechanisms and *in vivo* monitoring of ROS. *Circulation* 2003; 108:1912-1916.
 31. Aljada A, Dandona P. Effect of insulin on human aortic endothelial nitric oxide synthase. *Metabolism* 2000; 49:147-150.
 32. Mather K, Anderson TJ, Verma S. Insulin action in the vasculature: physiology and pathophysiology. *J Vasc Res* 2001; 38:415-422.
 33. Erdos B, Snipes JA, Miller AW, Busija DW. Cerebrovascular dysfunction in Zucker obese rats is mediated by oxidative stress and protein kinase C. *Diabetes* 2004; 53:1352-1359.
 34. Park JS, Hong GR, Baek SW, Shin DG, Kim YJ, Shim BS. Expression and regulation of endothelial nitric oxide synthase by vascular endothelial growth factor in ECV 304 cells. *J Korean Med Sci* 2002; 17:161-167.
 35. Miyazawa-Hoshimoto S, Takahashi K, Bujo H, Hashimoto N, Saito Y. Elevated serum vascular endothelial growth factor is associated with visceral fat accumulation in human obese subjects. *Diabetologia* 2003; 46:1483-1488.
 36. Naderali EK, Fatani S, Williams G. Fenofibrate lowers adiposity and corrects metabolic abnormalities, but only partially restores endothelial function in dietary obese rats. *Atherosclerosis* 2004; 177:307-312.
 37. Montagnani M, Golovchenko I, Kim I, Koh GY, Goalstone ML, Mundhekar AN, Johnsen M, Kucik DF, Quoni MJ, Draznin B. Inhibition of phosphatidylinositol 3-kinase enhance mitogenic actions of insulin in endothelial cells. *J Biol Chem* 2002; 277:1794-1799.

(Received August 15, 2008; Accepted August 29, 2008)

Drug Discoveries & Therapeutics

Guide for Authors

1. Scope of Articles

Drug Discoveries & Therapeutics mainly publishes articles related to basic and clinical pharmaceutical research such as pharmaceutical and therapeutical chemistry, pharmacology, pharmacy, pharmacokinetics, industrial pharmacy, pharmaceutical manufacturing, pharmaceutical technology, drug delivery, toxicology, and traditional herb medicine. Studies on drug-related fields such as biology, biochemistry, physiology, microbiology, and immunology are also within the scope of this journal.

2. Submission Types

Original Articles should be reports new, significant, innovative, and original findings. An Article should contain the following sections: Title page, Abstract, Introduction, Materials and Methods, Results, Discussion, Acknowledgments, References, Figure legends, and Tables. There are no specific length restrictions for the overall manuscript or individual sections. However, we expect authors to present and discuss their findings concisely.

Brief Reports should be short and clear reports on new original findings and not exceed 4000 words with no more than two display items. *Drug Discoveries & Therapeutics* encourages younger researchers and doctors to report their research findings. Case reports are included in this category. A Brief Report contains the same sections as an Original Article, but Results and Discussion sections must be combined.

Reviews should include educational overviews for general researchers and doctors, and review articles for more specialized readers.

Policy Forum presents issues in science policy, including public health, the medical care system, and social science. Policy Forum essays should not exceed 2,000 words.

News articles should not exceed 500 words including one display item. These articles should function as an international news source with regard to topics in the life and social sciences and medicine. Submissions are not restricted to journal staff - anyone can submit news articles on subjects that would be of interest to *Drug Discoveries & Therapeutics*' readers.

Letters discuss material published in *Drug Discoveries & Therapeutics* in the last 6 months or issues of general interest. Letters should not exceed 800 words and 6 references.

3. Manuscript Preparation

Preparation of text. Manuscripts should be written in correct American English and submitted as a Microsoft Word (.doc) file in a single-column format. Manuscripts must be paginated and double-spaced throughout. Use Symbol font for all Greek characters. Do not import the figures into the text file but indicate their approximate locations directly on the manuscript. The manuscript file should be smaller than 5 MB in size.

Title page. The title page must include 1) the title of the paper, 2) name(s) and affiliation(s) of the author(s), 3) a statement indicating to whom correspondence and proofs should be sent along with a complete mailing address, telephone/fax numbers, and e-mail address, and 4) up to five key words or phrases.

Abstract. A one-paragraph abstract consisting of no more than 250 words must be included. It should state the purpose of the study, basic procedures used, main findings, and conclusions.

Abbreviations. All nonstandard abbreviations must be listed in alphabetical order, giving each abbreviation followed by its spelled-out version. Spell out the term upon first mention and follow it with the abbreviated form in parentheses. Thereafter, use the abbreviated form.

Introduction. The introduction should be a concise statement of the basis for the study and its scientific context.

Materials and Methods. Subsections under this heading should include sufficient instruction to replicate experiments, but well-established protocols may be simply referenced. *Drug Discoveries & Therapeutics* endorses the principles of the Declaration of Helsinki and expects that all research involving humans will have been conducted in accordance with these principles. All laboratory animal studies must be approved by the authors' Institutional Review Board(s).

Results. The results section should provide details of all of the experiments that are required to support the conclusions of the paper. If necessary, subheadings may be used for an orderly presentation. All figures, tables, and photographs must be referred in the text.

Discussion. The discussion should include conclusions derived from the study and supported by the data. Consideration should be given to the impact that these conclusions have on the body of knowledge in which context the experiments were conducted. In Brief Reports, Results and Discussion sections must be combined.

Acknowledgments. All funding sources should be credited in the Acknowledgments section. In addition, people who contributed to the work but who do not fit the criteria for authors should be listed along with their contributions.

References. References should be numbered in the order in which they appear in the text. Cite references in text using a number in parentheses. Citing of unpublished results and personal communications in the reference list is not recommended but these sources may be mentioned in the text. For all references, list all authors, but if there are more than fifteen authors, list the first three authors and add "et al." Abbreviate journal names as they appear in PubMed. Web references can be included in the reference list.

Example 1:

Hamamoto H, Kamura K, Razanajatovo IM, Murakami K, Santa T, Sekimizu K. Effects of molecular mass and hydrophobicity on transport rates through non-specific pathways of the silkworm

larva midgut. *Int J Antimicrob Agents* 2005; 26:38-42.

Example 2:

Mizuochi T. Microscale sequencing of N-linked oligosaccharides of glycoproteins using hydrazinolysis, Bio-Gel P-4, and sequential exoglycosidase digestion. In: *Methods in Molecular Biology: Vol. 14 Glycoprotein analysis in biomedicine* (Hounsell T, ed.). Humana Press, Totowa, NJ, USA, 1993; pp. 55-68.

Example 3:

Drug Discoveries & Therapeutics. Hot topics & news: China-Japan Medical Workshop on Drug Discoveries and Therapeutics 2007. <http://www.ddtjournal.com/hotnews.php> (accessed July 1, 2007).

Figure legends. Include a short title and a short explanation. Methods described in detail in the Materials and methods section should not be repeated in the legend. Symbols used in the figure must be explained. The number of data points represented in a graph must be indicated.

Tables. All tables should have a concise title and be typed double-spaced on pages separate from the text. Do not use vertical rules. Tables should be numbered with Roman numerals consecutively in accordance with their appearance in the text. Place footnotes to tables below the table body and indicate them with lowercase superscript letters.

Language editing. Manuscripts submitted by authors whose primary language is not English should have their work proofread by a native English speaker before submission. The Editing Support Organization can provide English proofreading, Japanese-English translation, and Chinese-English translation services to authors who want to publish in *Drug Discoveries & Therapeutics* and need assistance before submitting an article. Authors can contact this organization directly at <http://www.iacmhr.com/iac-eso>.

IAC-ESO was established in order to facilitate manuscript preparation by researchers whose native language is not English and to help edit work intended for

international academic journals. Quality revision, translation, and editing services are offered by our staff, who are native speakers of particular languages and who are familiar with academic writing and journal editing in English.

4. Figure Preparation

All figures should be clear and cited in numerical order in the text. Figures must fit a one- or two-column format on the journal page: 8.3 cm (3.3 in.) wide for a single column; 17.3 cm (6.8 in.) wide for a double column; maximum height: 24.0 cm (9.5 in.). Only use the following fonts in the figure: Arial and Helvetica. Provide all figures as separate files. Acceptable file formats are JPEG and TIFF. Please note that files saved in JPEG or TIFF format in PowerPoint lack sufficient resolution for publication. Each Figure file should be smaller than 10 MB in size. Do not compress files. A fee is charged for a color illustration or photograph.

5. Online Submission

Manuscripts should be submitted to *Drug Discoveries & Therapeutics* online at <http://www.ddtjournal.com>. The manuscript file should be smaller than 10 MB in size. If for any reason you are unable to submit a file online, please contact the Editorial Office by e-mail: office@ddtjournal.com.

Editorial and Head Office

Wei TANG, MD PhD
Secretary-in-General
TSUIN-IKIZAKA 410
2-17-5 Hongo, Bunkyo-ku
Tokyo 113-0033
Japan
Tel: 03-5840-9697
Fax: 03-5840-9698
E-mail: office@ddtjournal.com

Cover letter. A cover letter from the corresponding author including the following information must accompany the submission: name, address, phone and fax numbers, and e-mail address of the corresponding author. This should include a statement affirming that all authors concur with the submission and that the material submitted for publication has not been previously published and is not under consideration for publication elsewhere and a

statement regarding conflicting financial interests.

Authors may recommend up to three qualified reviewers other than members of Editorial board. Authors may also request that certain (but not more than three) reviewers not be chosen.

The cover letter should be submitted as a Microsoft Word (.doc) file (smaller than 1 MB) at the same time the work is submitted online.

6. Accepted Manuscripts

Proofs. Rough galley proofs in PDF format are supplied to the corresponding author via e-mail. Corrections must be returned within 4 working days of receipt of the proofs. Subsequent corrections will not be possible, so please ensure all desired corrections are indicated. Note that we may proceed with publication of the article if no response is received.

Transfer of copyrights. Upon acceptance of an article, authors will be asked to agree to a transfer of copyright. This transfer will ensure the widest possible dissemination of information. A letter will be sent to the corresponding author confirming receipt of the manuscript. A form facilitating transfer of copyright will be provided. If excerpts from other copyrighted works are included, the author(s) must obtain written permission from the copyright owners and credit the source(s) in the article.

Cover submissions. Authors whose manuscripts are accepted for publication in *Drug Discoveries & Therapeutics* may submit cover images. Color submission is welcome. A brief cover legend should be submitted with the image.

Revised February 2008



Drug Discoveries & Therapeutics



Editorial Office

TSUIN-IKIZAKA 410
2-17-5 Hongo, Bunkyo-ku
Tokyo 113-0033, Japan

Tel: 03-5840-9697
Fax: 03-5840-9698
E-mail: office@ddtjournal.com
URL: www.ddtjournal.com

JOURNAL PUBLISHING AGREEMENT

Ms No:

Article entitled:

Corresponding author:

To be published in Drug Discoveries & Therapeutics

Assignment of publishing rights:

I hereby assign to International Advancement Center for Medicine & Health Research Co., Ltd. (IACMHR Co., Ltd.) publishing Drug Discoveries & Therapeutics the copyright in the manuscript identified above and any supplemental tables and illustrations (the articles) in all forms and media, throughout the world, in all languages, for the full term of copyright, effective when and if the article is accepted for publication. This transfer includes the rights to provide the article in electronic and online forms and systems.

I understand that I retain or am hereby granted (without the need to obtain further permission) rights to use certain versions of the article for certain scholarly purpose and that no rights in patent, trademarks or other intellectual property rights are transferred to the journal. Rights to use the articles for personal use, internal institutional use and scholarly posting are retained.

Author warranties:

I affirm the author warranties noted below.

- 1) The article I have submitted to the journal is original and has not been published elsewhere.
- 2) The article is not currently being considered for publication by any other journal. If accepted, it will not be submitted elsewhere.
- 3) The article contains no libelous or other unlawful statements and does not contain any materials that invade individual privacy or proprietary rights or any statutory copyright.
- 4) I have obtained written permission from copyright owners for any excerpts from copyrighted works that are included and have credited the sources in my article.
- 5) I confirm that all commercial affiliations, stock or equity interests, or patent-licensing arrangements that could be considered to pose a financial conflict of interest regarding the article have been disclosed.
- 6) If the article was prepared jointly with other authors, I have informed the co-authors(s) of the terms of this publishing agreement and that I am signing on their behalf as their agents.

Your Status:

- I am the sole author of the manuscript.
 I am one author signing on behalf of all co-authors of the manuscript.

Please tick one of the above boxes (as appropriate) and then sign and date the document in black ink.

Signature:

Date:

Name printed:

Please return the completed and signed original of this form by express mail or fax, or by e-mailing a scanned copy of the signed original to:

Drug Discoveries & Therapeutics office
TSUIN-IKIZAKA 410, 2-17-5 Hongo,
Bunkyo-ku, Tokyo 113-0033, Japan
E-mail: proof-editing@ddtjournal.com
Fax: +81-3-5840-9698

